A *Drosophila* Screen for neural proliferation mutants identifies *qless*, a gene required for CoQ synthesis.

Jennifer Grant

A thesis submitted to University College London for the degree of Doctor of Philosophy

Division of Developmental Neurobiology

National Institute for Medical Research

London

May 2008

ProQuest LLC
789 East Eisenhower Parkway
P.O. Box 1346
Ann Arbor, MI 48106-1346

I, Jennifer Grant, confirm that the work presented in this thesis is my own. Where information has been derived from other sources, I confirm that this has been indicated in the thesis.

Acknowledgements

I would first like to thank my supervisor Dr. Alex P. Gould for his help, encouragement, guidance and support throughout my Ph.D. His observations and recommendations were invaluable.

I would also like to thank all the Gould lab members for their help and feedback and for making the lab such a pleasant and friendly environment to work in. I am also very grateful to the "fly community" in general for their support and contributions at the divisional meetings and to the "cafe de la tarde" group for all the fun and great discussions.

Special thanks to Dr. Maximo Ibo Galindo for all his encouragement, help and belief in my work and who has been a great friend throughout my years of study.

Finally, I do not have enough words to thank all of my family who have always been there for me. They have given me their unfailing support, both economical and emotional throughout the years.

This thesis is dedicated to Nicholas, Carlos and Izan

Abstract

The final size and shape of the brain is specified during neurogenesis by complex spatiotemporal patterns of cell proliferation and cell death. Many of the developmental genes regulating these two cellular processes remain to be identified. In the holometabolous insect *Drosophila*, neurogenesis involves distinct embryonic and postembryonic phases. To identify new regulators of *Drosophila* postembryonic neurogenesis, I conducted two genetic screens. First, a screen of 350 mutagenised chromosomes was used to isolate 22 pupal-lethal mutations associated with an undersized and/or mis-shapened central nervous system. And second, a larger mosaic screen of 1,250 mutagenised chromosomes identified 68 embryonic-lethal mutations altering the number of neurons generated per neural progenitor (neuroblast).

Two of the mutations associated with neuroblast clones containing greatly reduced numbers of neurons were mapped to an uncharacterised gene, CG31005 that I have named *qless*. Sequence analysis indicates that *qless* encodes a fly orthologue of human prenyl diphosphate synthase subunit 1 (PDSS1), the mitochondrial enzyme that synthesises the isoprenyl side-chains of Coenzyme-Q (CoQ). CoQ is a potent antioxidant and plays a key role in generating cellular ATP via oxidative phosphorylation. Patients with mutations in *PDSS1*, present a range of pathologies including neural degeneration and mental retardation. In *Drosophila*, oxidative phosphorylation appears capable of utilising CoQ with anywhere between 4-10 isoprenyl groups as the *qless* phenotype can be rescued by dietary supplementation with CoQ4, CoQ9 or CoQ10. Neurons lacking *qless* activity express activated caspase and their mitochondria display elevated levels of a Cytochrome *c* epitope associated with apoptosis. Together, these studies of *qless* shed light on the poorly understood contribution of mitochondria to apoptosis in *Drosophila* and also provide a genetically tractable model for studying human CoQ deficiencies.

Table of Contents

Figures and Tables

Chapter 1

Introduction

1.Introduction

The final size and shape of the brain is specified during development by complex spatiotemporal patterns of cell proliferation and cell death. Neural cell number can be modulated by regulating the number of times a neural stem cell (NSC) or progenitor divides. In turn, this can be influenced by cell-cycle entry or exit and also by progenitor death. Although not discussed in this thesis, cell death can also regulate cell number after neurogenesis has been completed, via the editing out of post-mitotic neurons that fail to innervate their targets correctly (Oppenheim, 1991). The identification of new genes that control either proliferation or death of neural precursor cells will provide important insights into how brain size is regulated.

1.1.Mammalian neurogenesis

The building blocks of the mammalian central nervous system (CNS) are neural stem and progenitor cells. Two criteria are often used to define a cell as a stem cell, it has to be able to self-renew for many cell divisions and has to be multipotent with the ability to generate numerous differentiated cell types. Progenitor is the collective name for both stem cells and non-stem-cell progenitors. Neural non-stem-cell progenitors usually undergo symmetric differentiating divisions each of which produce two post-mitotic neuronal cells. In principle, neural progenitors can divide symmetrically or asymmetrically (Fig. 1.1). The purpose of symmetrical division is to give rise to two daughter cells of the same type, for example to increase the progenitor pool or to exit the cell cycle via two differentiated post-mitotic cells. The purpose of asymmetric division is to generate two different daughter cells, one of which is often identical to the mother cell and the other a more restricted intermediate or a differentiated cell type. Both types of division have been observed during vertebrate neurogenesis (Gotz and Hunter, 2005; Molyneaux et al., 2007). Live imaging of labelled progenitors in the CNS indicates that the majority of neurons, 84% in the hindbrain, are generated by symmetric divisions in the zebrafish (Lyons et al., 2003). During development of the mammalian cerebral cortex many of the details concerning when and where symmetric and asymmetric divisions are

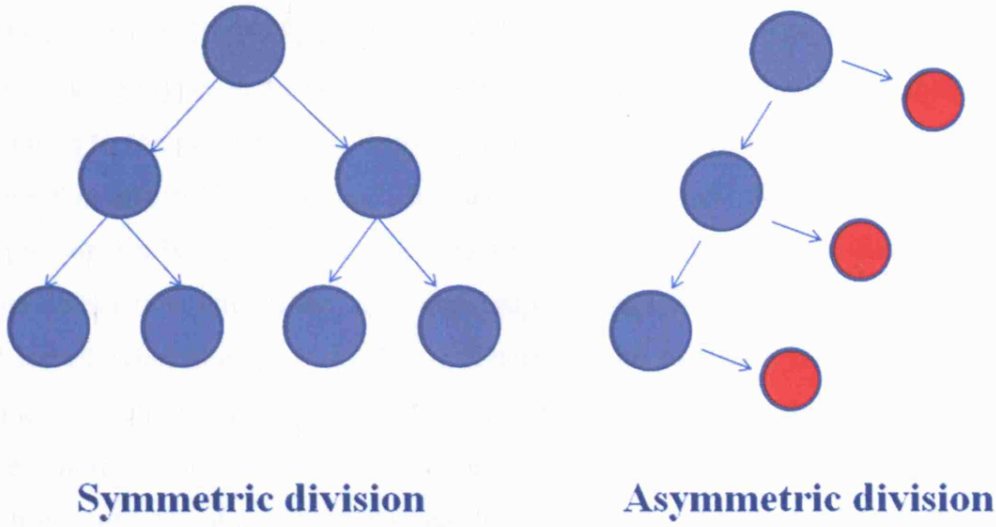

FIGURE 1.1. SYMMETRIC AND ASYMMETRIC DIVISION. Symmetric division of neural progenitors (blue) can increase the progenitor pool. Asymmetric division of progenitors can allow self-renewal and the production of differentiated cells such as neurons (red).

utilised remain to be worked out. However, early neuroepithelial cells are known to undergo extensive proliferation dividing symmetrically to expand the initial progenitor pool. These neuroepithelial cells then give rise to multipotent progenitors such as radial glia. These, in turn, appear to generate all the differentiated cells in the CNS via the production of intermediate precursors, also known as transit-amplifying cells, such as neuroblasts (NBs) and glioblasts (Doetsch et al., 2002; Lyons et al., 2003). Intermediate progenitors undergo repeated asymmetric divisions, self-renewing and producing several different types of neurons that migrate to a precise final destination. There are six distinct neuronal layers in the cerebral cortex, each layer consisting of neurons with specific morphology, function and connectivity. As each cortical layer develops, progenitors become progressively restricted from generating the earlier-born neuronal types. With the exception of the Cajal-Retzius cells which reside in layer 1, the cerebral cortex is formed in an "inside-out manner" (Berry et al., 1964). Layer 1 is produced first, followed by layers 6, 5, 4 and 2/3. Therefore, the birth-date of the neuron predicts its identity. Neurons which migrate to form the deepest 5^{th} and 6^{th} layers are born first while those destined for the more

superficial layers are the later born neurons (Brown et al., 2001; Hanashima et al., 2004; McConnell, 1988; Rakic, 1974; Shen et al., 2006). The first restriction in neuronal cell types in the cortex is the transition from the generation of Cajal-Retzius neurons to the production of deep-layer neurons. Research has now shown that one gene that affects this early cortical stage is *Foxg1*, which encodes a transcriptional repressor that is expressed in neuroblasts but not in early-born Cajal-Retzius cells. In loss-of-function mutations in mice, supernumerary Cajal-Retzius neurons are observed (Hanashima et al., 2004). Together, the evidence indicates that *Foxg1* functions cell-autonomously to repress the production of Cajal-Retzius neurons after their normal birth date, hence suppressing this early-born cell fate during the subsequent generation of the cortical laminae (Desai and McConnell, 2000; Frantz and McConnell, 1996; Hanashima et al., 2004; Shen et al., 2006). Other genes known to be crucial for the specification of the different cortical layers are LIM homeobox 2 (*Lhx2*), empty spiracles homologue 2 (*Emx2*) and paired box 6 (*Pax6*) (Cecchi, 2002; Molyneaux et al., 2007). Intrinsic cues appear to be involved in generating layer-specific neuronal identities from initial progenitors, as the process can be recapitulated by selected progenitors in vitro (Cecchi, 2002; Shen et al., 2006).

Birth-order dependent neuronal fates have also been observed in the vertebrate retina, hindbrain and spinal cord (Donovan and Dyer, 2005; Livesey and Cepko, 2001). In the vertebrate retina, for example, progenitors divide to produce seven major cell types, divided into the outer nuclear layer (rods and cones), the inner nuclear layer (horizontal, bipolar, amacrine and Müller) and the ganglion cell layer (Cepko, 1999; Chang and Harris, 1998; Hu and Easter, 1999; Young, 1985). Birth-dating and lineage studies in rat, mice, chicken and *Xenopus* have shown that the retina is generated from multi-potent progenitors that are biased to produce some cell types first and others later (Fekete et al., 1994; Holt et al., 1988; Moody et al., 2000; Pearson and Doe, 2004; Turner and Cepko, 1987; Turner et al., 1990; Wetts and Fraser, 1988). However, it is not yet known whether all cell types are born in the same order in all lineages, hence further studies to follow individual lineages are necessary. Both intrinsic and extrinsic cues are thought to be involved in the regulation of temporal identity e.g. early-born retinal cells are sensitive to extrinsic cues. When co-cultured with older cells, they were unable to generate early-born

amacrine cells and ganglion cells due to an inhibitory feedback loop from differentiated amacrine and ganglion cells (Belliveau and Cepko, 1999; Waid and McLoon, 1998). The ganglion-cell feedback loop is known to be mediated by Sonic hedgehog, but the identity of the signal for the amacrine cell feedback loop is unknown (Zhang and Yang, 2001). Most regions in the brain and spinal cord generate neurons first, followed by glia (Kessaris et al., 2001). This neuronal-to-glia switch is a good tractable system to investigate temporal patterning in the CNS. Olig2 and Neurogenin1 are required for early-born motor neuron identity whereas Olig2 and Nkx2.2 are needed for late-born glial cell identity (Mizuguchi et al., 2001; Novitch et al., 2001; Zhou et al., 2001). Although a few factors influencing temporal neuronal identities are known in mammals, the molecular timing mechanisms underlying birth-order dependent neurogenesis still remain elusive.

1.2. *Drosophila* neurogenesis

The holometabolous insect *Drosophila* goes through a remarkable metamorphosis in which the burrowing larva completely changes its body plan to become the adult fly, complete with new compound eyes, antennae, wings and legs (Fig.1.2.) (Truman et al., 1993). These two distinct body plans need to be powered by different nervous systems. Consequently, as the adult CNS develops from its larval predecessor, it is dramatically remodelled by several processes that are highly region specific. These processes include arrest and reactivation of neural progenitors and also programmed cell death (Bello et al., 2003; Truman and Bate, 1988; Truman et al., 1993).

1.2.1. Embryonic neurogenesis

Drosophila neurogenesis involves distinct embryonic and postembryonic phases. The primary precursor is the neuroblast (NB), a neuronal precursor cell similar to a mammalian stem cell in that it self-renews and is multi-potent, unlike the more restricted definition of a mammalian neuroblast. The multiple divisions of the neuroblast, produces with a few exceptions at the midline, all the different neuronal types and glia present in the brain. The formation of neuroblasts, their identification

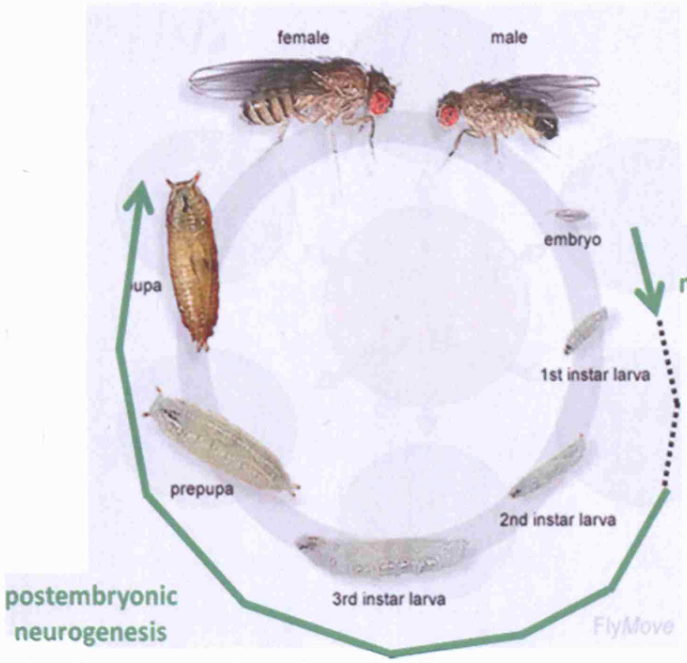

FIGURE 1.2. THE DROSOPHILA LIFE CYCLE. Periods of Neurogenesis are shown in green.

and description of their lineages have all been well documented (Technau GM, 2005; Urbach et al., 2003; Urbach and Technau, 2003a, b, 2004; Urbach R, 2004; Urbach et al., 2006). It has been shown that both the larval CNS and the adult CNS are formed from these precursor cells, which are generated early in embryogenesis with postembryonic neuroblasts (pNBs) sharing a lineage with their embryonic counterparts (Prokop et al., 1998; Prokop and Technau, 1991; Schmid et al., 1999; Schmidt et al., 1997; Urbach et al., 2003; Urbach and Technau, 2003a; Zhao et al., 2007).

Neuroblasts are derived from proneural clusters in the ventral neuroectoderm, with the brain deriving from the anterior procephalic neuroectoderm and the ventral cord from the more posterior ventral neuroectoderm (Campos-Ortega, 1997; Egger et al., 2007b; Skeath and Thor, 2003). Their formation is regulated by two opposing classes of genes, proneural genes such as *achaete-scute* that are basic helix-loop-helix transcription factors that promote neuroblast formation

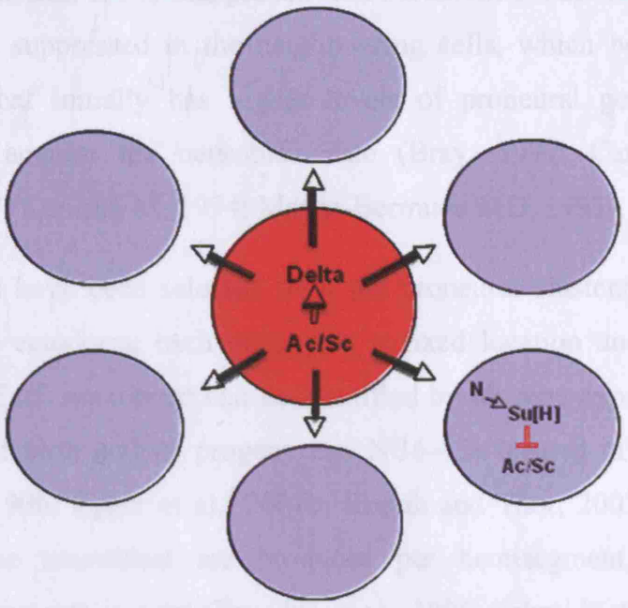

FIGURE 1.4. LATERAL INHIBITION IN THE PRONEURAL CLUSTER. The future neuroblast (red) expresses a higher level of Delta, which activates Notch in neighbouring cells. The Notch intracellular domain then activates Su[H] which in turn inhibits the proneural Achaete-Scute complex, leading to an epidermal fate (lilac).

(Skeath and Doe, 1996; Skeath and Thor, 2003; Urbach R, 2004) and neurogenic genes such as *Notch* and *Delta* that inhibit NB formation (Bhat, 1998; Hartenstein et al., 1994). Although all cells in each cluster are competent to become neuroblasts, normally only one cell does so. The remaining cells become ventral epidermal cells. A lateral inhibition process mediates this selection (Fig.1.3). Originally it was thought that stochastic fluctuations in the levels of proneural and neurogenic genes randomly selected one cell to become the neuroblast in each group.

However, it is now thought that, at least in some cases, region-specific factors can bias one cell, the future neuroblast, to express a higher level of the Delta ligand than the others. This activates the Notch receptor in neighbouring cells, cleavage of Notch results and its interior domain binds to Suppressor of Hairless [Su(H)]. This then translocates to the nucleus leading to activation of specific target genes, such as Enhancer of split [E(spl)]. Expression of Achaete-Scute is thus inhibited (Campos-

Ortega and Hartenstein, 1997; Campuzano and Modolell, 1992). This results in Delta expression being suppressed in the neighbouring cells, which become epidermal. Thus, the cell that initially has higher levels of proneural genes and/or Delta expression will acquire the neuroblast fate (Bray, 1997; Campos-Ortega and Hartenstein, 1997; Kunisch M, 1994; Martin-Bermudo MD, 1995).

After neuroblasts have been selected from the proneural clusters, they delaminate from the surface ectoderm, each occupying a fixed location and having its own unique identity. Each neuroblast can be identified by its gene expression profile, its time and place of birth and its progeny e.g. NB6-4 is located in column 6, row 4 (Bossing et al., 1996; Egger et al., 2007b; Skeath and Thor, 2003). 30 neuroblasts plus one midline neuroblast are produced per hemisegment, with the CNS comprising 13 segments in total (Broadus et al., 1995; Schmidt et al., 1997; Skeath and Doe, 1996). Neuroblasts divide asymmetrically in a budding process to self-renew and to generate a smaller ganglion mother cell (GMC). The GMC then divides symmetrically to produce two post-mitotic cells (A and B), which can either be neurons or glia (Doe and Bowerman, 2001; Doe and Skeath, 1996). [Where the A and B fates are different this can be explained by the asymmetric Numb partitioning which represses Notch signalling in one daughter cell (Doe, 2006; Van de Bor and Giangrande, 2001)].

Neuroblast asymmetrical division occurs perpendicular to the apical-basal axis such that basal complex genes go into the GMC, which is regulated by the apical complex (Fig.1.4). This requires cell polarity genes, important for cell differentiation and also for maintaining progenitor identity. The apical complex is composed of two sub-complexes linked by Inscuteable. One sub-complex has aPKC phosphorylation as its output and is involved in targeting proteins to the basal cortex, while the output of the other is G-protein signalling via Gαi, involved in spindle orientation and asymmetry. There are two basal complexes e.g. the Miranda complex functions to transfer Prospero into the GMC nucleus ensuring that the GMC divides only once. This involves aPKC phosphorylation of Lgl, part of the Lgl/Scrib/Dlg complex (lethal giant larva/scribble/ discs large) located at the neuroblast apical cortex, which subsequently dissociates from the plasma membrane. This results in uniform cortical distribution of the Lgl/Scrib/Dlg complex, reported to be

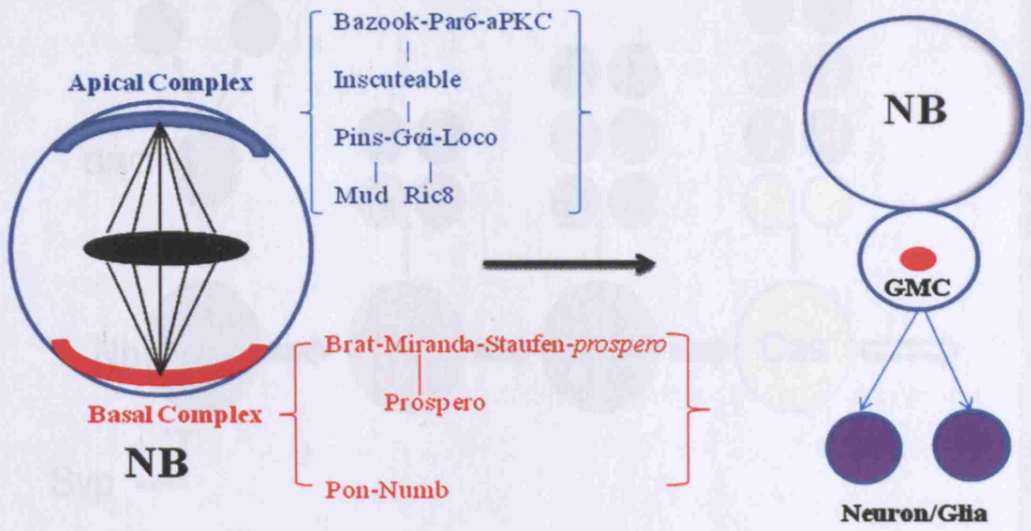

FIGURE 1.4. NEUROBLAST ASYMMETRIC DIVISION. Neuroblasts divide asymmetrically to self-renew and to generate a smaller ganglion mother cell (GMC) which then divides symmetrically producing two neurons/glia (Purple circles). The apical complex of the neuroblast (blue crescent) is responsible for targeting proteins to the basal cortex (red crescent). The output of the Miranda containing basal complex is the transference of Prospero to the GMC nucleus (red oval) where it turns off cell-cycle genes to ensure that the GMC divides only once. The output of Pon/Numb is to mediate the asymmetric fates of the daughter cells.

responsible for the basal targeting of Prospero/Miranda/Brat at metaphase, crucial for GMC fate. Mutations in *lgl, scrib* or *dlg* show defects in basal protein targeting, a smaller cortical domain and reduced spindle size, resulting in smaller neuroblasts and larger GMCs and hyperplasia (Albertson and Doe, 2003; Betschinger et al., 2003; Betschinger et al., 2006; Humbert, 2003; Lee et al., 2006a; Lee et al., 2006b; Wodarz, 2005).

1.2.2. Temporal Transcription Factor Series

Embryonic neuroblasts express members of a transcription factor series in a specific sequence, which gives a temporal identity to each neuroblast, with the GMC and

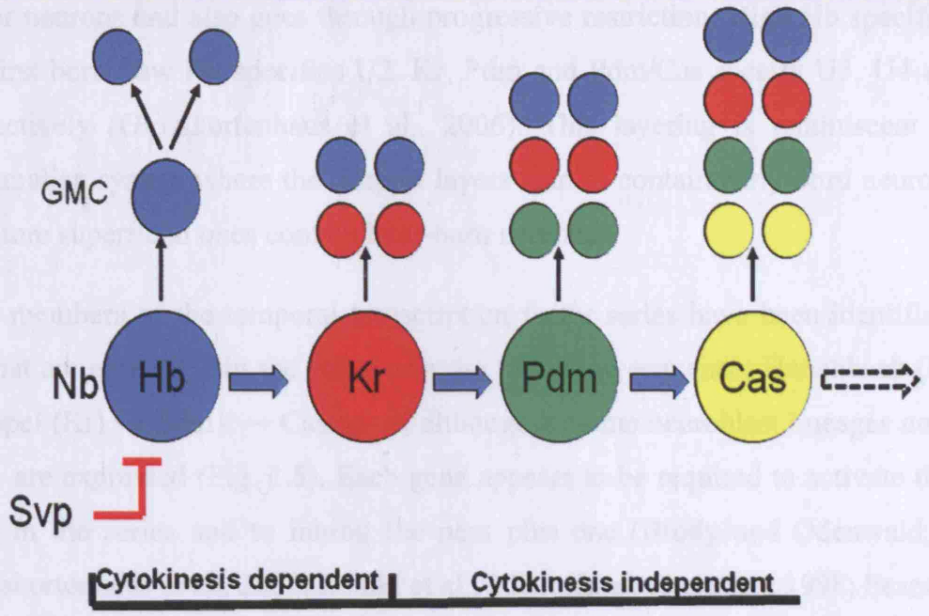

FIGURE 1.5. THE EMBRYONIC TEMPORAL TRANSCRIPTION FACTOR SERIES. Regulatory relationship between the transcription factors in the neuroblasts (large circles) confers identity to the progenies of successive ganglion other cells and the resulting post-mitotic cells (smallest circles). For clarity GMCs are omitted. The transition from Hb to Kr is regulated by Seven up and is cytokinesis dependent whereas Kr→Pdm1→Cas is not.

neurons sometimes expressing the same transcription factor as their progenitor (Brody and Odenwald, 2000; Isshiki et al., 2001; Kambadur et al., 1998). Early-born neurons tend to be located deep inside the CNS whereas the late-born neurons are located nearer the ventral surface of the CNS e.g. early-born neurons express Hunchback (Hb) and lie deep within the brain whereas later born neurons express Castor and lie in a more superficial layer (Fig.1.5) (Isshiki et al., 2001; Kambadur et al., 1998). For example, NB7-3 gives rise to four individual identifiable neurons generated from three distinct GMCs. Hunchback (Hb) is expressed in the early sub-lineage, while Pdm1 was found in the later born neurons (Novotny et al., 2002). Interestingly, 4 instead of 6 post-mitotic neurons are found in this lineage and several studies have shown that the cause of this is apoptosis among the progeny and requires Notch/Numb signalling (Karcavich and Doe, 2005; Lundell et al., 2003; Novotny et al., 2002; Rogulja-Ortmann et al., 2007). NB7-1 generates U1 to U5

motor neurons and also goes through progressive restriction. High Hb specifies U1, the first born, low Hb specifies U2, Kr, Pdm and Pdm/Cas specify U3, U4 and U5 respectively (Grosskortenhaus et al., 2006). This layering is reminiscent of the mammalian system where the deepest layers tend to contain early-born neurons and the more superficial ones contain later-born neurons.

Four members of the temporal transcription factor series have been identified thus far that are expressed in the embryo in the following sequence: Hunchback (Hb) → Kruppel (Kr) → Pdm1 → Castor →, although in some neuroblast lineages not all of these are expressed (Fig. 1.5). Each gene appears to be required to activate the next gene in the series and to inhibit the next plus one (Brody and Odenwald, 2005; Grosskortenhaus et al., 2005; Isshiki et al., 2001; Kambadur et al., 1998; Pearson and Doe, 2003). Studies have shown that the transition from Hb to Kr expression is regulated by Seven up (Svp) and is cell-cycle dependent, requiring cytokinesis (Grosskortenhaus et al., 2005; Grosskortenhaus et al., 2006; Kinai MI, 2005). Although Hb is switched off in the neuroblast, its expression is maintained in the first born GMC. Recent studies have reported that this maintenance is due to the transcription factor Prospero, which is asymmetrically segregated into the GMC nucleus and is crucial in determining the GMC fate and cell-cycle exit. Prospero inhibits the down regulation of Hb in the GMC by antagonising Svp activity. It also represses cell cycle genes to prevent the GMC from dividing more than once (Mettler et al., 2006). In addition, it appears that, unlike cell-cycle dependent Hb to Kr transition, Kr → Pdm1 → Cas are still sequentially expressed in *string* mutants where the cell is blocked in G2/M. This exciting observation suggests that the NB may possess an intrinsic clock mechanism independent of cell-cycle progression (Grosskortenhaus et al., 2005). At the end of embryonic neurogenesis, most abdominal neuroblasts die, leaving only 3 of 30 neuroblasts per hemisegment in comparison to 24 neuroblasts remaining in the thoracic region. This drastic reduction in abdominal neuroblasts is dependent upon the axial patterning Hox protein AbdA, which triggers the cell death mechanism of apoptosis mediated by the proapoptotic gene *reaper* (*rpr*) (Peterson et al., 2002; Prokop et al., 1998; White et al., 1994). This late elimination of neuroblasts in the embryo makes the first major contribution to the segment-specific sculpting of the adult CNS.

1.3. Postembryonic neurogenesis

The embryonic period is responsible for generating the larval CNS, whereas development of the larger, more complicated adult brain requires both phases (Fig.1.6). The adult CNS is comprised of 10% remodelled larval cells, born during embryogenesis, plus 90% imaginal cells generated in the larval and pupal stages. Most of the adult motoneurons derive from remodelled larval motoneurons, whereas all the adult interneurons are believed to be produced during postembryonic neurogenesis (Skeath and Thor, 2003). The larval CNS contains approximately the same number (400) of neurons in each head, thoracic and abdominal segments (Hartenstein et al., 1987; Maurange and Gould, 2005; Skeath and Thor, 2003). In contrast, the adult CNS develops by dramatic postembryonic proliferation of the head and thoracic neuromeres, while the abdomen expands very little, with abdominal neuroblasts undergoing apoptosis after only a few rounds of division (Bello et al., 2003). This difference in expansion is reflected by post-embryonic neuroblasts (pNBs) producing ~100 cells each in the thorax compared to ~10 cells in the abdomen (Bello et al., 2003; Cenci and Gould, 2005; Truman and Bate, 1988).

FIGURE 1.6. TIME COURSE OF DROSOPHILA NEUROGENESIS. Neuroblast divisions (black bars) for top to bottom: mushroom body NBs, central brain NBs, thoracic NBs, central abdominal NBs and terminal abdominal NBs, which show a gender specific proliferation window. The thoracic and abdominal neuromeres constitute the ventral ganglion. (Adapted from Maurange and Gould, 2005).

This is because neuroblasts in the anterior regions divide for much longer periods of time than they do in the posterior region (Fig.1.6).

Following embryonic neurogenesis (with the exception of the four mushroom body neuroblasts), neuroblasts enter a quiescent stage in which they exit the cell cycle and enter a G0 or G1-like quiescent state. However, the factors that induce this quiescent state are at present unknown. Interestingly, there are segmental differences in their quiescence time windows such that neuroblasts in the abdomen remain in the quiescent state longer than their thoracic and central brain counterparts. (Fig 1.5.) (Maurange and Gould, 2005; Truman and Bate, 1988; Truman et al., 1993). This region-by-region variation suggests that the exact time of exit from quiescence is regulated by local rather than global cues. Exiting the quiescent state and re-entering the cell cycle appears to depend on two types of extrinsic factors, humoral signals from the circulating hemolymph and more local signals such as Anachronism (Ana) from a glial cell-dependent stem cell niche (Maurange and Gould, 2005). The first stage of neuroblast reactivation is enlargement which is dependent on amino acids in the diet. An unidentified fat-body mitogen is produced in response to these nutritional amino acids and it has been reported that in starved larvae, this mitogen is not produced (Britton and Edgar, 1998). Other humoral cues include Juvenile Hormone, reported to induce quiescent neuroblasts to re-enter the cell cycle and ecdysone is also thought to play a role in *Drosophila* (Cayre et al., 2000; Datta, 1999; Egger et al., 2007b).

The second stage of reactivation is entry into S-phase which involves various factors (Truman and Bate, 1988). The gene *ana* encodes a secreted glycoprotein expressed in glial cells that are located next to the neuroblasts and although its receptor is unknown it appears to be required for maintenance of the quiescent state of central brain post-embryonic neuroblasts (pNBs), as loss-of-function mutations result in neuroblasts reactivating 8 hours earlier than normal (Ebens et al., 1993). Another factor involved in the reactivation of quiescent neuroblasts, is the protein encoded by the gene *terribly reduced optic lobes (trol),* as loss-of-function *trol* mutants show a severe delay in neuroblast reactivation. Although *trol* neuroblasts enlarge, they do not enter S phase. This can be rescued by over expression of *Cyclin E*, and reduced levels of Cyclin E are found in *trol* mutants, suggesting that *trol* neuroblasts may be arrested due to lack of Cyclin E (Caldwell and Datta, 1998). It has also been

demonstrated that Trol acts downstream of Ana to either bypass or inactivate its repressive effect on the cell cycle (Datta, 1995). *Trol* also modulates *hedgehog* and *branchless* signalling by binding FGF in cells adjacent to the neuroblasts to initiate division (Lindner et al., 2007). Another factor thought to be involved is the cell adhesion molecule DE-Cadherin which is expressed by pNBs, their progeny and glial cells. Expression of a dominant-negative Cadherin in neuroblasts or glia resulted in a severe phenotype where neuroblast mitotic activity was greatly reduced (Dumstrei et al., 2003). Thus it is thought that DE-Cadherin mediates neuroblast/glia interactions required for neuroblast proliferation Also involved is the transcription factor Grainyhead (Grh), which is expressed from late embryogenesis and maintained in pNBs throughout larval stages (Almeida and Bray, 2005; Bray et al., 1989; Cenci and Gould, 2005). It has been suggested that DE-Cadherin may be a direct target of Grh as expression is lower in *grh* mutant neuroblasts and the *DE-Cadherin* gene has Grh binding sites in its flanking sequences (Almeida and Bray, 2005; Cenci and Gould, 2005; Egger et al., 2007b).

1.3.1. Postembryonic neuroblast divisions

Postembryonic neurogenesis is a major contributor to the sculpting of the adult CNS. Postembryonic neuroblasts divide asymmetrically, as in the embryo, and utilise much of the same molecular machinery as embryonic neurogenesis. It is not known if the temporal transcription factor series continues or how many temporal identities of neurons exist postembryonically. However, a transcription factor called Chinmo has been revealed to confer temporal identity in a dose-dependent manner on the neuronal progeny (γ and α'β') of pNBs in the mushroom body (Zhu et al., 2006). Chinmo is not detected in the neuroblast itself, but seems to act on GMCs or early born neurons.

Thoracic neuroblasts continue to proliferate for a longer period of time (128hr ALH) in comparison to abdominal neuroblasts (72hr ALH) and employ a different mechanism to end proliferation. Recently, it has been shown that central brain and thoracic neuroblasts stop dividing via cell-cycle exit which is dependent on Prospero delocalizing to their nucleus (Maurange et al., 2008). In Prospero loss-of-function mutants, thoracic neuroblasts proliferate into adulthood, and when Prospero is

expressed earlier than normal, neuroblasts stop dividing prematurely. Abdominal neuroblasts stop dividing by undergoing apoptosis during third larval instar, triggered by a pulse of the Hox protein AbdA which activates one or more of the H99 cell death genes (*rpr, hid* and *grim*) (Bello et al., 2003). The progenitor-specific transcription factor Grainyhead (Grh) makes the neuroblast competent to respond appropriately to the AbdA signal (Almeida and Bray, 2005; Cenci and Gould, 2005; Egger et al., 2007a). The Polycomb (PcG) group of genes which maintain the inactivate states of Hox genes has recently been shown to be required for pNB survival (Bello et al., 2007). Proliferation defects are seen in mutants of the PcG genes due to loss of neuroblasts by apoptosis caused by the ectopic expression of the posterior Hox genes, *abdA* and *abdB,* confirming that Hox proteins have to be turned off in postembryonic neuroblasts to avoid them apoptosing (Bello et al., 2003). The result is that, at the end of postembryonic neurogenesis, each thoracic pNB has generated approximately 100 cells in 4 days whereas the abdominal pNBs only generate an average of 4 cells over a 1 day period. Interestingly, neuroblasts in the mushroom body (olfactory centre of the brain) do not undergo a quiescent phase and divide continuously, to generate about 500 cells each over 8 days (Maurange and Gould, 2005; Truman et al., 1993).

1.4. Apoptosis in vertebrates and insects

Programmed cell death is a fundamental process which functions during the development of multicellular organisms, either to eliminate surplus cells or cells that are damaged or infected and therefore detrimental to the organism. Cells in developing tissues compete to survive and proliferate and final organ size is the net result of integrating cell proliferation and cell death. In the developing CNS, neurons are dependent on a small group of highly specific proteins called neurotrophic factors, secreted from other neurons, glia and target tissues. Neurons are produced in excess and they compete with one another for survival. Neuronal death occurs in redundant neurons whose axons do not reach their target so are unable to receive neurotrophic factors and those whose axons have made erroneous connections (Brown et al., 2001; Oppenheim, 1991; Pettmann and Henderson, 1998).

The core apoptotic pathway was first discovered through genetic analysis in the nematode *C. elegans* and involves specific genes which cause cell death, such as the initiator and effector caspases and others which protect the cells from dying, for example, the IAP (inhibitor of apoptosis) and Bcl-2 anti-apoptotic proteins (Ellis and Horvitz, 1986; Horvitz, 1999; Liu and Hengartner, 1999). Caspases comprise a family of cysteine aspartate proteases that can be grouped into initiator caspases and effector caspases. The proteolytic initiator caspases activate the more downstream effector caspases triggering a cascade which results in apoptosis. The Bcl-2 family of proteins have two sub-groups, anti-apoptotic and pro-apoptotic proteins which are localized to the mitochondria (Igaki, 2000). Many components are conserved between species but there are also important differences as well. Animals with complex systems immune and nervous systems possess additional proteins, activators, adaptors and inhibitors of cell death which precisely regulate apoptosis (Jacobson et al., 1997; Putcha and Johnson Jr., 2004). The core apoptotic pathway in *C. elegans* is an intrinsic pathway involving 4 genes, *egl-1(egg laying abnormal)*, *ced-3(cell death abnormal)*, *ced-4,* pro-apoptotic genes and *ced-9* which is anti-apoptotic (Fig.1.7). CED-3, the initiator caspase, is activated by CED-4 and inhibited by CED-9 which blocks activation by physical interaction with CED-4. Endogenous CED-4 is localized to the mitochondria by CED-9 (anti-apoptotic Bcl-2 family), however if EGL-1 (pro-apoptotic Bcl-2 family) is expressed, the CED-4/CED-9 interaction ceases, CED-4 translocates to the nuclear membrane to activate CED-3 resulting in programmed cell death (Chen et al., 2000; del Peso et al., 2000). Each of these genes has *Drosophila* and mammalian orthologues (Fig. 1.7) and successive studies have uncovered 14 mammalian caspases, 1 -14 and at least 19 Bcl-2 family members divided into anti-apoptotic and pro-apoptotic subgroups (Riedl and Shi, 2004).

1.4.1. Mammalian apoptosis

Mammalian cells have two different pathways, the intrinsic pathway and the extrinsic pathway, whereas *C. elegans* only uses an intrinsic linear pathway. The extrinsic pathway in mammals is activated by extracellular cues, activating ligand-induced death receptors that lead to caspase activation and cell death. Cross talk

FIGURE 1.7. VERTEBRATE AND INVERTEBRATE APOPTOTIC PATHWAYS (adapted from (Riedl and Shi, 2004). Schematic of the pro-apoptotic and anti-apoptotic proteins involved in programmed cell death in *C. elegans*, mammals and *Drosophila*. Orthologues are depicted by the same colour code. The mitochondria play a key role in the intrinsic mammalian pathway, but its role in *Drosophila* apoptosis is still unclear.

between both pathways can amplify the apoptotic signal (Putcha and Johnson Jr., 2004; Shi, 2002; Twomey and McCarthy, 2005).

The intrinsic apoptotic pathway is dependent upon the depolarisation of mitochondria and the release of pro-apoptotic mitochondrial proteins. In mammals, mitochondria play a key role in apoptosis as cellular stress often causes the permeabilisation of the mitochondrial outer membrane and disruption of mitochondrial architecture, leading to the release of cytochrome c into the cytosol and subsequent caspase activation (McQuibban et al., 2006; Melzig et al., 1998; Youle and Karbowski, 2005). On mitochondrial depolarisation, the pro-apoptotic proteins are released into the cytosol and subsequently form a cytosolic complex called the apoptosome consisting of Apaf-1, cytochrome c, ATP and the initiator caspase-9. Apaf-1 (apoptotic protease-activating factor 1) the mammalian orthologue

of Ced-4 is required for the recruitment and autocatalytic activation of caspase-9 which triggers the caspase cascade leading to cell death. This requires ATP in mammals and nematodes and cytochrome *c* in mammals (Riedl and Shi, 2004; Zou et al., 1997) In addition to cytochrome *c*, other additional proteins are released from the mitochondria in mammals, such as Smac/Diablo which binds to IAPs (8 in mammals) inactivating them and thus triggering the caspase cascade and death. Other proteins released from mitochondria include AIF (apoptosis inducing factor), EndoG (endonuclease G) and Omi/HtrA2 (mitochondrial serine protease) (Twomey and McCarthy, 2005).

1.4.2. *Drosophila* apoptosis

Drosophila has an intermediate complexity between the nematode and mammals (Fig. 1.7), sharing many mammalian components but with less redundancy, compared to mammals (Hay and Guo, 2006; Hay et al., 2004; Richardson and Kumar, 2002). In *Drosophila*, there is widespread cell death during metamorphosis which is regulated by steroid hormones (Baehrecke, 2000; Richardson and Kumar, 2002; Rogulja-Ortmann et al., 2007). Several studies have identified apoptotic cells in the *Drosophila* CNS which require the proapoptotic gene *reaper* although how it is activated is still unclear (Karcavich and Doe, 2005; Lundell et al., 2003; Peterson et al., 2002). The Hox gene AbdA is required for apoptosis through one or more of the H99 (Reaper, Hid and Grim) proteins in abdominal pNBs, whereas the pioneer neurons dMP2 and MP1 found to undergo apoptosis in a region-specific manner need AbdB for their survival in the posterior segments of the CNS (Bello et al., 2003; Miguel-Aliaga and Thor, 2004; Miguel-Aliaga et al., 2008).

There are 7 *Drosophila* caspases, *Dcp-1, Dredd/DCP-2, Drice, Dronc, Decay, Strica/Dream and Damn/Daydream* and two Bcl-2 family proteins, Buffy/dBorg2 (anti-apoptotic) and Drob-1/Debcl/dBorg-1/dBok (pro-apoptotic) (del Peso et al., 2000; Igaki, 2000; Igaki et al., 2002; Quinn et al., 1999; Richardson and Kumar, 2002; Twomey and McCarthy, 2005; Zhang et al., 2000a). In addition, *Drosophila* has unique killer proteins in Reaper, Hid and Grim which have mitochondrial localization signals and bind to and inhibit dIAP (Brun et al., 2002; Wang et al., 1999; White et al., 1991). Although there is no sequence homology to *reaper, hid*

and grim, the mammalian protein Smac/Diablo shares functional similarities to them, in that it localises to the mitochondria and when released binds to the BIR (*baculovirus* IAP repeat) domain of the IAPs preventing them from inhibiting caspase activation in the same way as Reaper, Hid and Grim act on the dIAP (Denault et al., 2007; Denault and Salvasen, 2008; Salvesen and Riedl, 2008) (Fig.1.7).

Although *Drosophila* possess an *Apaf-1* homologue, *Ark,* there is no conclusive evidence that cytochrome *c* is required for cell death except in spermatid individualisation and in the retina (Arama et al., 2003; Mendes et al., 2006; Rodriguez et al., 1999). However, a cell death epitope of cytochrome *c* is unmasked in *Drosophila* when cells are programmed to undergo apoptosis (Dorstyn et al., 2004; Dorstyn et al., 2002; Varkey et al., 1999). Recently, the *Drosophila* DmHtrA2, homologue of the mammalian Omi/Htr2A, has been shown to reside in the mitochondria and on being exposed to UV-irradiation translocates to the extra mitochondrial compartment, cleaves dIAP and thus triggers cell death (Challa, 2007; Igaki, 2007). However, unlike the mammalian counterpart, which diffuses into the cytosol, DmHtr2A remains localised at mitochondria. Intriguingly, it appears to be an effector caspase-independent pathway possibly through DRONC, a fly counterpart of the initiator caspase, caspase-9 (Igaki et al., 2002). Although there are many similarities between the mammalian and *Drosophila* pathways, the involvement of mitochondria in programmed cell death in *Drosophila* is far from clear.

1.4.3. The importance of mitochondria in the CNS

Mitochondria generate cellular energy in the form of ATP which they accomplish via the coupling of electron transport to the generation of proton gradients for oxidative phosphorylation. All tissues require energy but each tissue has a different metabolic demand depending on its function. Tissues with high metabolic demands such as muscle, liver and the brain use large amounts of ATP and are therefore highly dependent on mitochondria which can be present in their hundreds or thousands or as a tubular network surrounding the nucleus of each cell (Chang and Reynolds, 2006). The CNS in particular uses enormous quantities of ATP, with 95% of this produced

by oxidative phosphorylation in the mitochondria (Chang and Reynolds, 2006; Thome Research, 2007).

Neurons are highly-active cells that often need to grow long processes during development and in the adult state must support many rounds of depolarisation-repolarisation, vesicle release and recycling (Chada and Hollenbeck, 2004). These are highly dynamic processes requiring large amounts of ATP and mitochondria have been shown to accumulate at the growth cones of growing axons by chemoattraction to the Nerve Growth Factor (NGF) (Chada and Hollenbeck, 2004). Synapses not only have a high metabolic demand but in addition have elevated intracellular calcium levels also regulated by the mitochondria, therefore mitochondrial transport to synapses along lengthy axons is an important requirement for normal neuronal development and signalling (Baloh, 2008; Chada and Hollenbeck, 2004; Chang et al., 2006; Chang and Reynolds, 2006; Kann and Kovacs, 2007). Once neurons are mature, ATP is essential to maintain the ion gradients across the plasma membrane required for the generation, processing and transmission of neural impulses. Mitochondria are therefore also localised at nodes of Ranvier as well as synapses (Chang and Reynolds, 2006).

Evidence that the CNS places a particularly high demand on mitochondrial function comes from several human mitochondrial diseases that have the strongest symptoms in the CNS such as Leigh syndrome, Alzheimer's, Parkinson's, Huntington's disease and Freidreich's Ataxia (Beal, 2007; Celotto et al., 2006; Dias-Santagata et al., 2007; Lin and Beal, 2006; Lopez et al., 2006; Mandemakers et al., 2007). In addition, mutations in the mitochondrial genome are found in infantile multisystemic syndromes including Lebers Hereditary Optic Neuropathy (LHON) which leads to blindness at an early age and MELAS (mitochondrial myopathies, encephalopathy, lactic acidosis and stroke-like symptoms (Bebel-Garcia et al., 2004; Quinzii et al., 2006)

1.5. Aims of the project

There have been many studies of the mechanisms involved in neuroblast formation and asymmetric division in the embryo. However, there have been no systematic

screens for genes controlling either the proliferation or death of neuroblasts. Identification of novel genes regulating these processes will provide important insights into how brain size is regulated during development. Key questions remain as to how NBs know when to start and stop dividing and how many times they should divide? To address this, I conducted two genetic screens of embryonic and pupal-lethal mutations on Chromosome III with the aim of isolating and characterising mutations causing neural growth defects. As a large proportion of *Drosophila* genes have human orthologues, at least some of the genes I identify are likely to have conserved functions during mammalian brain development.

Chapter 2

Materials and methods

2.1. *Drosophila* Stocks

Flies were maintained on standard cornmeal/yeast/agar (1% autolysed yeast, 5.8% cornmeal, 5% glucose and 0.6% agar) at 25°C unless otherwise stated. For the MARCM screen (Fig.2.1), the 3R "clonemaker" used was the Gould lab stock A15: *P{w$^+$elav-GAL4^{c155}}, P{ry$^+$ hsFLP}1; P{w$^+$ UASnlslacZ}20b,P{w$^+$UAS-CD8:GFP}LL5; P{ry$^+$,neoFRT82B} P{w[+],tubPGAL80}LL3/TM6 Tb Hu* Short genotype (*elavGAL4 hsFLP;UASlacZ UASGFP;FRT82BtubGAL80/TM6 Tb Hu*).

For selected mutants, another 3R "clonemaker" was used in MARCM experiments; *y w hsFLP^1 tubP-GAL4 UAS-GFPnls; UAS-y$^+$; tubP-GAL80 FRT82B/TM6B* (gift from Gary Struhl). *tub-GAL4* gives stronger GAL4 expression in progenitors than *elav-GAL4^{c155}*.

2.2. 3R MARCM Screen

FRT 82B males were starved for 19 h and then mutagenized by feeding with 26 mM EMS in 1% (w/v) aqueous solution of sucrose for 18 h. (W. Chia, King's College, London). FRT82B Males were then fed normally for 9 h to recover, after which they were mated to an excess of three times as many TM3,Sb/TM6B, Tb, Hu females for 3 days at 25°C. Virgin and male progeny were collected to establish stocks balanced with TM6B. This dose gave an average of 2.5 lethal hits per chromosome arm. A total of 1600 lethal lines were established for the embryonic (1,250) and pupal (350) lethal screens (collaboration with W.Chia's group). Pupal lethals die as 3rd instar larvae which enables the direct comparison of the mutant line CNS morphology with wild type CNS.

Mutations that are recessive lethal can only be maintained as heterozygotes. Lethal mutations on the 3rd Chromosome are maintained using a 3rd Chromosome balancer. Balancers are chromosomes that contain inversions and deletions and cannot recombine. The TM6,Tb, Hu balancer was used for both MARCM and pupal lethal CNS analysis as it carries the larval marker, Tubby.

Parents for the F1 MARCM screen cross (Lee and Luo, 1999) (Fig.2.1. and 2.2) were left to lay in vials for 24hrs at 25°C. 47 hours later, L1– L2 (0 – 48 hr ALH) larvae were heat shocked at 37°C for 85 minutes in a water bath. Vials were then kept at 18°C until wandering L3 larvae (96 hr ALH) appeared on the sides of the vial, 4-5 days later. Non-Tubby wandering L3 larvae were collected, partially dissected to expose CNS and discs and fixed in 1% Glutaraldehyde/PBS for 20 – 30 min. The fixed larvae were washed three times in PBS for 2 min. each, and stained overnight at room temperature in 1mg/ml X-gal in a X-gal stock solution (3.1mM K_3 $[Fe^{3+}(CN)_6]$, 3.1mM $K_4[Fe^{2+}(CN_6)]$, 1mM $MgCl_2$, 0.3% Triton-X-100, 500ml PBS). They were then washed in PBS, transferred to 50% glycerol/PBS for 45 min. and to 100% glycerol for a minimum of 45 min. Following this, the CNS was dissected and mounted in 100% glycerol under a coverslip.

2.3. Pupal-Lethal Screen

*FRT82B */TM6 Tb* X *FRT82B */TM6 Tb* → ***FRT82B */FRT82B ** (non-Tb)**

For the pupal lethal analysis, mutant homozygous 3rd instar wandering larvae (observed on side of vial) were selected for non-Tubby, having lost the Tubby marker. Homozygous mutant larvae from the above cross (* indicates EMS mutation) were raised at 25°C and dissected in PBS at wandering L3 larval stage (96 hr ALH). Samples were fixed in 4% Formaldehyde/PBS for 30 minutes on a rotating platform, washed 3 times in PBS for 10 mins and incubated in 0.5% Triton X-100/PBS for 45 mins, the CNS was then dissected and mounted in Vectashield plus DAPI (Vector Labs) under a coverslip and slides were sealed with transparent nail varnish.

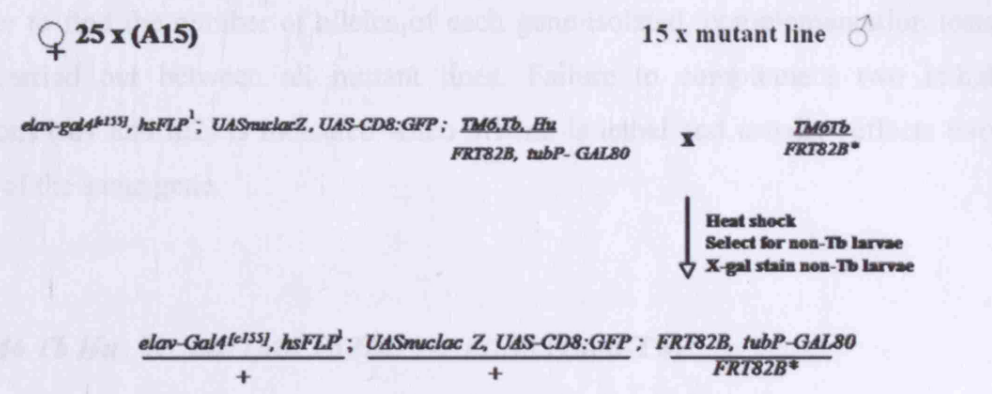

FIGURE 2.1. MARCM CROSSING SCHEME

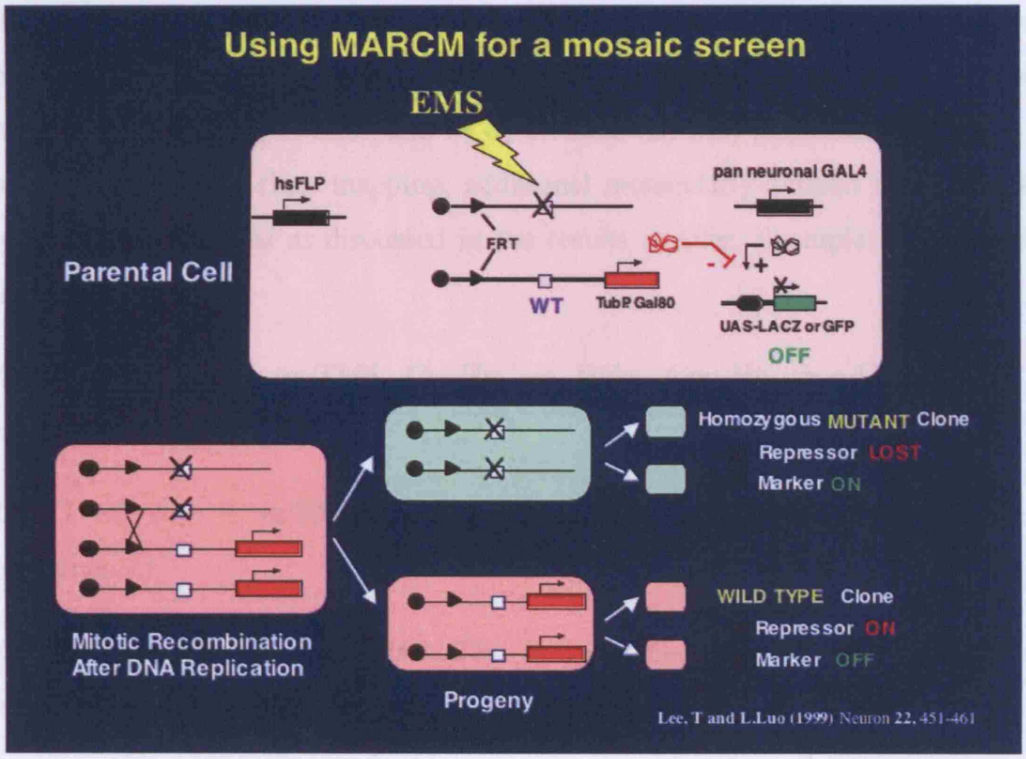

FIGURE 2.2. MOSAIC ANALYSIS WITH A REPRESSIBLE CELL MARKER (MARCM). A transgene which ubiquitously expresses a repressor of GAL 4 (*tub-Gal80*) is placed distal to the Flipase (FLP) recombinase target site (FRT). The homologue contains an identical FRT proximal to the mutation of interest. Prior to mitotic recombination, GAL80 represses the pan-neural GAL4, preventing *UAS-lacZ* and *UAS-GFP* expression. When mitotic recombination is induced in G2 using heat shock to activate FLP, the homozygous mutant progeny cells lose GAL80 and express *UAS-lacZ* and *UAS-GFP*. The WT progeny receive two copies of GAL80 and do not express the UAS reporters. Mutant clones can then be visualised by X-gal staining.

2.4. Complementation Testing and Deficiency mapping

In order to find the number of alleles of each gene isolated, complementation tests were carried out between all mutant lines. Failure to complement two lethal mutations (m1 and m2) is indicated when m1/m2 is lethal and usually reflects two alleles of the same gene.

m1/TM6 Tb Hu **X** ***m2/TM6 Tb Hu*** **→** ***m1/m2*** **(non-Tb)**

For mapping experiments, deficiency stocks for chromosome III were obtained from the Bloomington Stock Centre. For rough mapping, I assembled a 3R deficiency core kit of 91 deficiencies. This consists of 26 cytologically defined deficiencies from Bloomington and 65 molecularly-defined deficiencies. Of these, 41 were generated by Exelixis (Df Exel) and 24 by Drosdel (Df ED) (Appendix Table.2.1 at end of Chapter). For finer mapping, additional molecularly-defined from Drosdel and Exelixis were used as discussed in the results chapter. Examples of balancers used:

Df/TM2 Ubx **X** ***m/TM6 Tb Hu*** **→** ***Df/m*** **(**non-Hu, non-Ubx adults = complements.**)**

Df/TM3 Sb Ser **X** ***m/TM6 Tb Hu*** **→** ***Df/m(***non Sb/Ser, non-Hu adults = complements.***)***

Df/TM6B Tb Hu **X** ***m/TM6B Tb Hu*** **→** ***Df/m*** **(**non-Tb,non-Hu adults = complements.**)**

Mutant lines (*m/TM6B Tb Hu*) were crossed with the 91 deficiencies of the 3R core kit. Complementation tests were also carried out with all available lethal alleles in each candidate region. These lethal stocks were obtained from the Bloomington Stock Centre, Exelixis and Drosdel (Appendix Table 2.2). The MARCM screen only identifies phenotypes mapping to 3R whereas the pupal-lethal screen identifies phenotypes covering both arms of Chromosome III.

2.5. Immunostaining

Larvae were dissected in PBS to expose the CNS and discs and fixed in 4% Formaldehyde/PBS for 20 minutes. Samples were then washed 3 x 15 minutes in PBT (0.5% Triton-X-100/PBS), pre-incubated in normal goat serum (NGS):PBT (1:9) for 30 mins, and incubated with primary antibody/NGS:PBT at 4°C on a shaker overnight. Samples were then washed in PBT for 3 x 15 mins, incubated in secondary antibody in NGS:PBT at room temperature for a few hours, followed by 2 x 15 min washes in PBT and 1 x 30 min in PBS before being stored in Vectashield plus DAPI and mounted on slides. Primary antibodies used were mouse α-Mira (1:50), mouse α-GFP (1:1000), rabbit α-GFP (Invitrogen) (1:1000), rabbit α-mHSP60 (1:200) (Alonso et al., 2005), mouse α-Cytochrome C (1:200) (7H8 2C12, Invitrogen), rabbit α- pH3 (1:400) (Upstate Biotechnology) and mouse α-caspase 3 (Invitrogen) (1:75). Secondary antibodies were anti-mouse and anti-rabbit fluorescent conjugates with Alexa 594 (red) and Alexa 488 (green) at 1:200 (Molecular Probes). Images were collected using the Leica SP5 Confocal Fluorescence Microscope. All images show projections unless otherwise stated.

2.6. BrdU labelling

BrdU labels cells that have passed through S-phase. Larvae were raised on standard food mashed up with 1:33 of 0.2mg/ml BrdU in 40% ethanol (Sigma). BrdU-labelled larvae were collected, dissected and fixed in 4% formaldehyde/PBS for 30 min. Samples were rinsed three times in PBT, washed 2 x 15 min in DNase1 buffer (66mM Tris 7.5, 5mM $MgCl_2$, 1mM fresh β-mercaptoethanol), incubated at 37°C for 30 min in 25μl DNase1 + 0.5ml DNase1 buffer (Promega), washed 3 x 15mins in PBT and blocked in 10%NGS/PBT for 30 mins mouse anti- BrdU antibody (1:50) was added and incubated overnight at 4°C. After washing 3 x 15mins in PBT, samples were incubated in anti-mouse secondary antibody (1:100) and shaken at room temperature 2 -3 hours followed by 2 x 15 min washes in PBT and 1 x 30 mins in PBS before being stored in Vectashield plus DAP1 and mounted on slides.

2.7. Adult Cuticle Preps

Flies were dehydrated in iso-propanol, dissected and legs were mounted on slides with 2-3 drops of both iso-propanol and Euparal (Fisher Scientific). Slides were baked overnight in a 65°C oven with a 10g metal weight on top of the cover slip (M.I.Galindo personal communication).

2.8. Sequence analysis of *qless*

2.8.1. Quick Fly Genomic DNA prep.

Anesthetised flies were collected and stored frozen at -80°C. Genomic DNA was prepared by grinding 35 flies in 200 µl fresh Buffer A with a disposable tissue grinder. An additional 200µl of Buffer A (5ml Buffer A solution: 500µl 100mM Tris-HCl, 1000µl 100mM EDTA, 100µl 100mM NaCl, 250 µl 0.5% SDS (55°C) + 3150µl H_2O) was added, the flies were macerated until only cuticle fragments remained and then incubated at 65°C for 30 min. After incubation, 800µl of cold LiCl/KAc (1 part 5M KAc:2.5 parts 6M LiCl) solution was added and left to incubate on ice for at least 10 min, spun at 13,000rpm in a microcentrifuge at room temperature for 15 min then left on ice for a further 10 min. 1 ml of the supernatant was transferred to a new 2ml Eppendorf tube, avoiding the interface layer. Extraction with Phenol and Chloroform was then carried out by adding 500 µl phenol and 500µl chloroform to the sample and vortexing for 30 seconds and centrifuging at 13,000 rpm for 2 min in a microcentrifuge. The upper aqueous layer was transferred to another 2ml Eppendorf tube, taking care not to remove the white interface. 1ml of chloroform was added, the sample then vortexed for 30 seconds, spun at 13,000 rpm for 2 min in a microcentrifuged and the upper layer was again transferred to a new 2ml Eppendorf tube. 800µl of ice cold isopropanol was mixed with the sample, left at -20°C for 10 min then centrifuged at 13,000 rpm at room temperature for 15 min. The supernatant was carefully discarded, the pellet was washed in 70% ethanol, centrifuged at 13,000 rpm for 10 min and air dried. The DNA pellet was resuspended in 30µl TE buffer (1ml 1M Tris.Cl (pH8), 200µl 0.5M EDTA pH8, 8.8ml H_2O) and stored at -20C.

2.8.2. PCR protocol

PCR using the Robocycle (Stratagene) was carried out on the extracted DNA using the Expand High Fidelity Kit (Roche). Three pairs of primers (100μM synthesis from Eurogentec) covered the 8 exons of *qless*:

PAIR 1 – product size 1500bp, covers exons 6, 7 and 8.

Forward primer: JGIB - **TACGTGTATGGTTTATGTTAGGGTG**

Reverse primer: JG1E - **GTGTAGGGGAAACATTGCGAATTGC**

PAIR 2 – product size 2000bp, covers exons 2, 3, 4 and 5.

Forward primer: JG2A - **AGCATAAAATGTGCGAGGCACTTGG**

Reverse primer: JG2E - **GGCAAAACTTGTTAGACGTGACAC**

PAIR 3 – product size 500bp, covers exon 1.

Forward primer: JG3A - **GTATCTTTTCCTTTTCAAGTTTACCAG**

Reverse primer: JG3C - **CCTGTTGAATTCTGTGCCTGTGTCT**

PCR mix :	100ng/μl DNA	1μl
	Forward primer (10μM)	1μl
	Reverse primer (10μM)	1μl
	dNTPS	1μl
	Buffer (2)	5μl
	Enzyme (1)	0.5μl
	H_2O	40.5μl
		= 50μl

PCR Programme –	Initial denaturing	94°C for 2 min	
	Denaturing	94°C for 35 sec	40 cycles
	Annealing	58°C for 1min10sec	
	Extension	72°C for 1min10sec	
	Final extension	72°C for 9 min	

2.8.3. Gel extraction

For gel extraction and purification of PCR products, 45µl PCR product + 7.5µl loading buffer was run on a 1% agarose gel for 10 min at 120v then approximately 30 min at 100v. Bands were carefully excised under UV light and transferred to an Eppendorf tube. The amplified DNA was then purified using the Qiagen Gel Extraction kit and protocol and the DNA resuspended in 30µl H_2O. The purified DNA solution was then sequenced.

2.8.4. Sequencing

Sequencing was carried out by Cogenics. Forward primers for *qless* sequencing analysis were as follows:

Exon 1 – **GTATCTTTTCCTTTTCAAGTTTACCAG**

Exon 2 – **CTTAAGATTTGCGATTGGACATGG**

Exon 3 – **CGTTAGGTAATAACCACGAGTTC**

Exon 4 – **GGGCGTGTGTTTGGCTTTGTTTGCT**

Exon 5 – **AGCATAAAATGTGCGAAGGCACTTGG**

Exon 6 – **CACACTAATTGCCGAATTAAGCGGC**

Exon 7 – **CGATTTTTCTCTGTGCACACAACG**

Exon 8 – **TACGTGTATGGTTTATGTTAGGGTG**

2.9. Coenzyme Q feeding expts

Coenzymes Q_4, Q_9 and Q_{10} were all obtained from SIGMA Aldrich. All feeding experiments were carried out using 50μg CoQ per g fly food after an initial experiment using different concentration of 20μg, 50 μg, 100μg, 200μg and 500μg per gram food. The food in each vial was weighed and the corresponding amount of CoQ powder was then added and mixed thoroughly into the food to form a homogenous mixture. 25 virgins of the MARCM clonemaker, *y w hsFLP*^{1} *tubPGAL4 UAS-GFPnls; UAS-y*$^{+}$*; tubPGAL80 FRT82B/TM6B* were crossed with 15 FRT 82B *qless* or Frt82B^{+} males and the MARCM screen protocol was followed as described in section 2.2 and immunostained as described in section 2.5.

To assess whether embryonic lethality could be rescued by feeding parents with CoQ, 50 adult heterozygotes (*qless*/TM6B, Tu, Hu) were left for 48 hours in vials containing various concentrations of Coenzyme Q10 *i.e.* no CoQ10, 20μg/g food, 50μg/g food, 100μg/g food and 200μg/g food. They were then flipped out and the larvae left to grow in the vials. This was carried out for 3 generations to look for homozygote flies, (non-Tb, non-Hu).

For control purposes and to assess the effect of CoQ on WT flies, adult WT flies were left for 48 hours with the same CoQ concentrations as the *qless* mutant experiments and then flipped out and the larvae left to grow. The rate of development was observed on the different concentrations compared to non-fed WT flies.

2.10. Microscopy and Image Analysis

CNS images from both screens were recorded with the light or fluorescence microscope (Zeiss Axiophot) using a Leica Firecam and compared to wild-type CNS. The pupal-lethal screen CNS images used the nuclear marker DAPI and were recorded using fluorescent microscopy, whereas the MARCM screen images used X-gal staining and were recorded using light microscopy.

All further images were recorded by Confocal Fluorescence Microscopy (Leica SP5). All images were obtained with a 1.5 airy unit pinhole at a magnification of x 1000 (objective x 100). To calculate the number of cells in a clone and the number of clones present for wandering L3 larvae, we took advantage of the nuclear GFP used to mark the clone. For each clone image, a Z-projection of a stack up to 10 sections spaced by 1.5 microns was calculated using maximum intensity. A transparent lamina was placed over each Z section image and cell outlines were drawn using a black felt-tip pen to avoid double counting cells in adjacent z-stacks. Cell numbers were analysed using Microsoft Excel. On all figures, error bars are + 1 s.d. and p-values were calculated using the Student's t-test assuming equal sample variance and two tails.

Table 2.1.

TABLE 2.1. 3R CORE DEFICIENCY KIT		
Symbol	Estimated Cytology	Molecularly Defined
ED 5071	81F6;82E4	3R:22995..16113
ED 5138	82D5;82F8	3R:606794..1090605
ED 5147	82E;83A1	3R:912842..1193526
ED 5156	82F8;83A4	3R:1090655..1284574
EXEL 6144	83A6;83B6	3R:1328529..1438435
ED 5177	83B4;83B6	3R:1426351..1449817
EXEL7283	83B7;83C2	3R:1474080..1572399
ED 5196	83B9;83D2	3R:1510301..1833866
Df(3R)Tpl6	83D1-2;84A4-5	
Df(3R)LIN	84A4-5;84B1-2	
Df(3R)Antp-X1	84A4-5;84C2-3	
ED 7665	84B6;84E10	3R:2916249..3919805
ED 5230	84E6;85C3	3R:3803496..4478856
EXEL 6149	85A2;85A5	3R:4303420..4495213
ED 5300	85A5;85C3	
EXEL 6151	85C3;85C11	3R:4878567..4983814
Df(3R)BSC24	85C4-9;85D12-14	
EXEL 6286	85D2;85D15	
Df(3R)GB104	85D12;85E10	
EXEL 6154	85E9;85F1	3R:5619087..5754513
EXEL 6155	85F1;85F10	3R:5754513..5915190
Df(3R)BSC38	85F1-2;86C7-8	
EXEL 6159	86C3;86C7	3R:6464635..6715093
EXEL 7306	86C7;86D7	3R:6696747..6982569
ED 5514	86C7;86E14	3R:6710720..7394975
EXEL 6161	86E14;86E18	3R:7394952..7495415
EXEL 8154	86E17;86E18	3R:7472871..7585229
EXEL 7310	86F6:87A1	3R:7584321..7712831
ED 5558	86F9;87B10	3R:7654463..8269738
EXEL 7317	87B10;87C3	3R:8266959..8456337
Df(3R)Kar-Sz8	87C1-2;87D14-E1	
Df(3R)ry506-85C	87D1-2;88E5-6	
EXEL 6174	88F1;88F7	3R:11154373..1133206
EXEL 7326	88F7;89A5	3R:11363141..?
EXEL 6175	89A1;89A8	
EXEL 7328	89B1;89B9	3R:11835158..11983197
EXEL 7329	89B14;89B19	3R:12067151..12184534
EXEL 6269	89B17;89D2	3R:12131453..12328470
EXEL 6270	89D2;89D8	3R:12328472..12528639
Df(3R)DG2	89E7;90F1	
EXEL 8165	8E8;89E11	3R:12838670..12879721
EXEL 6176	89E11;89F1	3R:12879395..12974859
ED 5780	89E11;90C1	3R:12882199..13507523
ED 5794	90B3;90E4	
ED 5785	90C2;90D1	3R:13543832..13769792
ED 5797	90C2;90F10	3R:13543832..14068391
ED5185	90F4;91B8	3R:13993596..14484708
ED 2	91A5;91F8	3R:14224953..14922493
ED 5911	91C5;91F8	3R:14568649..14991505
ED 5942	91F12;92B3	3R:15052016..15660809
EXEL 6185	92E2;92F1	3R:16135262..16376403
Df(3R)H-B79	92B3;92F13	

Table 2.1. continued

Symbol	Estimated Cytology	Molecularly defined
Df(3R)BSC43	92F7-93A1;93B3-B6	
ED 10820	93A4;93B8	3R:16774462..16937182
EXEL 6272	93A7;93B13	3R:16783442..16938073
Df(3R)e-BS2	93C3-6;93F14-94A1	
ED 6076	93E7;93F14	3R:17459227..17868550
EXEL 6189	93F14;94A2	3R:17859431..17950482
ED 6093	94A2;94C4	3R:17959510..18552029
ED 6096	94B5;94E7	3R:18413403..19047691
EXEL 6280	94E5;94E11	3R:19007696..19112013
EXEL 9012	94E9;94E13	3R:19096137..19162766
Df(3R)slo3	94D4-10;96A18	
EXEL 6200	96A20:96B4	3R:20585721..20711086
EXEL 6220	96A7;96C3	3R:20369520..21009495
EXEL 6201	96C2;96C4	3R:20954218..21013378
EXEL 9056	96C4;96C5	3R:21013378..21025666
EXEL 6202	96D1;96E2	3R:21109376..21330760
EXEL 6203	96E2;E6	3R:21330985..21452963
EXEL 6204	96F9;97A6	3R:21821474..22076526
Df(3R)Espl3	96F1;97B1	
ED 6235	97B9;97D12	3R:22360956..22806229
EXEL 6205	97D12;97E1	3R:?..22885211
EXEL 6206	97E1;97E5	3R:22885211..22972573
Df(3R)R38.3	97E3-11;98A	
Df(3R)Sq219	97F1-2;98A	
Df(3R)BSC42	98B1-2:98B3-5	
EXEL 6259	98C4;98D6	3R:24141831..24416263
EXEL 6209	98D6;98E1	3R:24416263..24490049
EXEL 6210	98E1;98F5	3R:24490049..24806106
EXEL 6211	98F5;98F6	3R:24806106..24879352
Df(3R)3450	98E3;99A6-8	
Df(3R)Dr-rv1	99A1-2;99B6-11	
Df(3R)01215	99A6;99C1	
Df(3R)127	99B5-6;99F1	
Df(3R)B81	99D3;3Rt	
EXEL 7378	99F8;100A5	3R:26378312..26610043
Df(3R)tll-e	100A2;100C2	
Df(3R)awd-KRB	100C;100D	
Df(3R)faf-BP	100D;100F5	
Df(3R)04661	100D2;100F5	

Table 2.2.

TABLE.2.2.DEFICIENCIES FOR COMPLEMENTATION TESTING		
Deficiency	Cytological Location	Molecularly Defined
Pupal Lethal 2v71		
Df(3R)3450	98E3;99A6-8	
Df(3R)Ptp99A[R3]	99A7;99A7	
Df(3R)L127	99B5-6;99F1	
EXEL6213	99C5;99D1	3R:25692182..25827836
4420 (l(3)99Dj)	99D6;99E3	
4421 (l(3)99Di[4])	99D6;99E3	
4425 (l(3)99Ea[1])	99D6;99E3	
10348 (l(3)j2D5)	99F1;99F2	
Df(3R)X3F	99D1-2;99E	
EXEL 6209	98D6;98E1	3R:24416263..24490049
EXEL 6215	99F6F8	3R:?..26378570
EXEL 6216	99F6;99F7	3R:26281120..26347656
Df(3R)Dr-rv1	99A1-2;99B6-11	
EXEL 6214	99D5;99E2	3R:25914470..26018056
12161 (*Takr99D*)	99C8;99D1	3R:25776512..25795169
15298 (CG7920)	99D1	3R:25836188..25841086
17649 (*Axn*)	99D2;99D3	3R:25848566..25861035
7340 (*Med*)	100C7;100D1	3R:27436770..27441478
11483 (*Fer2LCH*)	99F2	3R:26213554..26216306
11497 (*Fer1HCH*)	99F2	3R:26211290..26213851
Df(3R)tll-g	99F1-2;100B4-5	
12410 (*hdc*)	99E4;99F1	3R:26103656..26187891
15960 (*aralar1*)	99F4;99F5	3R:26271360..26281589
EXEL 9020	100A4;100A5	3R:26571483..26610037
EXEL 8194	100A4;100A7	3R:26571483..26703333
EXEL 6217	100A6:100A7	3R:26635749..26703333
EXEL 7379	100B2;100B3	3R:26917412..?
2455 (*dco*)	100B2	3R:26880904..26886931
EXEL 6219	100B4;100B8	3R:27126307..27277252
15221 (*Gycβ*)	100B4;100B5	3R:26960192..26997242
15328 (CG1815)	100D1	3R:27494956..27503703
15509 (*pasha*)	100D1	3R:27443700..27447197
18944 (CG1792)	100D1	3R:27442062..27443559
12165 (l(3)rM731)	100C1	
15857 (*Rpl6*)	100C7	3R:27420508..27421967
15597 (*CycG*)	100C7	
11589 (*heph*)	100D3;100E1	3R:27676732..27819000
10565 (*krz*)	100E3	3R:27873828..27877711
11795 (*mod*)	100E3	3R:27877794..27880696
Pupal Lethal 2v106		
Df(3R)T-55	86F1;87A7	
Exel 6173	86F1;87A7	
Df(3R)M(3)76A	87E8;93C	
Df(3R)sbd105	88F9;89B10	
11627 (*Akt*)	89B3	3R:11924938..11930239
Df(3R)P115	89B7;89E7	
Df(3R)sbd104	89B5;89C	
11012 (CG3590)	89E8	3R:12844496..12846810
Df(3R)Sri16	90D1;90E1	
Df(3R)DG4	90D2;90F3	
14930 (*alt*)	90C1	3R:13505448..13505448
5949 (*osa*)	90C1;90C2	3R:13513540..13544059
12827 (*cpo*)	90D1	3R:13769785..13769785
1034 (*DnaseII*)	90E1	3R:13845099..13846883
19261 (*htl*)	90E2	3R:13875093..13875130
18397 (*Actn*)	89E5	3R:12801620..12803382
17153 (CG3534)	89E6	3R:12822174..12825172
Df(3R)Cha7	90F1;91F5	
EXEL 6178	90E7;91A5	3R:13992164..14223904

Table 2.2

Deficiency	Estimated Cytology	Molecularly Defined
Pupal Lethals 2v290 and 2v316		
Df(3R)Espl22	96F10-11;96F11	
ED 6232	96F10;97D2	3R:21862598..22624704
Df(3R)Tl-P	97A;98A1-2	
199 [E(spl)]	96F10	3R:21866046..21866585
2124 (*groucho*)	96F10	3R:21867432..21875634
Pupal Lethal 2v206		
ED 6235	97B9;97D12	3R:22360956..22806229
12159 (*scrib*)	97B9;97C1	3R:22362068..22421912
Embryonic Lethal 63		
11664 (*Nmdar1/Itp-r83A*)	83A6;83A7	3R:1334544..1349046
16420 (*Itp-r83A*)	83A7;83B1	3R:1342825..1364584
18865 (*noi*)	83B4	3R:1415317..1417180
22248 (*Rheb*)	83B2	3R:1394618..1396213
10214 (*noi/vha*)	83B4	3R:1417453..1420429
8461 (*Snm*)	83B1;83B2	3R:1380812..1383514
16244 (*mia*)	83B1	3R:1374074..1376355
Embryonic Lethals 47/87		
ED 5577	86F9;87B13	3R:7654463..8303300
ED 5559	86E11;87B11	3R:7394904..8269738
EXEL 6161	86E14;86E18	3R:7394952..7495415
EXEL 6276	86E11;86E14	3R:7394911..7495408
18576 (CG6946)	86F9	3R:7648449..7650647
EXEL 6163	87A1:87A4	3R:7712923..7824992
17825	87A1	3R:7708517..7718107
8707 (*Lk6*)	86E18	3R:7578506..7590179
10275 (*neo*)	86E18	3R:7595335..7604826
Embryonic Lethals 109/264 (*qless*)		
EXEL 6218	100B5;100B8	3R:26994861..27126217
EXEL 7379	100B2;100B3	3R:26917412..?
11509 l(3R)00720	100B5;100B7	
12165 l(3R)rM731	100C1	
17207 CG31005	100B8	3R:27061752..27078326
Df(3R)tll-g	99F1;100B4-5	
18226 CG31004	100B5	3R:27005304..27021484

Note: Bloomington lethal stocks are given as stock number, then the allele in brackets.

Chapter 3

Two Genetic Screens for neural growth mutants

3.1. Introduction

Although there have been many studies on neuroblast formation, asymmetric division and lineage mapping in the *Drosophila* embryo, none thus far have systematically screened for genes controlling neural proliferation and growth. Many questions therefore remain as to how neuroblasts know when to start and stop dividing and which factors are required to maintain their survival and mitotic activity. To address these issues, I have conducted two genetic screens of chemically-induced recessive-lethal mutations on chromosome III. The mutagen used, EMS (ethyl methane sulfonate), is an alkylating agent commonly used as a *Drosophila* mutagen for inducing point mutations, although at low frequency it can also produce rearrangements or small chromosomal deletions (Greenspan, 1997). The first screen, involving 350 pupal-lethal EMS lines aims to identify mutations in genes on both arms of chromosome III with either cell autonomous or non-cell autonomous requirements for CNS growth. These lines fail to develop after late 3rd instar and do not form pupae. The second screen of 1,250 embryonic-lethal EMS lines analyses mutations in genes on the right arm of chromosome III. MARCM is used to generate marked homozygous-mutant clones in a heterozygous background. This type of screen identifies genes with cell-autonomous requirements within the neuroblast lineage. I first describe the pupal-lethal and mosaic screens, and then characterise several mutants selected for further study.

3.2. Pupal-Lethal Screen

In the pupal-lethal screen, gene function is removed from the whole animal such that only those 350 lethal chromosomes surviving in the homozygous state until late L3 and pupal stages can be analysed (for crossing scheme see Section 2.3). The screen involves dissecting L3 larvae, staining nuclei with DAPI and comparing the overall size of the CNS from homozygous mutants(non-Tb) with wild-type. From 350 pupal-lethal lines, I identified 25 pupal-lethal mutants whose brain size and morphology differed considerably from the wild type. All 25 phenotypes were confirmed by rescreening. The phenotypes recovered fall into three classes (Fig. 3.1.and 3.2). Class A, represented by 6 lines, shows smaller than normal optic lobes

(OL) and thorax (Th) (Fig.3.1.2 and 3.1.3). Class B, represented by 18 lines, has all regions of the CNS (OL, CB, Th, Ab) undersized (Figure 3.1.4 and 3.1.5). Class C, represented by only 1 line, shows elongation of the CNS (Figures 3.1.6). As this screen looks at the overall size of the CNS, neural proliferation, cell death and/or condensation defects could be involved.

3.2.1. Selection of mutants for mapping and characterisation

Before selecting which pupal-lethal mutations to map, I performed complementation tests (Table 3.1). Lines 197, 321 and 66 failed to complement each other, indicating three hits in one gene. In addition, lines 22 and 162 failed to complement each other, indicating two hits in one gene. The remaining 20 mutations represent single hits. To maximise the chances of mapping a new gene in the time frame available, I selected six pupal-lethal mutations, 2v71, 2v106, 2v206, 2v237, 2v290, and 2v316 for further characterisation. Although only one allele was identified for each, their CNS phenotypes were dramatically different from wild type and covered all three phenotypic classes. Three mutants, 2v237, 2v290 and 2v316 have the Class B phenotype of an undersized CNS (Fig.3.1.), whereas 2v71 and 2v206 have the Class A phenotype of region-specific abnormalities *i.e.* undersized brain lobes and thorax and possible overgrowth of the abdomen (Fig. 3.1.). Finally, 2v106 was chosen as it is the only pupal-lethal mutant with a Class C phenotype of an oversized, elongated CNS (Fig 3.1). The CNS phenotypes and larval morphology of each selected pupal lethal is described below.

2v71 (Class A)

The pupal lethal 2v71 (Fig 3.1.3) shows reduced thoracic neuromeres, optic lobes and central brain and also oversized abdominal neuromeres. The mutant phenotype is fully penetrant in that all L3 homozygotes show similar CNS and larvae are slimmer and more transparent than wild-type. Less than 1% develop into pharate adults that do not eclose from the pupal case. Even less manage to eclose but these all have severe mobility impairments, lack a proboscis and die 2-3 days later. In preliminary

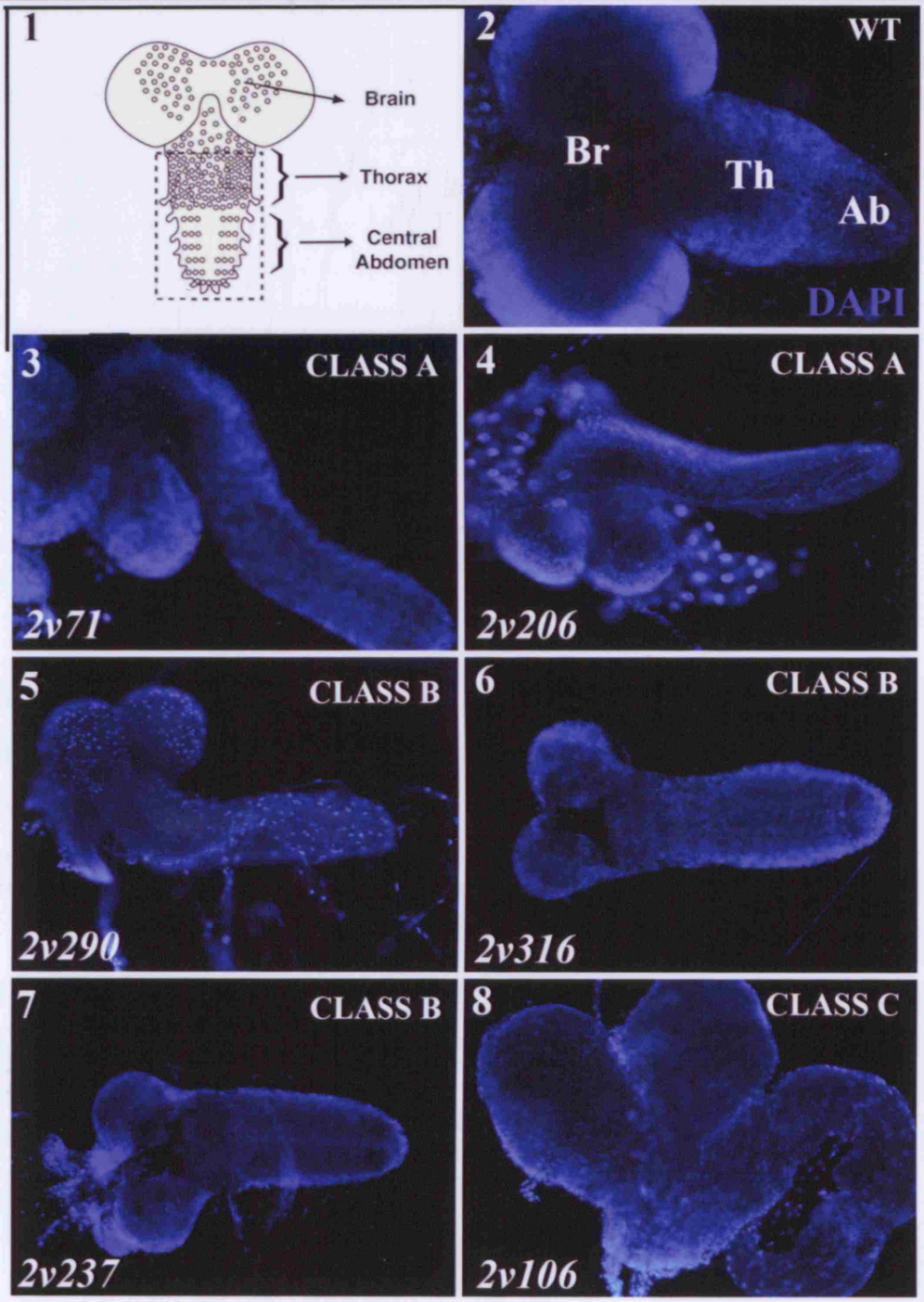

FIGURE 3.1 PUPAL-LETHAL CNS PHENOTYPES. (1) Schematic of larval CNS. **(2-8)** All images show L3 CNS at 96 hr. Anterior is to the left and magnification is 200x. **(2)** Wild type. **(3** and **4) Class A** phenotype shows undergrowth of brain lobes and thorax, and overgrowth of abdomen. **(5, 6** and **7) Class B** phenotype reveals undergrowth of the CNS. **(8) Class C** shows an elongated CNS phenotype, with oval-shaped brain lobes.

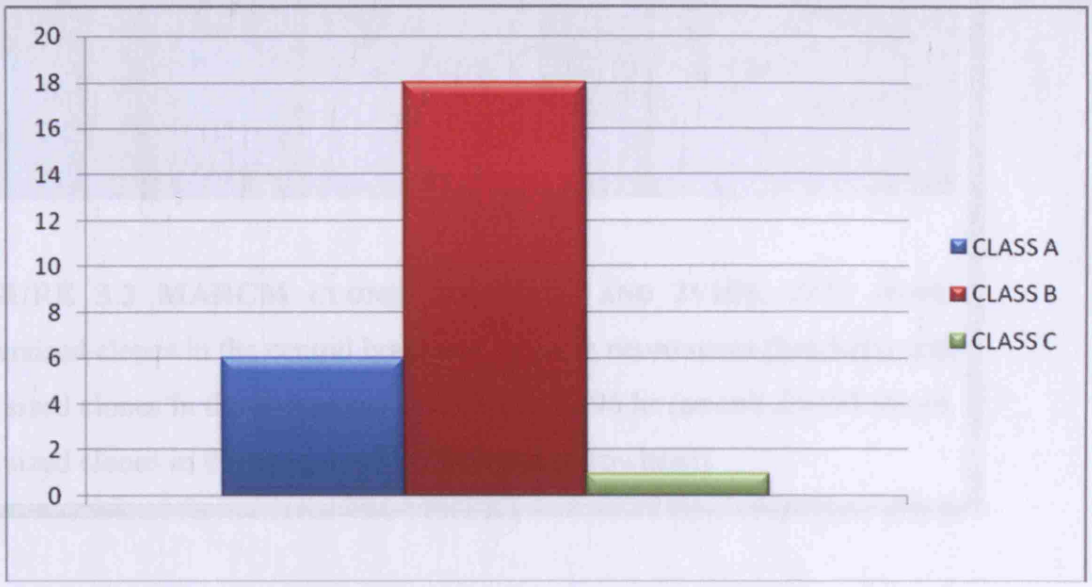

FIGURE 3.2. PUPAL LETHAL SCREEN. CLASS A phenotype of undergrowth in the brain lobes and thorax and overgrowth of abdomen is represented by 6 lines. CLASS B phenotype of undergrowth of the CNS is represented by 18 lines. CLASS C phenotype of oversized CNS is represented by 1 line.

	106	206	237	290	326	331	316	336	122	321	197	133	66	135	327	303	308	181	287	22	263	244	162	1080
71	C	C	C	C	C	C	C	C	C	C	C	C	C	C	C	C	C	C	C	C	C	C	C	C
106		C	C	C	C	C	C	C	C	C	C	C	C	C	C	C	C	C	C	C	C	C	C	C
206			C	C	C	C	C	C	C	C	C	C	C	C	C	C	C	C	C	C	C	C	C	\
237				C	C	C	C	C	C	C	C	C	C	C	C	C	C	C	C	C	C	C	C	\
290					C	C	C	C	C	C	C	C	C	C	C	C	C	C	C	C	C	C	C	\
326						C	C	C	C	C	C	C	C	C	C	C	C	C	C	C	C	C	C	\
331							C	C	C	C	C	C	C	C	C	C	C	C	C	C	C	C	C	\
316								C	C	C	C	C	C	C	C	C	C	C	C	C	C	C	C	\
336									C	C	C	C	C	C	C	C	C	C	C	C	C	C	C	\
122										C	C	C	C	C	C	C	C	C	C	C	C	C	C	\
321											F	C	F	C	C	C	C	C	C	C	C	C	C	\
197												C	F	C	C	C	C	C	C	C	C	C	C	\
133													C	C	C	C	C	C	C	C	C	C	C	\
66														C	C	C	C	C	C	C	C	C	C	\
135															C	C	C	C	C	C	C	C	C	\
327																C	C	C	C	C	C	C	C	\
303																	C	C	C	C	C	C	C	\
308																		C	C	C	C	C	C	\
181																			C	C	C	C	C	\
287																				C	C	C	C	\
22																					C	C	F	\
263																						C	C	\
244																							C	\
162																								\
1080																								

TABLE 3.1. COMPLEMENTATION TESTS OF THE PUPAL LETHALS. C=complements F=Failure to complement, indicating hits in the same gene.

FIGURE 3.3 MARCM CLONES FOR 2V71 AND 2V106. *2v71* shows undersized clones in the central brain and thoracic neuromeres (brackets) and oversized clones in the abdominal neuromeres at 96 hr (arrow). *2v106* shows oversized clones in the abdominal neuromeres (arrowhead).

studies to test whether the 2v71 gene is required intrinsically within the NB lineage or whether the CNS defects are a consequence of a deficit elsewhere in the larva, I conducted a MARCM clonal analysis. 2v71 shows a MARCM phenotype of undersized clones in the thoracic neuromeres and central brain, ectopic clones in the abdomen and normal-sized clones in the eye discs and optic lobes (Fig. 3.3), indicating that the gene lies on 3R and its requirement is intrinsic within the neuroblast lineage, at least within the central brain, thorax and abdomen.

2v106 (Class C)

2v106 was the only homozygote with an over-sized CNS (Fig.3.1.8). The phenotype is fully penetrant and comprises a longer ventral ganglion (Th and Ab) than wild type. The brain lobes, however, are oval-shaped but do not appear to be larger than normal. As with 2v71, the larvae themselves are slimmer and more transparent than wild type. Homozygous animals do not survive after L3 and as such are larval lethal. The fat body cells are round and present in strings rather than a flat epithelial sheet. To ascertain whether the 2v106 phenotype is autonomous to the NB lineage, I conducted a MARCM analysis (Fig 3.3). Ectopic 2v106 clones were observed in abdominal neuromeres, although the optic lobe, central brain and thoracic clones all

appear undersized. This indicates that the gene lies on 3R and has a neuroblast lineage-intrinsic phenotype of abdominal neuromere overgrowth.

2v206 (Class A)

2v206 has an undergrowth phenotype in the brain lobes and thoracic neuromeres. (Fig.3.1.4) The larvae are viable until late L3, very transparent, slimmer than wild type and the fat body is abnormal showing the same phenotype as 2v106 i.e. fat body cells are present in strings rather than organised in into an epithelial sheet.

2v237, 2v290 and 2v316 (Class B)

2v237, 2v290 and 2v316 (Fig. 3.1.5, 6 and 7) show similar CNS and larval phenotypes. The homozygous CNS is dramatically undersized throughout with rounded brain lobes, but the larval body is of normal size and appearance. 2v237 and 2v316 homozygotes die at late L3 and do not form pupae, while 2v290 homozygotes form a puparial case but no pupa develops.

3.3. The MARCM screen

To study the late effect of mutations which cause embryonic lethality, genetic mosaics have to be generated. I therefore used mosaic analysis with a repressible cell marker (MARCM), a technique that creates labelled homozygous mutant clones in an unlabelled heterozygous background (see Fig. 2.1, Fig. 2.2 & Section 2.2). To mark clones specifically in the developing CNS and eye disc, I used the pan neural *elav-Gal4* driver to express UAS reporter genes. *elav-GAL4* is expressed in neural progenitors, postmitotic neurons and photoreceptors (Bello et al., 2003). Used with the FRT82B recombination site, this allows screening of the right arm of chromosome III for genes required intrinsically within the neuroblast lineages. To assess whether mutant phenotypes are CNS specific, clones within the eye disc were used as an internal control. As a control for wild-type clone size in the CNS, clones were made with FRT82B on an otherwise wild-type chromosome III. Figure 3.4B

shows the wild-type pattern, observed after X-gal staining, with large blue clones present in the central brain, optic lobes and thoracic neuromeres. As abdominal clone size is small (~6 cells) and due to the perdurance of GAL80 after recombination, few or no clones are observed in the central abdomen. Occasionally small blue clones can be recovered at the tip of the abdomen where neuroblasts proliferate longer than other abdominal NBs. (Truman and Bate, 1988).

After screening 1,250 lines, I identified 70 with MARCM phenotypes falling into three categories (Fig. 3.4). Class I show a reduced clone size in the central brain and thoracic neuromeres such that many clones are barely detectable by X-gal staining (Fig. 3.4.C). Class II display clones in abdominal neuromeres indicating overgrowth compared to the small undetectable clones in the wild type in this region (Fig. 3.4.D and E). Clonal overgrowth in the central brain, optic lobes and thoracic neuromeres is more difficult to detect by X-gal staining and would require accurate counts of cell number using antibody staining. Class III have a phenotype of reduced clone size in thoracic neuromeres (Fig. 3.4.F). Class I is represented by 6 lines, Class II is represented by 52 lines and Class III is represented by 12 lines. Of the 52 Class II mutants, 30 show a strong clonal overgrowth phenotype whereas 22 mutants have a weaker and more variable overgrowth.

I selected four of the embryonic lethal mutants, 47, 72, 63 and 109 for mapping and further characterisation, as these had the strongest phenotypes. 109 shows a Class I phenotype (Fig. 3.4.C) whereas 47, 63 and 72 show Class II phenotypes (Fig. 3.4.D and E). Complementation tests between each of the four selected mutants and all other mutants in the same phenotypic class resulted in the discovery that 47 is allelic with a second mutation, 87. In addition, 109 is allelic to 264. These complementation tests define 5 complementation groups in Class I and 51 complementation groups in Class II with neuroblast lineage-autonomous effects on neural growth (Table 3.2).

3.4. Discussion

I successfully completed two genetic screens of 1,600 mutant EMS lines in which a total of 90 mutants with neural growth defects were identified. Each of the 90 mutant lines was re-tested to confirm all of these mutant phenotypes are reproducible. This

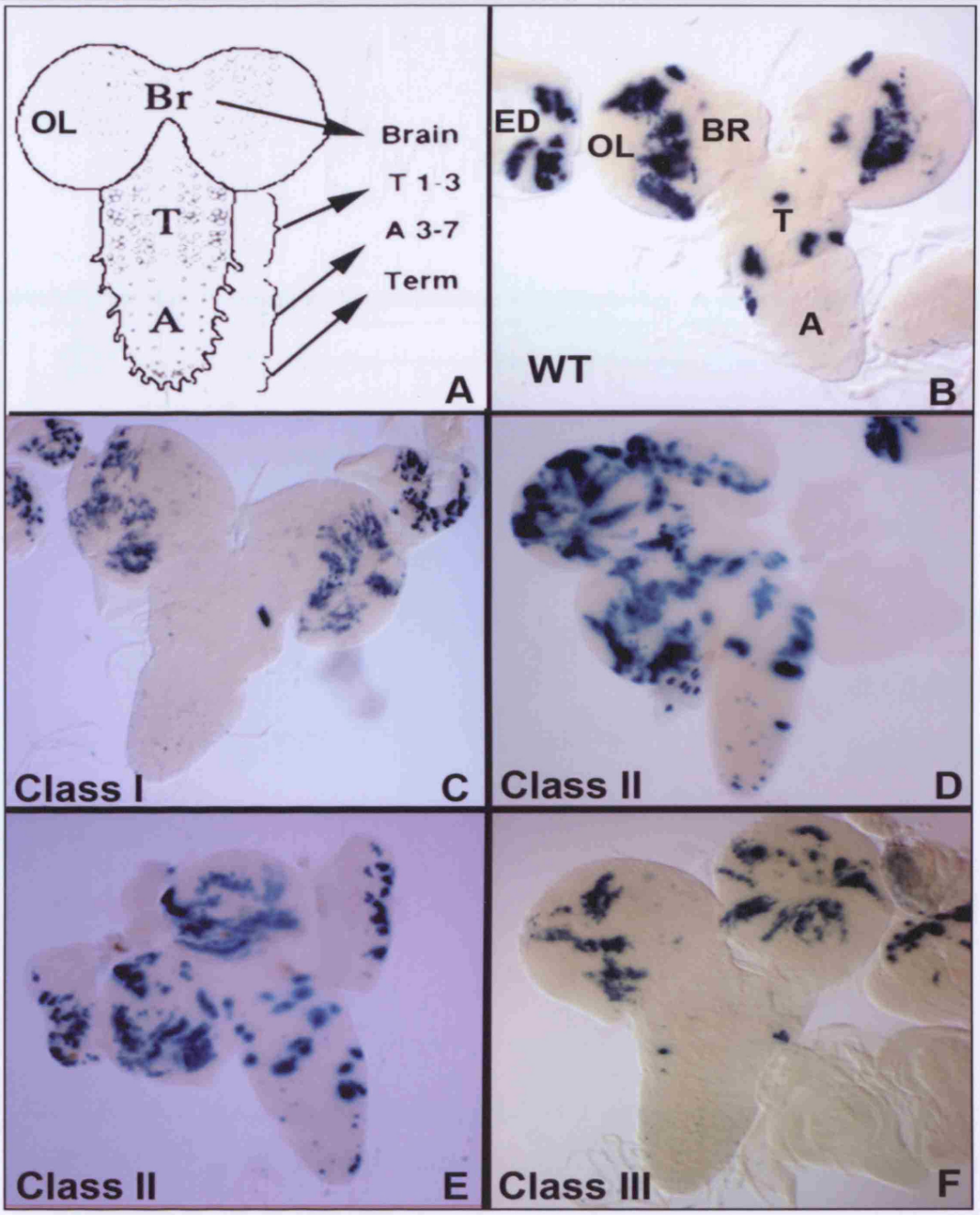

FIGURE 3.4. MARCM PHENOTYPES. **A)** Schematic of a larval brain OL= Optic Lobe, Br=Central Brain, T=Thorax, A=Abdomen, ED=Eye Disc (B). **B)** wild-type pattern of clones stained with X-gal. **C) Class I** phenotype shows reduced clone size in the brain lobes and thoracic neuromeres. **D** and **E) Class II** phenotype shows an increase in clone size in the abdomen. **F) Class III** phenotype shows a reduced clone size in thoracic neuromeres.

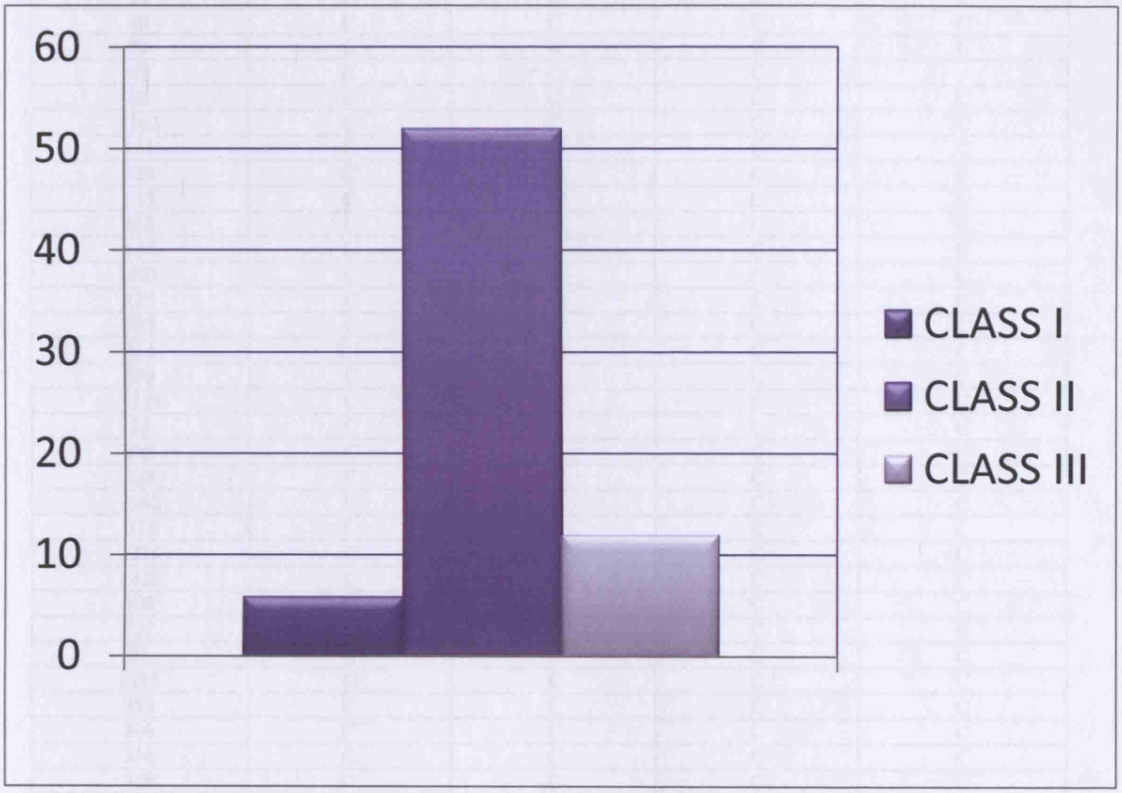

FIGURE 3.5 MARCM SCREEN. CLASS I phenotype of undersized clones in the central brain and thoracic neuromeres is represented by 6 lines. CLASS II, the most abundant phenotype of oversized clones in the abdominal neuromeres is represented by 52 lines. CLASS III phenotype of undersized clones in the thoracic neuromeres is represented by 12 lines.

TABLE 3.2. COMPLEMENTATION TEST FOR SELECTED MARCM MUTANTS

Mutant	109	47	72	63
47	C	-	C	C
109	-	C	C	C
72	C	C	-	C
87	C	F F	C	C
7	C	C	C	C
107	C	C	C	C
14	C	C	C	C
48	C	C	C	C
91	C	C	C	C
63	C	C	C	-
83	C	C	C	C
1162	C	C	C	C
121	C	C	C	C
929	C	C	C	C
123	C	C	C	C
883	C	C	C	C
130	C	C	C	C
1081	C	C	C	C
137	C	C	C	C
783	C	C	C	C
264	F F	C	C	C
396	C	C	C	C
1219	C	C	C	C
28	C	C	C	C
385	C	C	C	C
288	C	C	C	C
1202	C	C	C	C
373	C	C	C	C
1216	C	C	C	C
1038	C	C	C	C
198	C	C	C	C
737	C	C	C	C
91	C	C	C	C
1105	C	C	C	C
383	C	C	C	C
366	C	C	C	C
310	C	C	C	C
368	C	C	C	C
249	C	C	C	C
356	C	C	C	C
375	C	C	C	C
348	C	C	C	C
254	C	C	C	C
386	C	C	C	C
705	C	C	C	C
695	C	C	C	C
795	C	C	C	C
1036	C	C	C	C
341	C	C	C	C
304	C	C	C	C
345	C	C	C	C
315	C	C	C	C
394	C	C	C	C
287	C	C	C	C
282	C	C	C	C
369	C	C	C	C
743	C	C	C	C
186	C	C	C	C

C = complementation, FF = a confirmed second hit in the same gene.

represents 5.6% of the total, roughly twice that found in the 3L screen carried out in the Gould lab (C. Maurange, L. Cheng, J. Pendred and A. Gould, unpublished), in which 90 mutants with altered clone size were recovered from 3000 EMS lines. The difference is probably due to a higher effectiveness of lethal EMS hits in the 3R mutagenesis. In fact, the average number of lethal hits per chromosome arm was 1.5 for 3L versus 2.5 for 3R. As the vast majority of neural growth phenotypes map to complementation groups with only one member, it is clear that neither the 3L nor 3R mutagenesis were anywhere close to saturation.

The most abundant phenotype recovered from the pupal-lethal screen was undergrowth of the CNS with only one oversized CNS identified. This contrasts with the MARCM screen where the most abundant phenotype was oversized clones in the abdominal neuromeres. This suggests that many mutations which produce overgrowth in the CNS are embryonic lethal and can only be revealed by generating mosaic organisms. In addition, there may be fewer of these genes in the genome. Furthermore, the MARCM technique is biased towards this phenotype as it is simple to detect the presence of blue clones in the abdominal neuromeres compared to the few or no clones in the wild type. On the plus side, this indicates that MARCM is likely to be very efficient for dissecting the AbdA-dependent neuroblast apoptosis programme. Although X-gal staining provides a rapid assay for clone size, accurate cell counts within clones require higher-resolution labelling using antibodies to β-gal or GFP reporters. It is important to point out that the primary screens using both MARCM and pupal-lethal screens do not distinguish whether altered CNS or clonal growth is due to altered cell proliferation, cell size or cell death. To distinguish between these possibilities would require secondary screening, for example using BrdU incorporation to measure proliferation and α-activated caspase staining to detect dying cells.

Interestingly, the pupal-lethal screen showed that in some cases normal sized larvae can have small sized brains and tiny L3 larvae can have wild-type brains, suggesting that diploid cells and polyploid cells have different growth requirements.

To represent all growth phenotypic classes, I selected 10 mutants with interesting and strong phenotypes for mapping and further characterisation. Six are pupal lethals, five of which have a smaller than normal CNS, either region specific or the

whole CNS, while one has an oversized CNS. The four remaining mutants are embryonic lethals, two of which have a second allele. Three have oversized abdominal clones while one has undersized clones in both the optic lobes and thoracic neuromeres.

Chapter 4

Mapping and Characterisation of Selected Mutants

4.1. Introduction

This chapter discusses the mapping and characterisation of 10 selected mutants, six from the pupal-lethal screen and four from the MARCM screen (See chapter 3). To rough map each selected mutant, complementation tests were set up with a custom-made kit of 91 deletions assembled using the classical, Drosdel and Exelixis deficiencies. The classical deficiency kit available from the Bloomington Stock Center provides maximum coverage with a minimum number of stocks and covers a predicted 94.5% of the right arm of chromosome III (See appendix chapter 2, Table 2.1). However, due to the breakpoints of these classical deficiencies being determined at the cytological level, there are normally grey areas on the molecular genome map either side of the deficiency *i.e.* there is uncertainty about how many genes are deleted. In contrast, the Exelixis and Drosdel deficiencies are molecularly defined to exact DNA coordinates and thus were used, where possible, to bridge the grey areas. Failure to complement a deficiency uncovers the candidate region in which the gene of interest is located (see sections 2.4.1 and 2.4.2). Once this candidate region has been identified, it can then be narrowed down by further complementation testing with every available deficiency in the region. Finally, all known lethal mutations previously mapped to the candidate region are also crossed with the mutation in question to establish whether a known gene is affected.

4.2.Failure to map *2v237, 2v316 and 72*

2v237 homozygotes have a Class B phenotype of reduced brain lobes and thoracic neuromeres although the larval body is of normal size and morphology (see Fig. 3.1.5). This mutation complemented all of the 91 deficiencies covering 3R. However, as the mutation was recovered as a pupal lethal not a 3R MARCM phenotype, the relevant gene may well lie on 3L. As this study was focused on genes on 3R, no further characterisation of *2v237* was carried out.

2v316 homozygous larvae have a Class B phenotype of an undersized CNS, with reductions in all regions including the optic lobes, thoracic and abdominal neuromeres (see Fig. 3.1.4). This is specific to the CNS as L3 larvae are of normal size and external morphology. The *2v316* mutation failed to complement the

Df(3R)Exel6204 deficiency which is molecularly defined with predicted cytological breakpoints of 96F9-97A6. Fine mapping revealed a failure to complement *Df(3R)Espl22* which narrowed this cytological location to 96F10;96F11. However, L3 larvae of the genotype *2v316/Df(3R)Espl22* show normal CNS morphology suggesting that the 96F10;96F11 lethal is not the primary cause of the CNS phenotype. As *Df(3R)Espl22* is the only 3R deficiency that I found to fail to complement *2v316*, the lethal hit associated with the undersized CNS phenotype may map to 3L. *2v316* was therefore not characterised further.

The embryonic lethal *72* has a Class II phenotype in FRT82B clones and is therefore located on 3R and autonomously required within the neuroblast lineage, at least for abdominal clone size (see Fig. 3.4.D). However, crossing *72* with each of the 91 deficiencies on 3R resulted in no cases of failure to complement. One possible reason for this is incomplete coverage by the deficiency kit (Section 4.1). Another possible reason is that the clonal phenotype is synthetic, resulting from the combined effects of multiple viable mutations on 3R.

4.3.Pupal lethal *2v290* is an allele of *E(spl)m8*

The pupal lethal *2v290* has a Class B phenotype of a reduced-size CNS and normal larvae. When rough mapped with the 91 deficiencies for 3R, it failed to complement with *Df(3R)Espl3* whose breakpoints are 96F1;97B1. The *2v290/Df(3R)Espl3* CNS, when dissected at 96hr, was found to have the same CNS phenotype as *2v290* homozygotes, indicating that the relevant mutation lies in 96F1;97B1. Fine mapping resulted in failure to complement with *Df(3R)Exel6204* (96F9;97A6) and *Df(3R)Espl22* (96F10;96F11) and complementation with *Df(3R)ED6232* (96F10;97D2). This leaves a candidate interval containing 5 genes of the Enhancer of split complex: *HLHm5*, *m6*, *HLHm7*, *E(spl)m8* and *groucho*. Lethal mutations were available for two of these genes, $E(spl)m8^{rv1}$ and *groucho*. *2v290* failed to complement with $E(spl)m8^{rv1}$ (Fig. 4.1). *E(spl)m8* encodes a HLH transcription factor that is a tumour suppressor and a target of Notch (Bray, 1997).

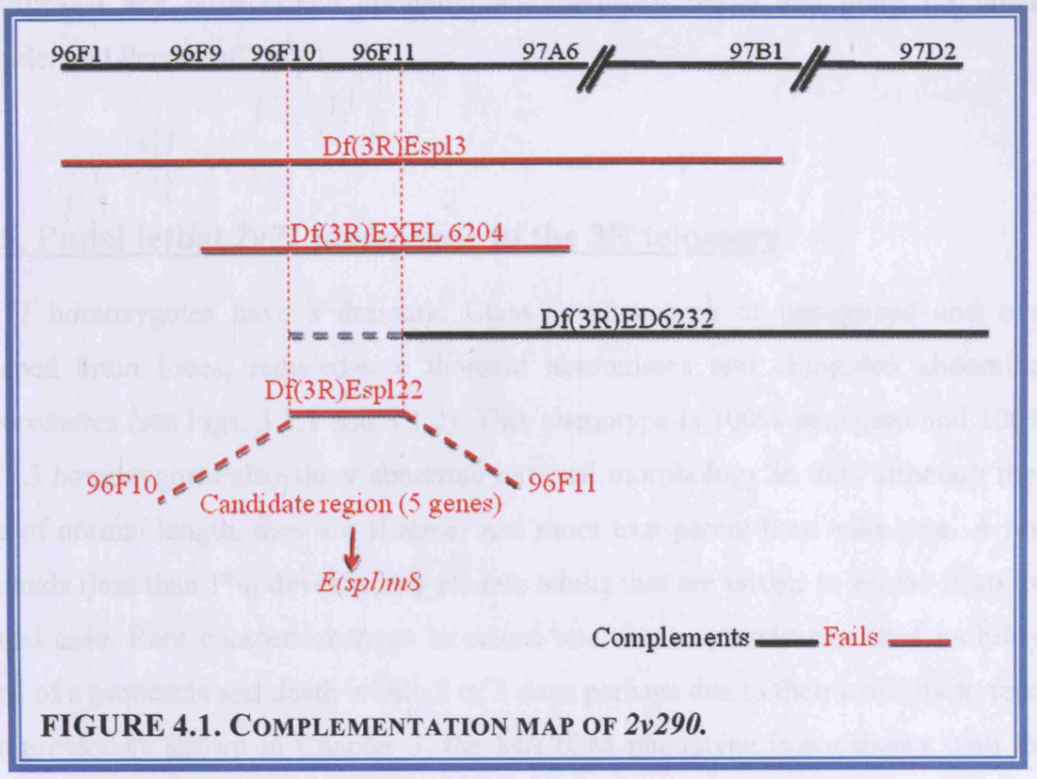

FIGURE 4.1. COMPLEMENTATION MAP OF *2v290*.

4.4. *2v206* is a mutation in *scribble*

2v206 has a Class A phenotype similar to that of *2v71,* showing reduced brain lobes and thorax (Fig. 3.1.3). L3 homozygous larvae are slimmer than wild type and more transparent. Transparency is likely due to abnormal fat body morphology. Indeed fat body cells appear rounded and fail to form an epithelial sheet. Homozygous pupae are not found, indicating that the lethal-phase occurs during late larval development. *2v206* failed to complement the 3R deficiency *Df(3R)ED6235* whose cytological breakpoints are 97B9;97D12. To facilitate mapping of the EMS mutations, we exchanged lists of selected mutant lines with William Chia's group, who had screened the same EMS mutant collection for Mira mislocalisation phenotypes (Slack et al., 2006). They found that the lethal mutation on the *2v206* chromosome maps to 97B9;97C1 which contains *scribble*. To confirm that *2v206* corresponds to *scribble*, I crossed it to *scribble[j7B3]* which resulted in failure to complement. *scribble* is a well characterised and documented gene encoding a tumour suppressor and cell-polarity protein. Reported loss-of-function *scribble* mutations show

overgrown and unstructured epithelial and neuronal tissue and giant L3 larvae (Bilder and Perrimon, 2000).

4.5. Pupal lethal *2v71* maps close to the 3R telomere

2v71 homozygotes have a dramatic Class A phenotype of undersized and oval shaped brain lobes, reduced-size thoracic neuromeres and elongated abdominal neuromeres (see Figs. 3.1.1 and 3.1.2). This phenotype is 100% penetrant and 100% of L3 homozygotes also show abnormal external morphology in that, although they are of normal length, they are slimmer and more transparent than wild-type. A few animals (less than 1%) develop into pharate adults that are unable to eclose from the pupal case. Rare escapers manage to eclose and show severely impaired mobility, lack of a proboscis and death within 2 or 3 days perhaps due to their inability to feed. As previously shown in Chapter 3, the MARCM phenotype is consistent with the pupal-lethal phenotype as ectopic clones are observed in the abdomen and clones in the central brain and thoracic neuromeres are greatly reduced in size (see Fig. 3.2).

To examine whether the distribution or mitoses of neuroblasts were affected in *2v71* mutants, I used Miranda (Mira) to label neuroblasts and phospho Histone 3 (pH3) to mark cells in M-phase. *2v71* homozygotes have fewer-than-normal Mira-positive neuroblasts in both the brain lobes and thorax and correspondingly less pH3-positive cells in both regions at L3 (Fig. 4.2.A-F). Abdominal neuromeres, in marked contrast, contain ectopic Mira-positive neuroblasts and pH3 positive cells (Fig. 4.2.A-F). This analysis indicates that neuroblasts are reduced in number in the brain and thorax. In the abdomen, however, some escape the normal process of apoptosis at 72 hrs and continue to divide for at least an additional 24 hr. This would suggest that *2v71* genetically interacts in some way with AbdA, Grh or H99 proapoptotic genes during this process (See Chapter 1).

To examine further alteration in cell proliferation in *2v71* mutants, larvae were continuously fed with BrdU from 0-96 hr (Fig. 4.3). In comparison to the wild-type CNS, *2v71* shows ectopic neural BrdU incorporation in the abdomen (Fig. 4.3.A and D) which is consistent with the Mira and pH3 labellings. There also appears to be less BrdU incorporation in the thorax and brain lobe regions than in the wild type,

consistent with the reduced clone size observed in these regions of MARCM clones. Together, these results suggest that the observed size reduction in brain lobes and thoracic neuromeres and the expanded abdominal neuromeres of the *2v71* homozygotes can both be accounted for by lineage-autonomous effects on neuroblast number and mitotic activity.

To map *2v71*, complementation tests were set up with all of the 3R deficiencies. Only *Df(3R)B81* with cytological breakpoints 99D3:3Rt failed to complement the *2v71* lethality. *2v71/Df(3R)B81* hemizygotes die as pharate adults unable to eclose from the pupal case with no escapers. When dissected from the pupal case, these hemizygous animals were found to lack a proboscis similar to that of the homozygotes. In addition, 100% of hemizygotes displayed malformed legs with varying degrees of severity ranging from axis duplication to truncations (Fig. 4.4.A, B and C). This, together with the previous observations of altered external morphology in *2v71* homozygotes, demonstrates that *2v71* is not a CNS-specific mutation but rather it likely affects many larval and imaginal tissues.

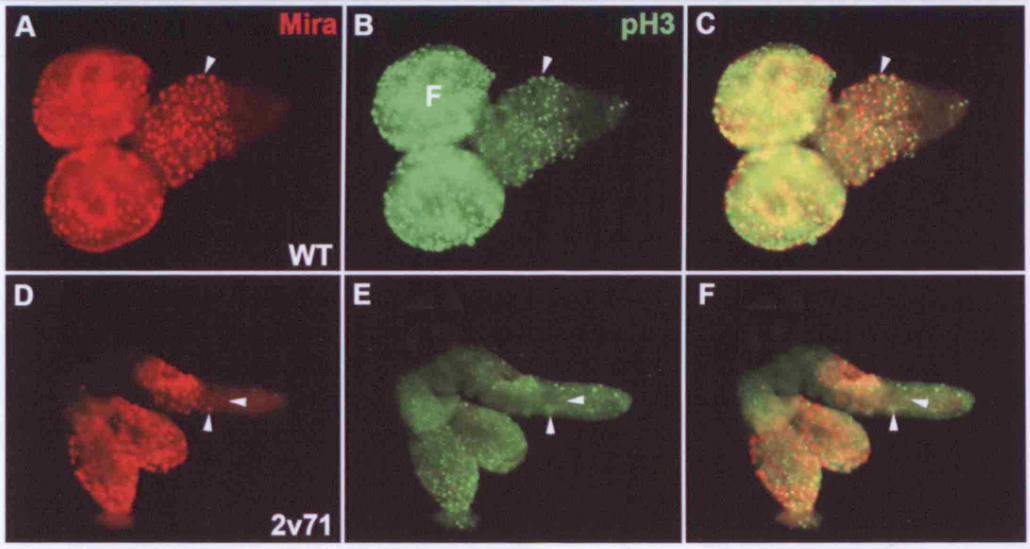

FIGURE 4.2. 2V71 HOMOZYGOTES SHOW REGION-SPECIFIC ALTERATIONS IN NEUROBLAST NUMBER. **A-C** show wild-type Mira/pH3 staining at 96 hr. **D-F** Mira/pH3 expression at 96 hr in *2v71* homozygotes reveals fewer than normal Mira-positive neuroblasts in the brain lobes and thoracic neuromeres and correspondingly less pH3-positive cells in both regions whereas the abdominal neuromeres contain ectopic Mira-positive neuroblasts that are pH3-positive and therefore are in M-phase (arrowheads).

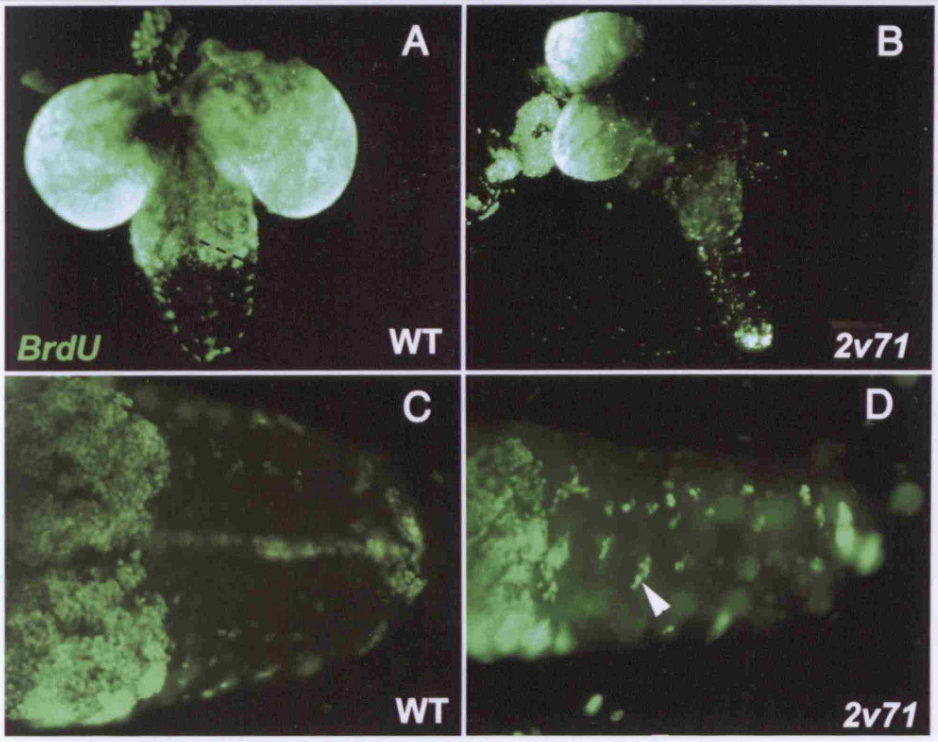

FIGURE.4.3. 2V71 HOMOZYGOTES SHOW REGION-SPECIFIC CHANGES IN NEUROBLAST PROLIFERATION. **(A** and **C)** show wild type BrdU incorporation. **(B** and **D)** ***2v71*** shows ectopic neural BrdU incorporation in the abdomen (arrowhead) whereas the thorax shows less BrdU incorporation.

FIGURE 4.4. 2V71/DF(3R)B81 LEG PHENOTYPES. **(A)** wild-type leg. Dotted line denotes junction between tibia and 1st tarsal segment. **(B)** ***2v71/Df(3R)B81*** shows axis-duplication phenotype of the tarsal segments. **(C)** ***2v71/Df(3R)B81*** shows leg-truncation phenotype of the tarsal segment.

2v71 was fine mapped by crossing it with an additional 23 deficiencies and 25 point mutations available in the candidate region of 99D3;3Rt (Chapter 2, Appendix, Table 2.2). *2v71* complemented all the deficiencies covering the region between 99A7 and 100F5. Unfortunately, no deficiencies covering the most distal candidate region from 100F5 to 3Rt were available. Together, the mapping results strongly suggest that the 2v71 mutation lies close to the 3R telomere. Intriguingly, Flybase does not report any protein-coding genes lying between 100F5 and the 3R telomere. This does not necessarily mean that there are none, as the heterochromatin in this region has not yet been well studied. In addition, genome annotation can miss small genes e.g. microRNAs. Although *2v71* has a very interesting and dramatic phenotype, the inability to map the gene responsible precluded further genetic study.

4.6. Embryonic lethal *63*

The embryonic lethal *63* has a Class II MARCM phenotype of large clones in the abdomen similar to *47/87* (Fig.3.4D). Crossing with all 91 deficiencies on 3R revealed a failure to complement *Df(3R)Exel6144* (83A6;83B6) and complementation with *Df(3R)ED5177* (83B4;83B7) giving a candidate region spanning 83A6;83B4, consisting of 16 genes. Further crossing to 7 available lethal mutations in this region, indicated complementation with *Nmdar1* (83A6;83A7),

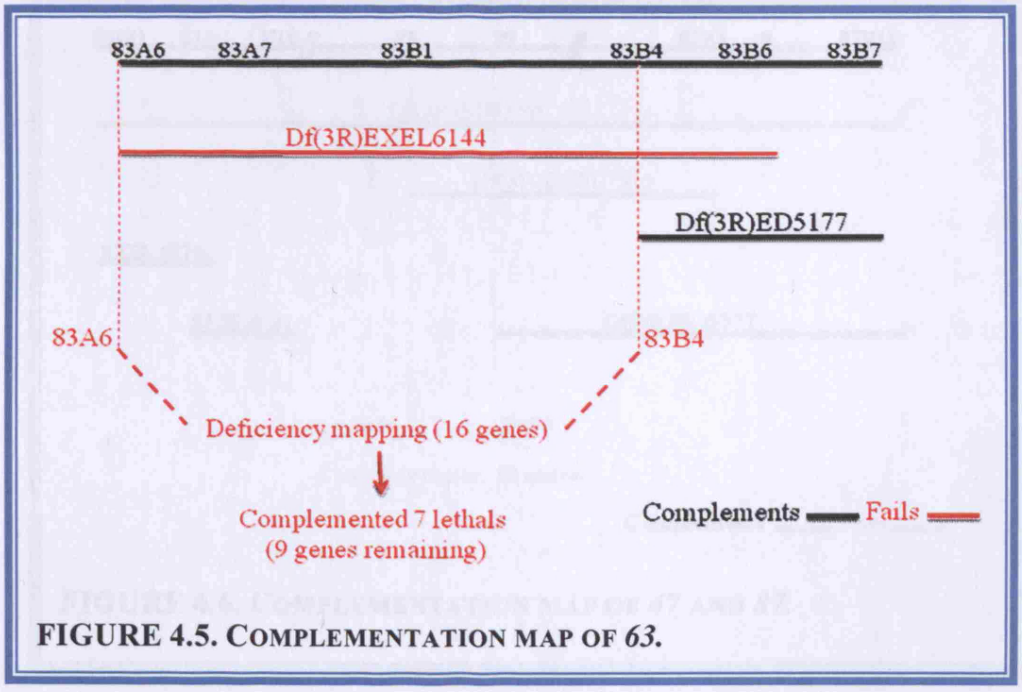

FIGURE 4.5. COMPLEMENTATION MAP OF *63*.

Itp-r (83A), noi (83A7;83B), *Rheb* (83B2), *noi/vha* (83B4), *Snm* (83B1;83B2) and *mia* (83B1). This suggests that *63* corresponds to one of the remaining 9 genes; *CG2519*, *Pcmt*, *Pi4KIIalpha*, *CG14671*, *CG12746*, *CG2931*, *CRMP*, *CG2926*, and *rev7*.

4.7.Embryonic lethal alleles *47* and *87*

The embryonic-lethal alleles *47* and *87* fail to complement each other and both give a Class II MARCM phenotype *i.e.* overgrowth of abdominal CNS clones (see Fig. 3.4E). Both mutations were crossed with the 91 deficiencies on 3R. *47* had two lethal hits, *Df(3R)Exel6174* (88F1;88F7) and *Df(3R)Exel7310* (86F6;87A1), however allele *87* only failed with *Df(3R)Exel7310*. This indicates that *Df(3R)Exel7310* contains the mutation responsible for the MARCM overgrowth phenotype. Both *47* and *87* alleles were then crossed with 9 available lethal stocks in the candidate region (Chapter 2, Table 2.2). Both failed with *Df(3R)ED5559* (86E11;87B11) but complemented *Df(3R)Exel5184* (86E17;86F6) and *Df(3R)ED5577* (86F9;87B13), *Df(3R)Exel6276* (86E11:86E14) and *Df(3R)Exel6161* (E14;E18). This narrowed down the candidate region to 86F6;86F9 (Fig.4.6). This region contains 8 genes: *CG17360*, *CG14723*, *CG6939*, *CG31116*, *CG14727*, *CG14724*, *CG6950* and *CG6959*. Although no lethal mutations are available for any

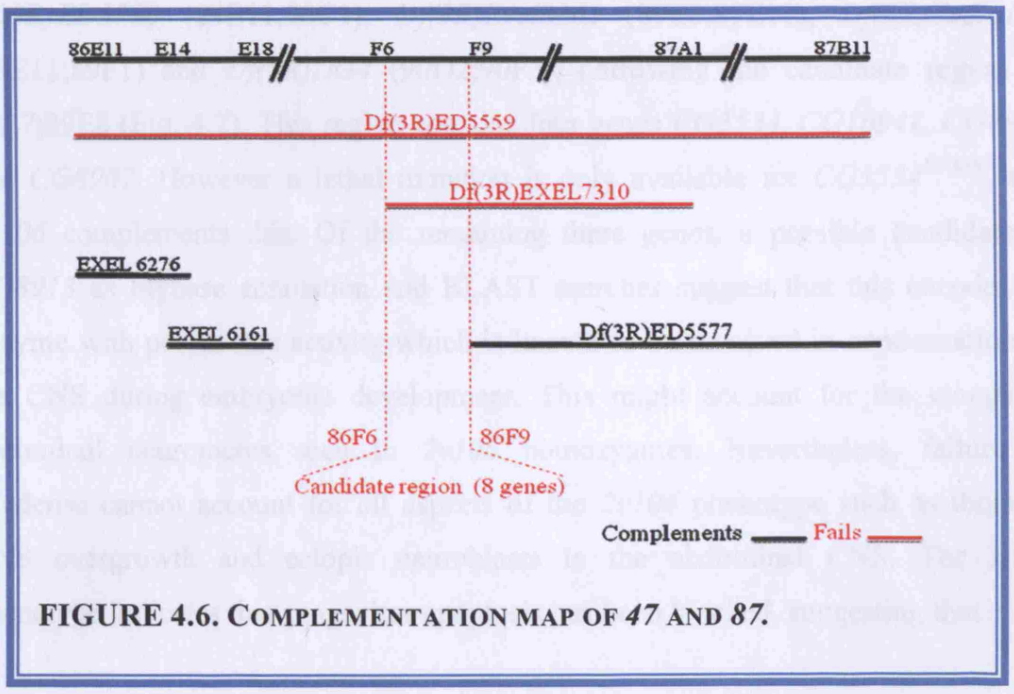

FIGURE 4.6. COMPLEMENTATION MAP OF *47* AND *87*.

of these, *CG6939* is a possible candidate as it encodes Sbf, a transcription factor with a yeast orthologue known to be involved in cell proliferation and growth. Yeast Sbf regulates the cell cycle at the G1 to S phase transition and is a target of the MAP kinase cascade which is required for the maintenance of cell integrity during asymmetric cell growth. (Madden et al., 1997).

4.8. *2v106* corresponds to CG16941, CG8913 or CG8907

The homozygous Class C phenotype of *2v106* differs dramatically from wild type and is the only one recovered from the pupal-lethal screen that possesses an oversized CNS (see Fig. 3.1.A and E). It has a 100% penetrant phenotype with a longer-than-normal ventral ganglion (thoracic and abdominal neuromeres) and larger-than-normal oval-shaped brain lobes. Homozygous *2v106* larvae are comparable in length to wild type at L3 (96hr) but are slimmer and more transparent. MARCM analysis revealed that the *2v106* has a lineage-autonomous overgrowth phenotype in abdominal neuromeres (see Fig. 3.3C). Initial mapping with the 3R deficiency kit indicated that *2v106* fails to complement *Df(3R)DG2* with cytological breakpoints 89E1;90F1. I then fine mapped the mutation by crossing *2v106* to 25 additional, available deficiencies in this region, but it complemented all of them (See Chapter 2, Table.2.2). In particular, *2v106* complemented *Df(3R)P115* (89B7;89E7), *Df(3R)ED5780* (89E11;90C1), *Df(3R)Exel8165* (89E8;89E11), *Df(3R)Exel6176* (89E11;89F1) and *Df(3R)DG4* (90D2;90F3), narrowing the candidate region to 89E7;89E8 (Fig. 4.7). This region contains four genes *CG3534, CG16941, CG8913* and *CG8907*. However a lethal mutation is only available for $CG3534^{EP3669}$ and *2v106* complements this. Of the remaining three genes, a possible candidate is *CG8913* as Flybase annotation and BLAST searches suggest that this encodes an enzyme with peroxidase activity which is known to be involved in condensation of the CNS during embryonic development. This might account for the elongated abdominal neuromeres seen in *2v106* homozygotes. Nevertheless, failure to condense cannot account for all aspects of the *2v106* phenotype such as thoracic CNS overgrowth and ectopic neuroblasts in the abdominal CNS. The latter phenotype indicates that progenitor apoptosis has been blocked, suggesting that

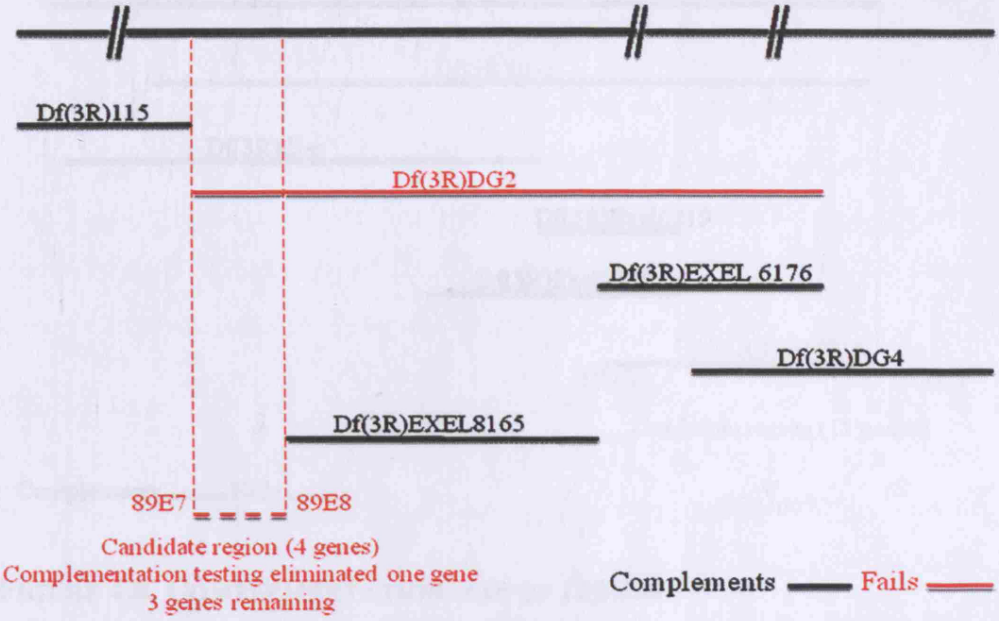

FIGURE 4.7. COMPLEMENTATION MAP OF *2v106*.

2v106 blocks the AbdA/Grh/H99 proapoptotic pathway at some level during this process (See Chapter 1). I conclude that either the *CG8913* peroxidase enzyme has a previously uncharacterised role in proliferation or that *2v106* maps to *CG16941* or *CG8907*.

4.9. Embryonic lethals *109* and *264* are alleles of *CG31005*.

The embryonic-lethal alleles *109* and *264* fail to complement each other and have a Class I MARCM phenotype *i.e.* undergrowth of the brain lobes, central brain and thoracic neuromeres. MARCM clones also show undergrowth in eye discs, indicating that the phenotype is not CNS specific (see Fig. 3.4C). *109* failed to complement two non-overlapping deficiencies from the 3R core kit, namely *Df(3R)tll-e* (100A2;100C1) and *Df(3R)Exel6206* (97E1;97E5), indicating there are two lethal hits on 3R. *264,* however, failed to complement *Df(3R)tll-e* alone, indicating that the mutation responsible for the CNS phenotype lies within 100A2;100C1. Finer mapping resulted in a failure to complement with *Df(3R)Exel6218* (100B5;100C1) and complementation with *Df(3R)Exel7379*

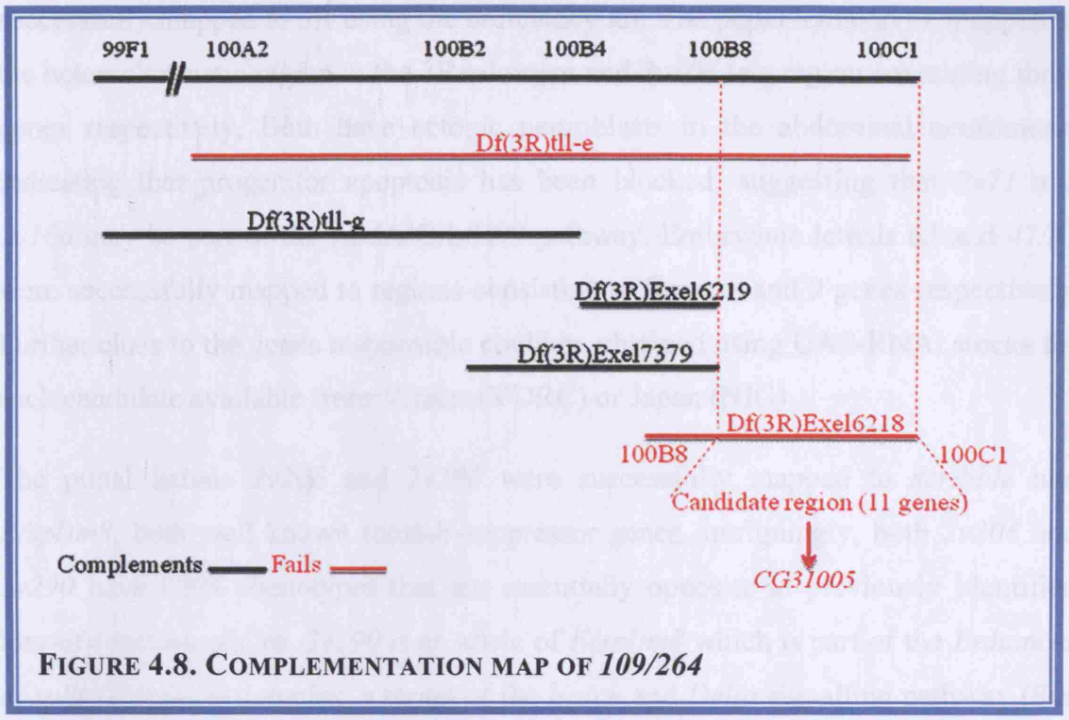

FIGURE 4.8. COMPLEMENTATION MAP OF *109/264*

(100B2;100B8), *Df(3R)Exel6219* (100B4;100B8) and *Df(3R)tll-g* (99F1;100B5) indicating that the *109/264* gene lies within the region 100B8;100C1, encompassing 11 genes. Lethal mutations for 2 genes in this region were available and $CG31005^{EP594}$ failed to complement both *109* and *264* (Fig. 4.8). *CG31005* is an uncharacterised gene that according to Flybase electronic annotation and BLAST searches, encodes a trans-hexaprenyl transferase. This gene will be the focus of Chapter 5.

4.3. Discussion

Of the ten selected mutations, three failed to map to 3R. The pupal lethal *2v237* complemented all of the 3R deficiency kit indicating that it most probably lies on 3L. The pupal lethal *2v316* failed to complement one of the 3R deficiencies, but this did not uncover the relevant CNS phenotype, again suggesting that the gene in question lies on 3L. The embryonic lethal *72* complemented all the 3R deficiencies but as this has an FRT82B MARCM phenotype, the relevant gene must lie on 3R, either in areas not covered by the 3R deficiency kit or, alternatively, that multiple non-lethal genes are responsible for the phenotype. Seven out of ten mutations were

successfully mapped to 3R using the deficiency kit. The pupal lethal *2v71* mapped to the heterochromatic region at the 3R telomere and *2v106* to a region containing three genes respectively. Both have ectopic neuroblasts in the abdominal neuromeres indicating that progenitor apoptosis has been blocked, suggesting that *2v71* and *2v106* may be part of the AbdA/Grh/H99 pathway. Embryonic lethals *63* and *47/87* were successfully mapped to regions consisting of 8 genes and 9 genes respectively. Further clues to the genes responsible could be obtained using UAS-RNAi stocks for each candidate available from Vienna (VDRC) or Japan (NIG).

The pupal lethals *2v206* and *2v290* were successfully mapped to *scribble* and *E(spl)m8*, both well known tumour-suppressor genes. Intriguingly, both *2v206* and *2v290* have CNS phenotypes that are essentially opposite to previously identified loss-of-function alleles. *2v290* is an allele of *E(spl)m8* which is part of the *Enhancer of split [E(spl-C)]* complex, a target of the *Notch* and *Delta* signalling pathway (See Chapter 1). These are well characterised neurogenic genes required for lateral inhibition leading to the segregation of neural progenitor cells (neuroblasts) from the proneural clusters in the neuroectoderm during embryonic neurogenesis (see Chapter 1). As there is some redundancy between the helix-loop-helix genes of the *[E(spl-C)]*, *groucho* is the only one of these genes which when mutated shows an overproliferation phenotype of variable penetrance, resulting in some epidermal cells adopting the neuroblast fate (Knust et al., 1992; Schrons et al., 1992). When the whole complex is deleted the phenotype shows a much more severe neural hyperplasia. The extent of neural hyperplasia depends on the number of genes deleted in the complex, the more genes that are deleted the more severe is the phenotype (Bray, 1997; Ziemer et al., 1988). A reported homozygous deficiency for *m7* and *m8* makes it to adulthood with neural hyperplasia whereas *2v290* homozygotes only survive to L3 with a much reduced CNS. Other studies also show neural hyperplasia on *E(spl)* loss-of-function mutations (Buescher et al., 2002; Corbin et al., 1991; Knust et al., 1992; Schrons et al., 1992; Ziemer et al., 1988).

2v206 is an allele of *scribble* with homozygous L3 larvae being slimmer, more transparent than normal, with a reduced-size CNS and abnormal fat body. In contrast to this, reported loss-of-function alleles of *scribble* induce neural overgrowth(Bray, 1997). *scribble* mutations are also reported to have unstructured imaginal discs with brain cells of homozygous L3 larvae losing apical-basal polarity, becoming rounded,

lose adhesion and are able to migrate forming metastatic tumours (Bilder and Perrimon, 2000). L3 larvae do not pupariate and can grow for a further two weeks longer than normal, becoming giant bloated larvae before dying (Humbert, 2003; Wu et al., 2001). Scribble forms a complex at the septate junction with Discs large (Dlg) and Lethal Giant larvae (Lgl) and the Scrib/Lgl/Dlg complex is reported to regulate cortical polarity, cell size and mitotic-spindle asymmetry. During prophase/metaphase this complex localises to the apical cortical region, then localises uniformly to the cortex. Mutants have defects in basal protein targeting, a smaller cortical domain and reduced spindle size, resulting in undersized neuroblasts and larger-than-normal GMCs (Albertson and Doe, 2003). In mutant larvae, neuroblasts and GMCs over proliferate to form neoplastic (overgrown and unstructured) tissue. These proteins are also thought to regulate negatively Cyclin E, which controls the G1/S cell-cycle transition. In *scribble* mutants, the cell cycle slows down but cells do not exit the cell cycle and continue to proliferate resulting in overgrown tissue (Bilder and Perrimon, 2000; Humbert, 2003). Interestingly, there is one report that *scribble* affects the organization of the fat body with cells losing their structure and rounding up, due to loss of cell polarity (Wu et al., 2001). This is highly reminiscent of the effect of *2v206* on the fat body. Although *scribble* has been well characterised and documented, the *2v206* allele is highly atypical and therefore very interesting to study. One possibility is that this allele may display a tissue-specific phenotype in tissues such as the fat body, which may indirectly lead to a non-cell autonomous phenotype of under-proliferation in the CNS, due to the possible loss of fat-body mitogens (Britton and Edgar, 1998). This hypothesis might be supported if MARCM clones in the CNS had no undersized phenotype.

Finally, the embryonic-lethal alleles *109/264* were successfully mapped to a previously uncharacterised gene, *CG31005.* In the next chapter I concentrate on this gene as it fulfils the initial aim of the screens, which was to discover novel genes required for neural growth. Together, these results show that a combination of cytologically and molecularly-defined deficiencies provide an efficient tool kit for mapping mutations. However, there are limitations in that it is not always possible to map the mutation to a single gene, largely due to the unavailability of lethal alleles for all candidate genes.

Chapter 5

Characterisation of the qless gene

5.1. Introduction

The embryonic lethal alleles *109* and *264,* show an undergrowth MARCM phenotype in the brain lobes, thoracic region and eye discs. They map to a single uncharacterised gene *CG31005,* which I have named *qless*. Flybase electronic annotation indicates that *CG31005* encodes a *trans*-prenyl transferase, a lipid enzyme catalysing the addition of isoprenoid subunits.

Prenyl transferases are referred to as polyprenyl-diphosphate synthases and are crucial to the biosynthesis of more than 23,000 natural isoprenoid products, which have different structures and consist of various numbers of five-carbon isoprenyl pyrophosphate (IPP) units (Liang et al., 2002; Ohnuma et al., 1998). There are three types of prenyl transferases: Protein prenyltransferases catalyze the addition of an isoprenyl pyrophosphate (isoprenoid) 5C unit to a protein or a peptide such as Ras or Rab to activate signal transduction; Prenyltransferases generate cyclic isoprenoids found in cholesterol and steroid hormones; Isoprenyl pyrophosphate synthases (*cis* or *trans*-prenyl transferases) catalyse chain elongation with substrates that are not protein or cholesterol derivatives. Instead allylic pyrophosphate substrates undergo consecutive condensation reactions with isoprenyl pyrophosphate (IPP) to produce linear polymers (Fig. 5.1). The *cis*-type produce long isoprenoid chains of more than 50 carbons (*i.e.* more than 10 isoprenoid units) such as rubber which consists of thousands of units. *Trans*-prenyl transferases are responsible for the biosynthesis of shorter linear isoprenoid chains of between 6 and 10 units that are synthesized from farnesyl pyrophosphate (C_{15} FPP) and IPP (Liang et al., 2002) (Fig.5.1). The all-*trans* isoprenoid side chains extend linearly within the cell membranes, although long side chains may form folded structures (Guo et al., 2004).

Most research on the structure of *trans*-prenyl transferases has been carried out in bacteria, yeast and plants (*Arabidopsis*) although there is some characterisation of the rat solanesyl diphosphate synthase. (Saiki et al., 2005). These enzymes possess seven conserved domains including two aspartate rich DDxxD motifs which act as the catalytic sites, the first is the FPP binding site and the second is the IPP binding site. Site-directed mutagenesis in yeast has shown that all of the aspartic residues

FIGURE 5.1. SYNTHESIS OF LINEAR ISOPRENOID CHAINS BY CIS AND TRANS PRENYL TRANSFERASES. GPP (geranyl diphosphate), FPP (farnesyl diphosphate) GPPS (geranylgeranyl diphosphate synthase) HexPPs (hexaprenyl diphospate synthase [C_{30}]), HepPPS (C_{35}), OPPS (C_{40}), SPPS (C_{45}) and DPPS (decaprenyl) which produces a side chain length of (C_{50}) (adapted from (Liang et al., 2002).

except the last in the second more carboxyl terminal domain are required for catalytic activity. Removal of any of these abolishes catalytic activity completely. Other crucial residues are the small amino acids alanine and serine that regulate side-chain length and are located in the 4th and 5th position upstream from the first DDxxD domain (Song and Poulter. C, 1994). In the avian FPPS mutants A116W and N114W, a side-chain length of 20 carbons instead of 30 carbons is generated. (Fernandez et al., 2000; Guo et al., 2004; Koyama et al., 1995; Koyama et al., 1994; Liang et al., 2002). The corresponding positions in the *Bacillus stearothermophilis* FPPS enzyme are naturally large residues, namely tyrosine and leucine. In this context, if the tyrosine residue is replaced by a smaller glycine residue, the side-chain length is increased from C_{25} to C_{30}. These results show that catalytic activity and side-chain length are highly regulated by key amino acid residues upstream and

within the active site which are critical to their structure and function (Ohnuma et al., 1998).

5.2. Results

qless has a Class I MARCM phenotype of smaller-than-normal clones in the thorax, brain lobes and eye discs (See Fig. 3.4. B, C).This could be due to defective cell proliferation or increased cell death. To identify which *trans*-prenyl transferase *CG31005* is most closely related to, I performed a BLAST search against the protein database. This revealed that *CG31005* matches human *PDSS1* (prenyl diphosphate synthase sub-unit 1) with an e-value of 1e-106 which indicates that the probability of this being a random match is only 10^{-106}. This sub-family of *trans*-prenyl transferases are all involved in ubiquinone (Coenzyme Q) synthesis.

5.2.1. Biosynthesis and function of Coenzyme Q

Coenzyme Q (CoQ) also known as ubiquinone, is found naturally in all cells and

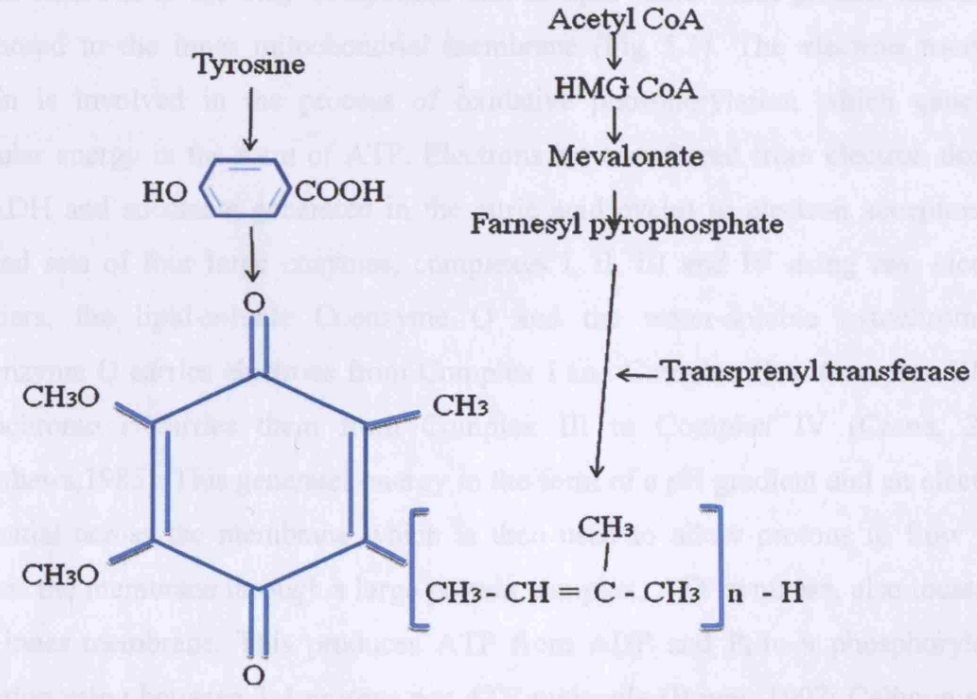

FIGURE.5.2. BIOSYNTHESIS AND STRUCTURE OF COENZYME Q.

membranes in variable amounts depending on the specific requirements of a particular cell or tissue. It is found in all organisms, microorganisms and plants in addition to animals (Crane, 2001; Lopez et al., 2006; Turunen et al., 2003). The endogenous biosynthesis of Coenzyme Q (CoQ) is a complicated process which requires two different multistep pathways. One leads to the synthesis of the ring structure from tyrosine or phenylalanine and consists of a redox-active 2,3-dimethoxy-5-methylbenzoquinone ring and the second leads to the formation from acetyl-CoA residues, via the mevalonate pathway, of a hydrophobic isoprenoid side chain in the 6 position due to the catalytic action of *trans* prenyl transferase (Fig.5.2). The different CoQs vary from each other in the length of their side chain which is indicated by a number (n) following the name. The principal coenzyme Q in humans and most mammals (primates, rabbit, sheep, horse, goat, pig and cow) is CoQ_{10} which indicates that the side chain contains 10 units or 50 carbon atoms (Turunen et al., 2003). CoQ_9 is also present but to a much lesser extent (4% in humans). Rats, mice and worms use mainly CoQ_9 while yeast uses CoQ_6 and *E.coli* uses CoQ_8.

The most studied function of CoQ is its role in the mitochondrial electron transport chain where it is the only component that is lipid rather than protein and is not anchored to the inner mitochondrial membrane (Fig 5.3). The electron transport chain is involved in the process of oxidative phosphorylation which generates cellular energy in the form of ATP. Electrons are transferred from electron donors, (NADH and succinate generated in the citric acid cycle) to electron acceptors via linked sets of four large enzymes, complexes I, II, III and IV using two electron carriers, the lipid-soluble Coenzyme Q and the water-soluble cytochrome c. Coenzyme Q carries electrons from Complex I and Complex II to Complex III and cytochrome *c* carries them from Complex III to Complex IV (Crane, 2001; Matthews,1985). This generates energy in the form of a pH gradient and an electrical potential across the membrane which is then used to allow protons to flow back across the membrane through a large protein complex, ATP synthase, also located in the inner membrane. This produces ATP from ADP and P_i in a phosphorylation reaction using between 3-4 protons per ATP molecule (Boyer, 1997; Calhoun et al., 1994; Cecchini, 2003; Hunte et al., 1990; Schultz and Chan, 2001; Trumpower, 1990; Yoshida et al., 2001; Yoshikawa et al., 2006; Young et al., 2007).

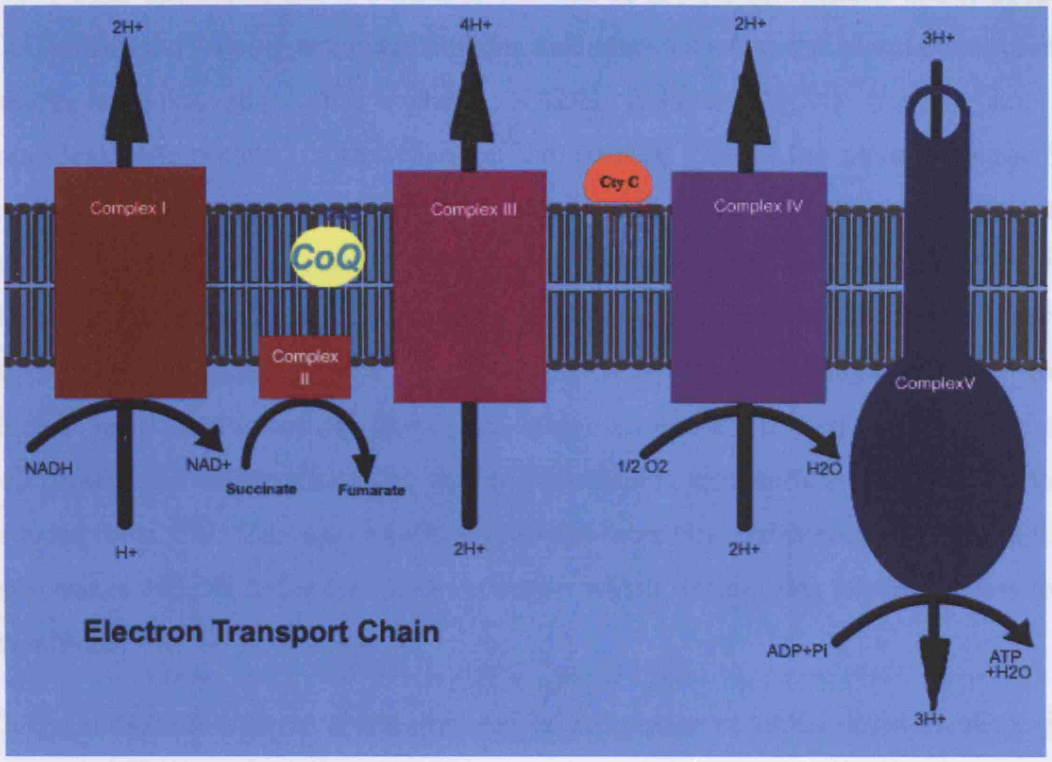

FIGURE 5.3. ELECTRON TRANSPORT CHAIN IN THE INNER MITOCHONDRIAL MEMBRANE. CoQ moves within the membrane as an electron carrier transferring electrons from Complex I and II to Complex III. Complex V, ATP synthase, uses the proton gradient across the membrane to drive the synthesis of ATP from ADP and (P_i).

Oxidative phosphorylation can be a potential generator of reactive oxygen species (ROS). To combat the toxic effects of ROS, the cell has various anti-oxidants such as vitamin C and E and enzymes namely catalase, superoxide dismutase and peroxidases. Coenzyme Q itself in its reduced form, $CoQH_2$, is also a very powerful anti-oxidant (Rattan, 2006; Valko et al., 2007). $CoQH_2$ maintains the integrity of cellular membranes by preventing lipid peroxidation, free radicals and therefore preventing membrane disruption (Crane, 2001; Turunen et al., 2003).

New roles for Coenzyme Q in other cellular functions have been found in recent years which include regulation of transcription factor activity and cell signalling through redox reactions in non-mitochondrial membranes such as those of lysosomes, peroxisomes, golgi apparatus and plasma membranes (DeHahn et al.,

1997; Gille and Nohl, 2000; Morre, 1994; Sun et al., 1992; Turunen et al., 2003). CoQ carries out redox reactions in cellular membranes such as the plasma membrane which in eukaryotic cells contains NADH oxidase (NOX) that is not a transmembrane protein, rather it lies on the external side of the membrane and is involved in electron transport. At the cytosolic side, a quinone reductase is present which catalyses the reduction of CoQ to $CoQH_2$ in the presence of NADH. $CoQH_2$ then shuttles electrons to NOX which is able to reduce ascorbyl radicals, produce superoxide and reduce protein disulfides. These NOX interchange activities are thought to respond to growth factors and hormones and are related to the control of cell growth and differentiation as well as maintaining extracellular ascorbate in the reduced form. CoQ also seems to be involved in lysosome redox reactions due to the presence of NADH-dependent CoQ reductase which translocates protons across the membrane.

CoQ_{10} is thought to counteract mitochondrial membrane potential depolarization via the mitochondrial permeability transition pore (PTP). Disruption to the membrane due to increased permeability through the opening of the PTP e.g. due to high levels of Ca^{2+}, has been proposed as an early indicator of apoptosis resulting in cytochrome c release and caspase activation in mammals. CoQ_{10} seems to be able to prevent this as studies show that it can counteract membrane depolarisation, cytochrome *c* release and caspase-9 activation through inhibition of the opening of the PTP and therefore acts as an apoptotic inhibitor (Turunen 2004, Papucci 2003).

CoQ is also involved in the regulation of gene expression and cell signalling through its redox activities. Electron transport is the primary generator of peroxide, H_2O_2 which activates transcription factors such as NFκB which results in gene expression and regulation of calcium signalling. CoQs can also participate in the oxidation of ion channels and also of thiol groups on growth factor receptors and consequently is involved in the regulation of cell proliferation, however this is a new area of study which requires further research (Crane 2001). Another area in which CoQ plays a role is in the immune system. CoQ_{10} increased phagocytic activity in tumour-induced mice and was also found to increase immunoglobins and decrease the levels of tumour necrosis factor-α and interleukin-6. In addition, several clinical trials suggest that it has a tumour suppresser effect and inhibits metastases (Premkumar et al., 2007).

It is clear that the CoQs are involved in various biological processes in all cells and are not just limited to their function as electron carriers. In consequence they are vital molecules in all organisms.

5.2.2. The *CG31005* mutation responsible for the *qless* phenotype is identified

To identify the mutations in *CG31005* responsible for the *qless* phenotypes, sequence analysis was carried out on both $qless^{109}$ and $qless^{264}$ (see Material and Methods 2.5.2, 2.5.3 and 2.5.4). Although the $qless^{264}$ DNA lesion was not found, this analysis revealed $qless^{109}$ is a G to A missense mutation in exon 4 (Fig.5.4.A) which changes a conserved serine to an asparagine, S214N (Fig.5.4.B). The *qless* mutation is located 10 amino acids downstream from the first DDxxD domain of the catalytic site and is probably positioned at the entrance of the tunnel-shaped crevice (Fig. 5.5.) To date, studies have shown that critical amino acids at the catalytic site are the aspartate residues and the 4th and 5th amino residues upstream. This result identifies another crucial amino acid downstream of the first active site that is required for *PDSS1* function.

5.2.3. Dietary Coenzyme Q supplementation rescues *qless*

The BLAST sequence analysis strongly suggests that *qless* is the *Drosophila* orthologue of *PDSS1*, the enzyme that synthesises CoQ. To ascertain whether embryonic lethality can be rescued by breeding flies continuously on a CoQ_{10} supplemented diet, *qless*/TM3actGFP flies were fed for three generations on concentrations of 20, 50 and 100µg CoQ_{10} per gram of food. No non-GFP *qless* homozygous larvae were found indicating a failure of CoQ_{10} to rescue *qless* lethality.

To determine directly if the *qless* phenotype is due to a defect in CoQ synthesis, MARCM clones were generated in wild-type and *qless* larvae fed concentrations of CoQ_{10} varying from 10µg to 500µg per gram of food. All concentrations rescued the MARCM undergrowth phenotype to varying extents but 10µg and 20µg were less effective than the rest, and 200µg and 500µg produced fewer, viable L3 larvae (data

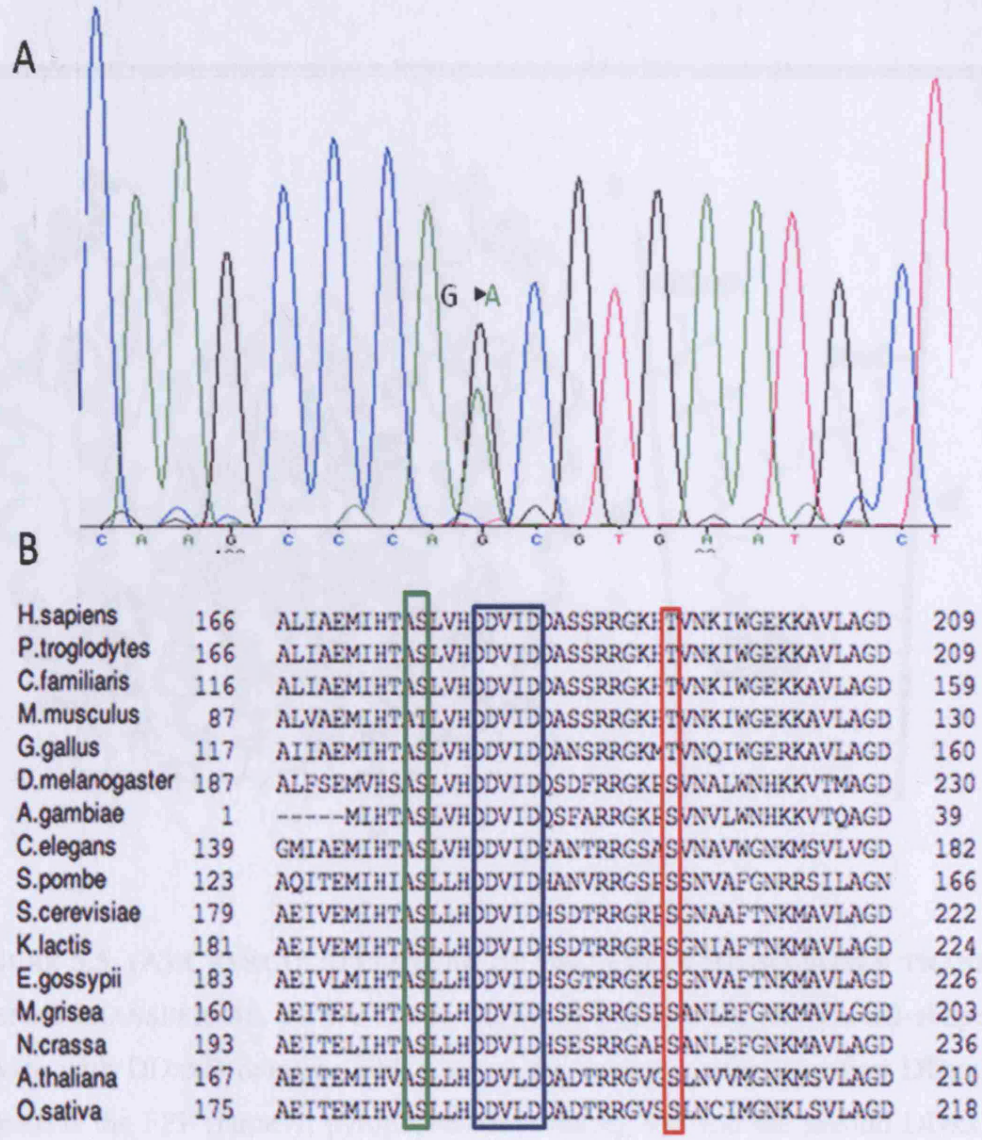

FIGURE 5.4. SEQUENCE ANALYSIS OF *qless*^{109}. (A) The *qless*^{109} sequence trace has a double peak showing a G to A mutation at position 214 within the *CG31005* gene. **B)** Red box shows the conserved serine/threonine of the *PDSS1* family in several different species. This changes to an asparagine in the *qless*^{109} mutation. Blue box is the first catalytic DDxxD domain. Green box shows critical residues for side-chain length

FIGURE 5.5. (A) CRYSTAL STRUCTURE OF THE AVIAN HOMO-DIMER TRANS-PRENYL TRANSFERASE. Active site is shown by red arrows. **(B)** Tunnel-shaped crevice with DDxxD domains which act as the catalytic sites. The first DDxxD domain is the FPP (farnesyl pyrophosphate) binding site and the second DDxxD domain is the IPP binding site. Black circle represents the amino acid upstream from the catalytic sites which is important for side-chain length. Isoprenoids are shown in the crevice. (Adapted from Liang *et al*. Eur. J. Biochem. 269, 3339-3354).

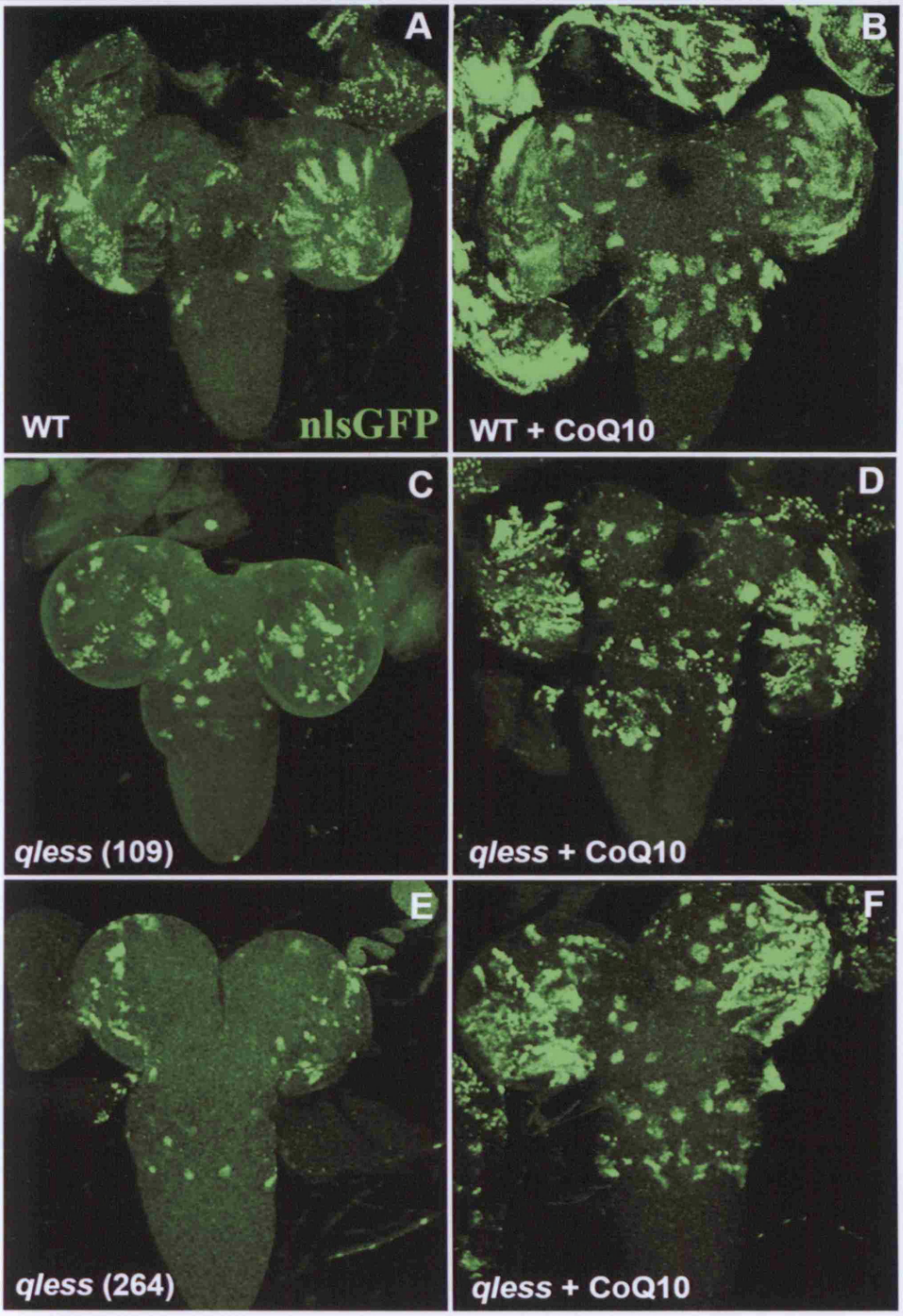

FIGURE 5.6. COENZYME Q SUPPLEMENTATION RESCUES *qless*. **(A)** Wild type pattern of clones stained with nlsGFP at 96hr ALH. **(B)** Wild type + CoQ_{10} reveals an increase in clone number. **(C)** and **(E)** ***qless*** shows a dramatic undergrowth phenotype. **(D)** and **(F)** 50 µg/g food of CoQ_{10} efficiently rescues *qless* undergrowth. An increase in number of clones is also observed.

not shown). Taking these results into consideration, 50μg per gram of food was used as the optimal concentration in subsequent feeding experiments as this produced abundant larvae while efficiently rescuing the clonal undergrowth phenotype of both *qless*^{109} and *qless*^{264} (Fig 5.6.). These results directly demonstrate that the *qless* undergrowth phenotype results from a CoQ deficiency and shows that *qless* encodes a *trans*-prenyl transferase.

To quantify the degree of rescue by CoQ_{10}, clone size (*i.e.* number of cells per clone) was analysed in the CoQ feeding experiments. Due to difficulties counting cells in large optic lobe clones, analysis was restricted to the central brain (CB) and Thorax (Th). The average sizes of central brain and thoracic *qless* clones were 8 cells (n=30) and 4 cells (n=30) respectively compared to wild-type values of 40 and 29 cells (Fig.5.7). CoQ_{10} supplementation for wild type central brain and thoracic neuromeres gave an average size of 41 and 31 cells respectively with a p-value of 0.18 (Fig. 5.8). This indicates that CoQ supplementation does not significantly increase the size of wild-type neuroblast clones. For *qless,* CoQ supplementation gave an increase of average clone sizes from 8 to 40 cells (central brain) and from 4 to 24 cells (thoracic neuromeres), with a p-value of 0.003 which is highly significant. This compares closely with wild-type clone sizes of 40 and 29, indicating complete rescue (Fig.5. 8). Eye disc clones were also fully rescued (data not shown).

5.2.4 A Method to Increase MARCM clone frequency

The CoQ_{10} supplementation experiments show that wild-type clone size is not noticeably altered. Interestingly, however, addition of CoQ_4, CoQ_9 or CoQ_{10} does increase the frequency of labelled MARCM clones, both in wild-type and mutant cases. The average thoracic wild-type clone number increases with CoQ supplementation from 8 to 25 per CNS (n=6 larvae) (Fig 5.9 and 5.10). A similar three-fold increase in clone number is also observed with *qless* rescue (Fig. 5.6). These results show that CoQ can be used to increase the frequency of MARCM clones. Importantly, CoQ_{10} supplementation has no ability to induce MARCM clones in the absence of heat shock (data not shown). One possibility is that the increase in frequency is due to CoQ increasing the efficiency at which Flipase

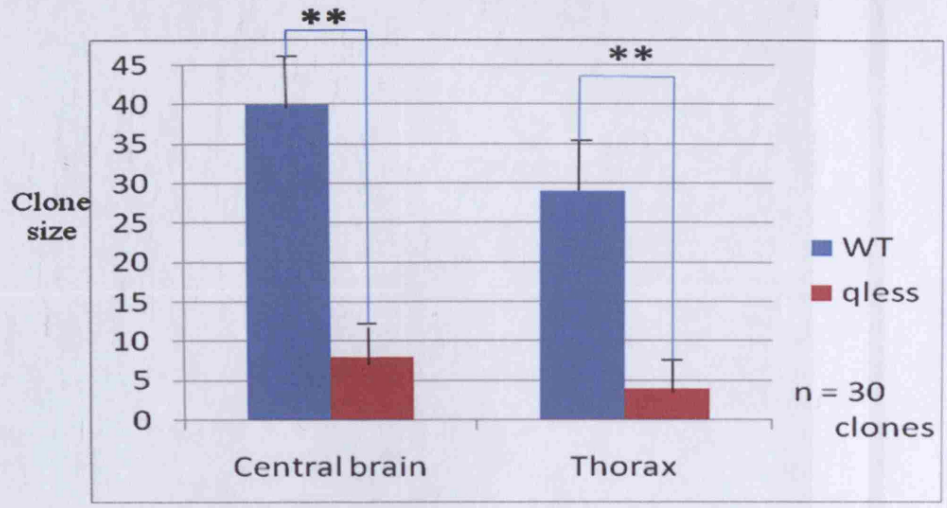

FIGURE 5.7. CLONE SIZE IS DRAMATICALLY REDUCED IN *qless* CLONES COMPARED TO WILD-TYPE.(p-value = 0.003) Wild-type central-brain and thoracic MARCM clones show an average clone size of 40 and 29 cells compared to 8 and 4 cells in *qless* clones.

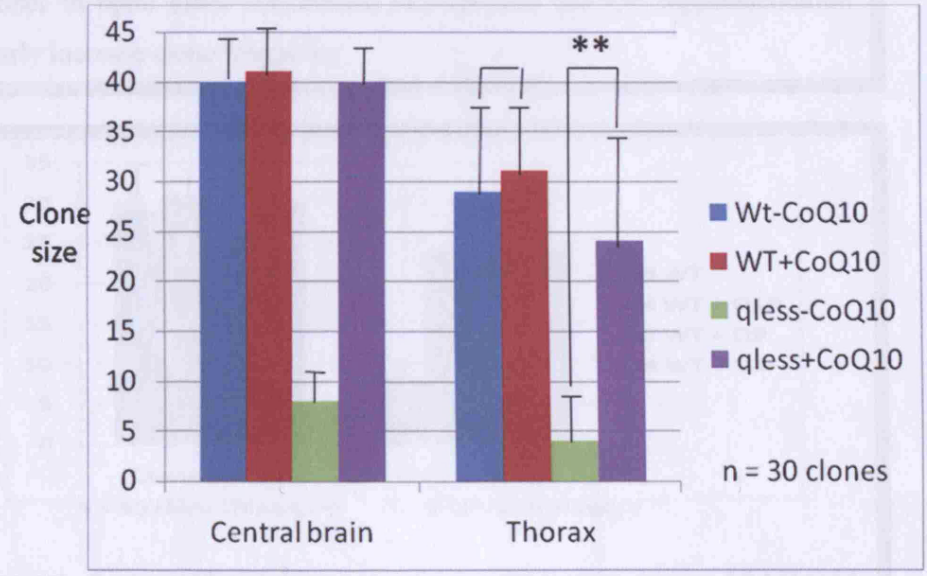

FIGURE 5.8. CoQ10 SUPPLEMENTATION RESCUES *qless* CLONE SIZE. Importantly it does not increase size of wild-type clones (p-value=0.18, not significant). *qless* clones are rescued in the central brain and thorax showing an increase from 8 and 4 cells respectively to 40 and 24 cells which is comparable wild-type clone size of 40 and 29 cells (p-value = 0.003).

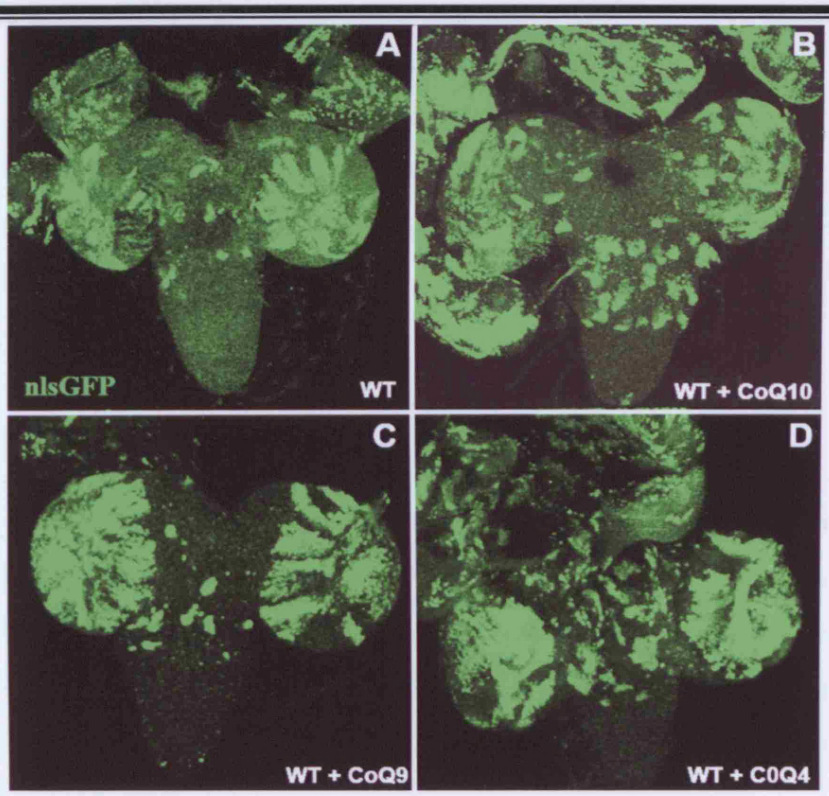

FIGURE5.9. Q4-Q10 SUPPLEMENTATION INCREASES FREQUENCY OF MARCM CLONES. **(A)** Wild-type pattern of clones stained with nlsGFP at 96hr ALH. **(B)** Q10 supplement increases frequency of clones in optic lobes and thorax. **(C)** Q9 and **(D)** Q4 supplementation similarly increase clone frequency.

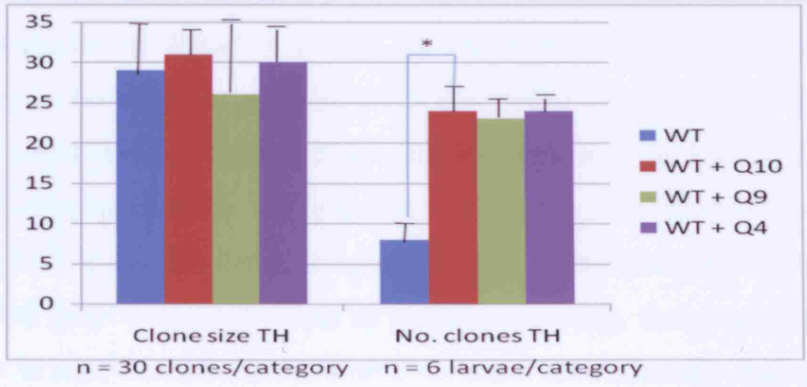

FIGURE 5.10. Q4-Q10 INCREASES FREQUENCY OF MARCM CLONES BUT NOT CLONE SIZE. Clone size of thoracic neuromeres does not alter significantly from wild type without CoQ (29cells) and with Q4 (30), Q9 (26) and Q10 (31). Frequency of clones alters significantly (*p-value 0.02) from 8 clones in wild-type thoracic clones to 24 (Q4), 23 (Q9) and 24 (Q10).

induces homologous recombination between chromosomes. CoQ supplementation could therefore be a useful tool for increasing the frequency of MARCM or even other FLP-induced clones in cases where they are normally very rare e.g. in the embryo.

5.2.5 Different CoQ side-chain lengths can rescue *qless*

The literature indicates that different CoQ side-chain lengths can, in some cases, substitute for one another (Farley et al., 1966; Hihi et al., 2003; Okada, 1998; Saiki et al., 2005; Scholler et al., 1970). To test whether this is the case, 50μg per gram of food of CoQ_{10}, CoQ_9 or CoQ_4 was fed to wild-type controls and *qless* larvae. All three CoQs increased clone frequency similarly for wild type and *qless.* In the case of wild type, none of the CoQs affected clone size significantly (Fig.5.9 and 5.10). In the case of *qless,* average thoracic clone size is increased from 4 to 24 cells (plus Q_{10}), to 23 cells (plus Q_9) and to 21 cells (plus Q_4) (Fig.5.11 and 5.12). This indicates that side-chain lengths of 4 -10 isoprenoid units are similarly active in rescuing *qless.*

To establish the effects of loss-of-activity of *qless* and CoQ supplementation on neuroblasts, MARCM analysis was carried out using Mira as a neuroblast marker. Neuroblasts are found in almost all wild-type clones in the brain lobes and the thorax, with and without CoQ_4, CoQ_9 and CoQ_{10} (Figs 5.13 and 5.14). In the central brain, neuroblasts can be seen in some *qless* clones (Fig.5.15 A, A', A'') and, with CoQ supplementation, the frequency of clones containing a neuroblast increases (Fig.5.15 B-D). Similarly, in *qless* thoracic neuromeres at 96 hr, a neuroblast is present only in a small subset of clones. Typically, these rare clones are only 1-2 cells in size whereas clones with 3 or more cells normally lack a neuroblast (Fig. 5.16 A, A', A''). Supplementation with CoQ_4, CoQ_9 or CoQ_{10}, not only increases clone size but rescues the presence of the neuroblast (Fig. 5.16 B-D). These results indicate that dietary CoQ supplementation rescues the presence of neuroblasts as well as cell number in *qless* clones. They also provide additional evidence that isoprenoid side-chain lengths between 4 and 10 can functionally substitute for one another.

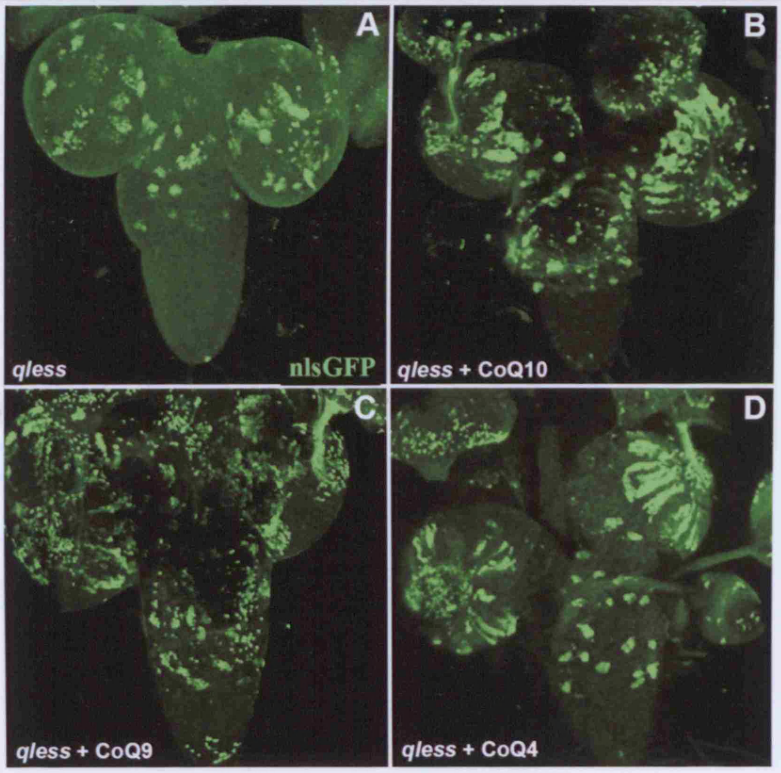

FIGURE 5.11. DIFFERENT COQ SIDE-CHAIN LENGTHS RESCUE *qless* CLONE SIZE. All images show L3 CNS at 96hr ALH. Magnification is 200x. nlsGFP labels clones. **(A)** *qless* undergrowth phenotype. **(B-D)** show complete rescue of *qless* on supplementation with CoQ10, Q9 and Q4 respectively.

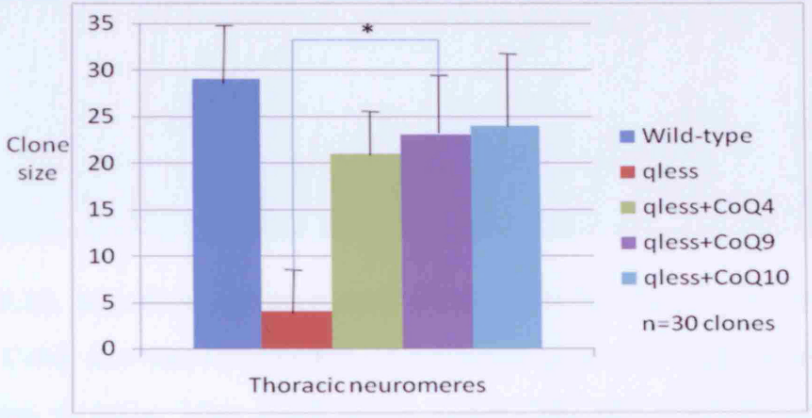

FIGURE 5.12. DIFFERENT SIDE-CHAIN LENGTHS RESCUE *qless* CLONE SIZE. Wild type has an average thoracic clone size of 29 cells whereas *qless* has an average clone size of 4 cells. On supplementation with CoQ clone size increases to 21 (Q4), 23 (Q9) and 24(Q10) which shows rescue of clone size similar to wild type (*indicates p-value = .004).

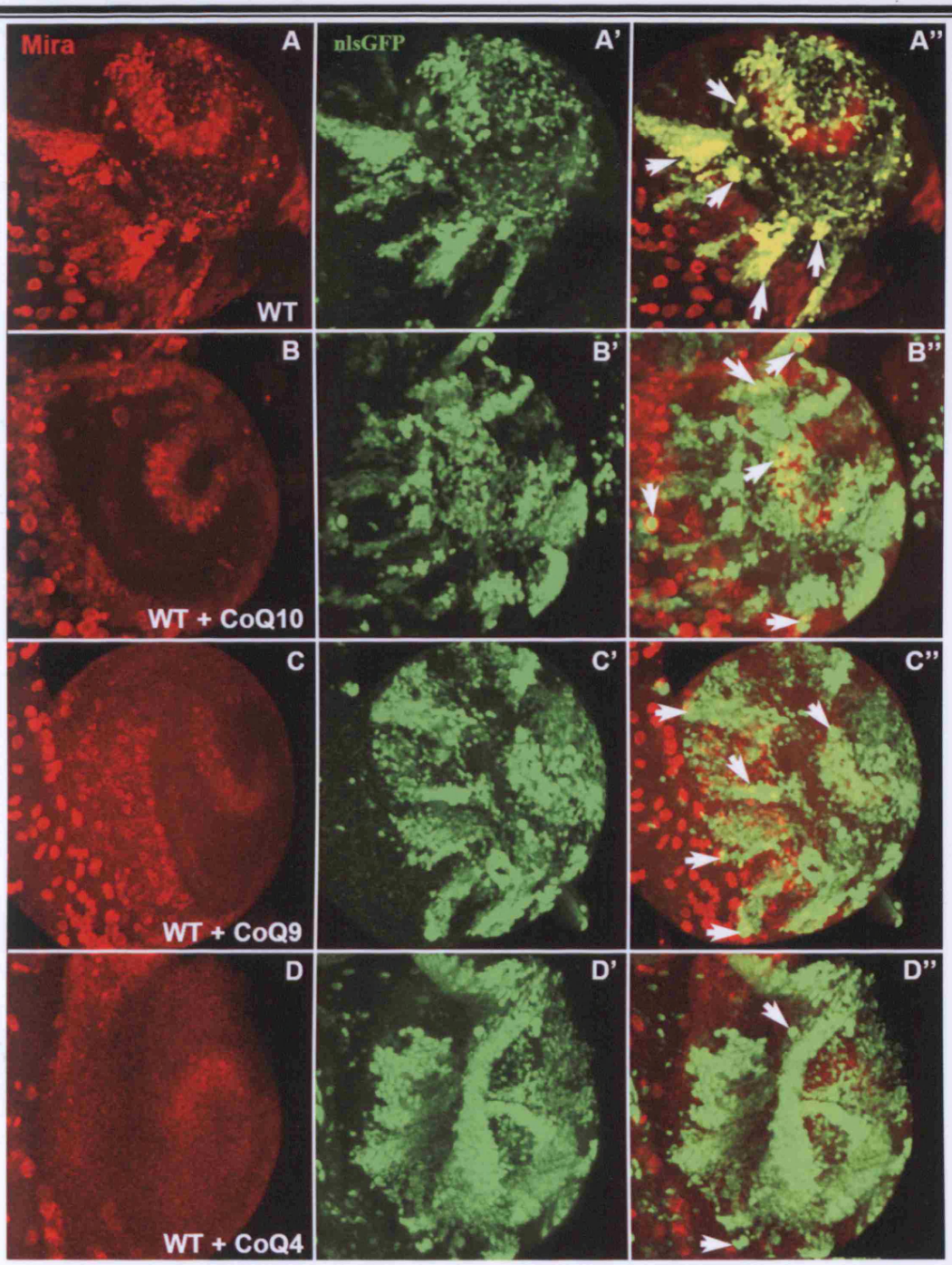

FIGURE 5.13. NEUROBLAST PATTERN IN WILD-TYPE BRAIN LOBES WITH AND WITHOUT CoQ SUPPLEMENTATION. All images show L3 brain lobes at 96 hr. Magnification is 600x. Mira (red) labels neuroblasts and nlsGFP (green) labels clones. Arrows indicate neuroblasts in clones (not all indicated). **(A)** Wild-type neuroblast activity without CoQ and **(B-D)** show similar neuroblast activity on supplementation with CoQ10, CoQ9 and CoQ4 respectively. **(B-D)** also show an increase in clone frequency compared to wild-type, as indicated earlier.

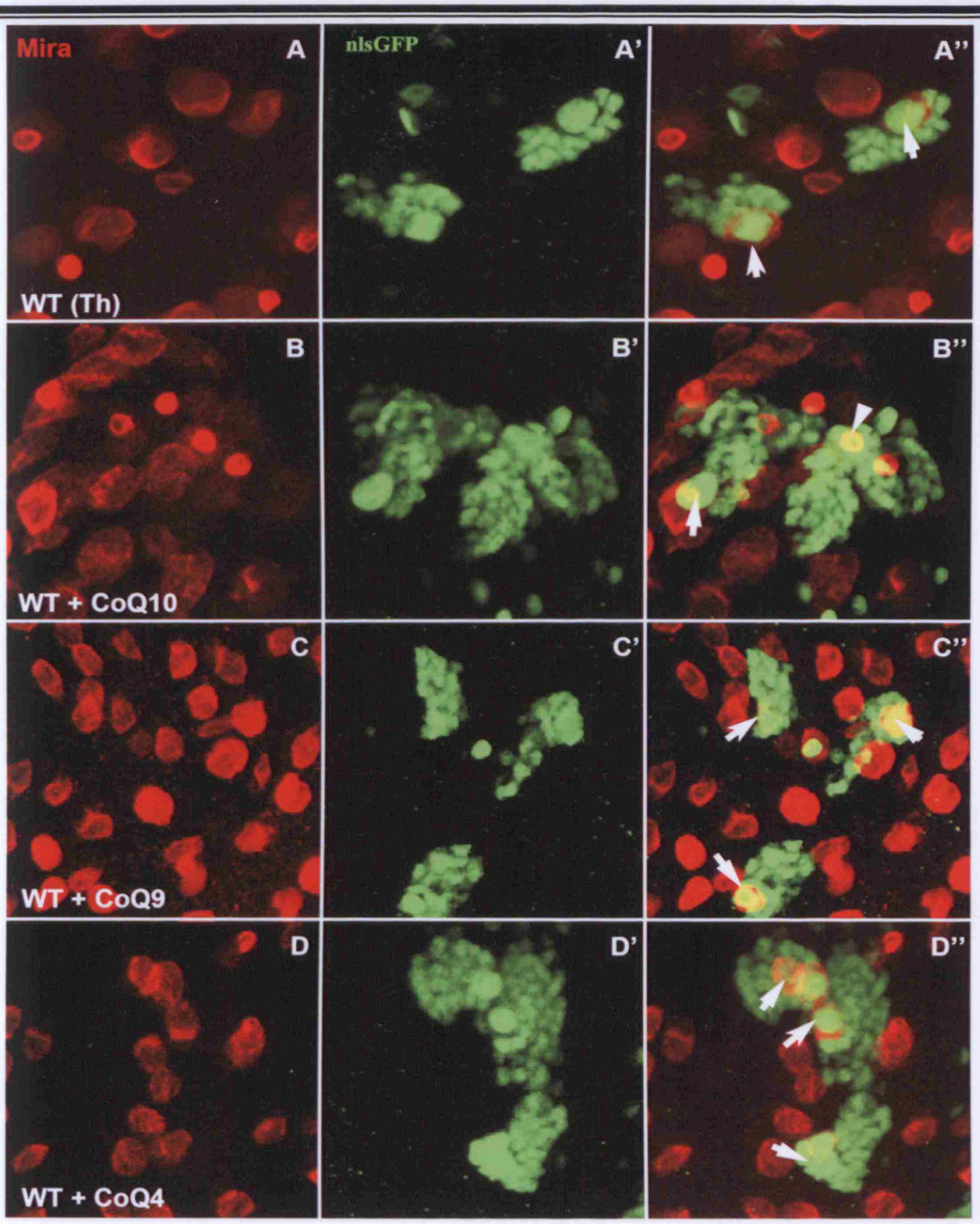

FIGURE 5.14 NEUROBLAST ACTIVITY IN WILD-TYPE THORACIC NEUROMERES WITH AND WITHOUT CoQ SUPPLEMENTATION. All images at 96 hr ALH, magnification 1000x. Mira (red) labels neuroblasts and nlsGFP (green) labels clones. Arrows indicate the active neuroblast in clones. **(A)** All wild-type thoracic neuromeres contain a neuroblast. **(B-D)** Supplementation of CoQ10, CoQ9 and CoQ4 similarly show the presence of a single neuroblast in every clone.

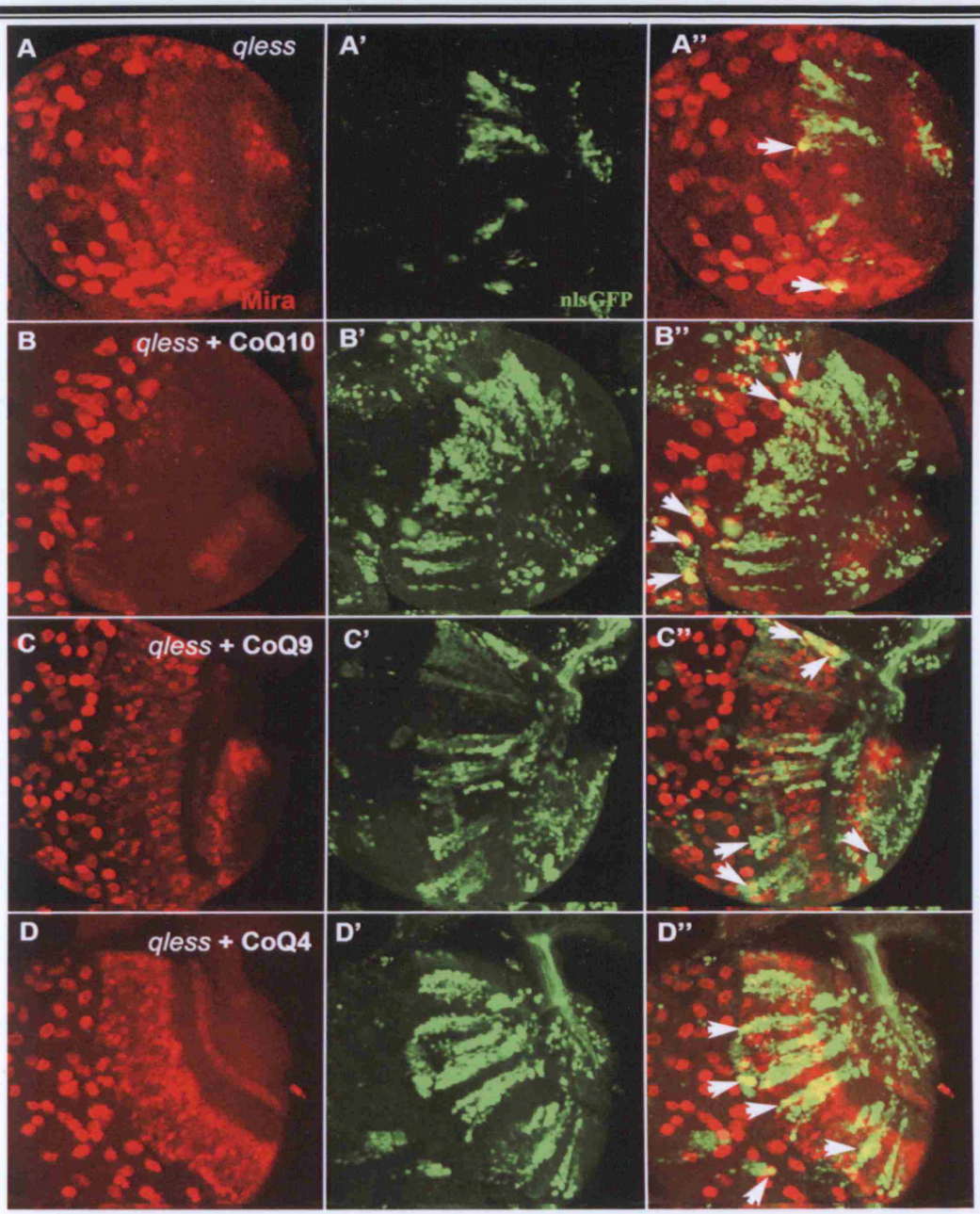

FIGURE 5.15. DIFFERENT COQ SIDE-CHAIN LENGTHS RESCUE NEUROBLAST ACTIVITY IN *qless* BRAIN-LOBE CLONES. All images at 96hr ALH. Mira(red) marks the neuroblast and nlsGFP (green) labels clones. Magnification 600x. **(A)** Most *qless* brain-lobe clones do not contain a neuroblast and where a neuroblast is present the clone contains only 1-2 cells (arrow). **(B-D)** Supplementation with CoQ10, CoQ9 or CoQ4 rescues neuroblast activity in *qless* clones (arrows).

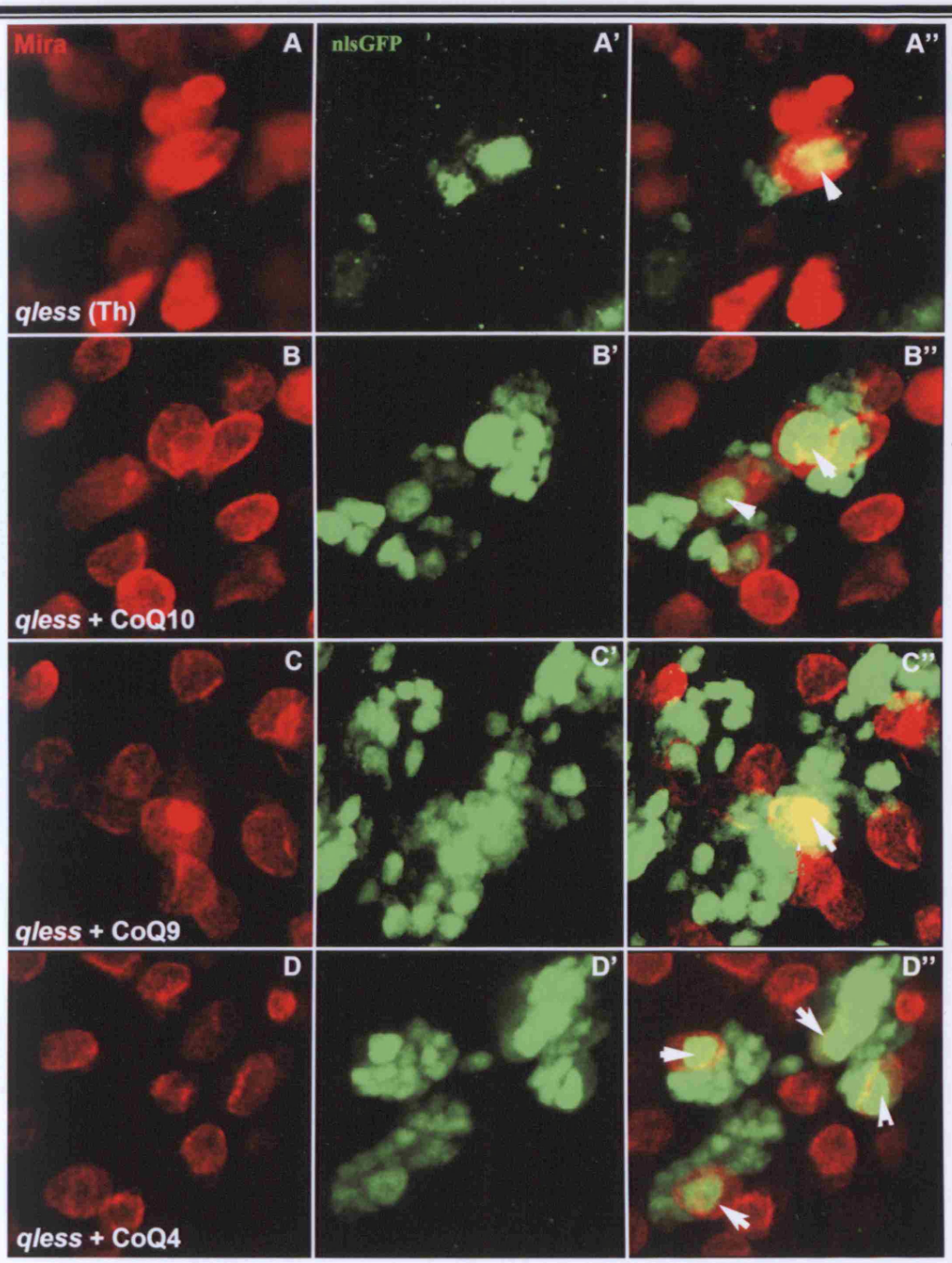

FIGURE 5.16. *qless* NEUROBLAST ACTIVITY IN THORACIC NEUROMERES IS COMPLETELY RESCUED WITH DIFFERENT CoQ SIDE-CHAIN LENGTHS. All images show L3 thoracic neuromeres at 96 hr ALH. Magnification is 1000x. nlsGFP (green) labels clones and Mira (red) labels neuroblasts. Arrows indicate a neuroblast within a clone. **(A)** *qless* clones without CoQ. One clone of 2 cells contains a neuroblast and another clone contains no neuroblast. **(B-D)** Supplementation with CoQ10, Q9 and Q4 respectively completely rescues neuroblast activity in every clone and rescues clone size.

5.2.6. The mitochondrial stress marker Hsp60 is upregulated in *qless* clones

To examine the effects of loss of CoQ in mitochondria, I used Hsp60 which is a marker for mitochondrial stress. The *Drosophila* Hsp60 protein is a molecular chaperone located in mitochondria and is up-regulated during mitochondrial stress (Alonso et al., 2005; Arya et al., 2007). Co-labelling for nlsGFP and Hsp60 indicated that there is an up-regulation of Hsp60 in *qless* clones compared to heterozygous tissue outside the clones or to wild-type clones (Fig 5.17). Although I cannot rule out that this reflects an increase in mitochondrial number, this observation suggests that *qless* mitochondria are under stress.

5.2.7. The Cytochrome *c* cell death epitope is unmasked in *qless* clones

Next, to test whether increased mitochondrial stress might be associated with cell death, the mitochondrial protein Cytochrome *c* (Cyt *c*), was analysed. I used an antibody specific to an epitope of Cyt *c* that is unmasked when the outer mitochondrial membrane is disrupted. In mammals and *Drosophila* this unmasking occurs during apoptosis (Dorstyn et al., 2002; Varkey et al., 1999; Zou et al., 1997). Co-labelling *qless* clones with nlsGFP and anti-Cyt *c* reveals that the cell-death epitope is unmasked in the *qless* clones (Fig. 5.18 A-C). Together with the previous Hsp60 results, these results suggest that mitochondrial membranes lacking CoQ become permeabilised in a way that resembles known mitochondrial changes accompanying apoptosis.

5.2.8. Caspase activation in *qless* clones

The previous mitochondrial results suggest that cells in *qless* clones might be undergoing apoptosis. Co-labelling with mGFP and CM1, an antibody to activated caspase 3, was used to look at cell death. In *qless* clones, most cells *i.e.* neuroblasts and neurons, are CM1-positive indicating that they are undergoing programmed cell death (Fig. 5.19). Together with the analysis of clone size and neuroblast frequency, the caspase results strongly suggest that the *qless* undergrowth phenotype is, at least in part, the result of apoptosis in progenitors and post-mitotic neurons.

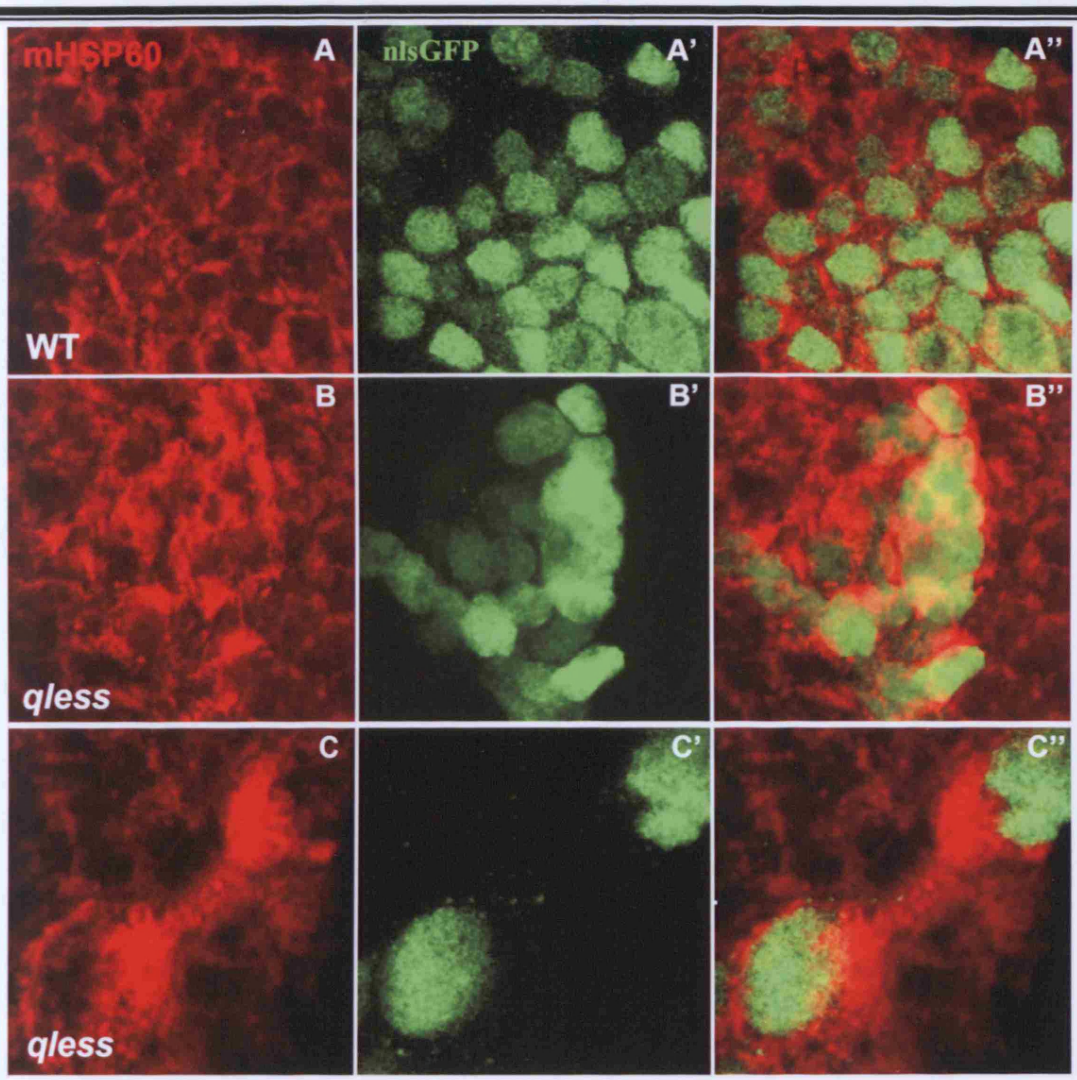

FIGURE 5.17. THE HSP60 MITOCHONDRIAL STRESS MARKER IS UP-REGULATED IN *qless* CLONES. Images taken at 96hr ALH. Magnification of A and B is 1000x and C is 5000x. Clones are labelled with nlsGFP (green) and mitochondria are labelled with Hsp60 (red). **(A)** Wild type clones show no difference in the Hsp60 levels either inside or outside the clone. **(B)** A *qless* clone has up-regulated Hsp60 whereas outside the clone Hsp60 levels are lower. **(C)** Higher magnification of a 2-cell clone which reveals up-regulation of Hsp60 within the clone.

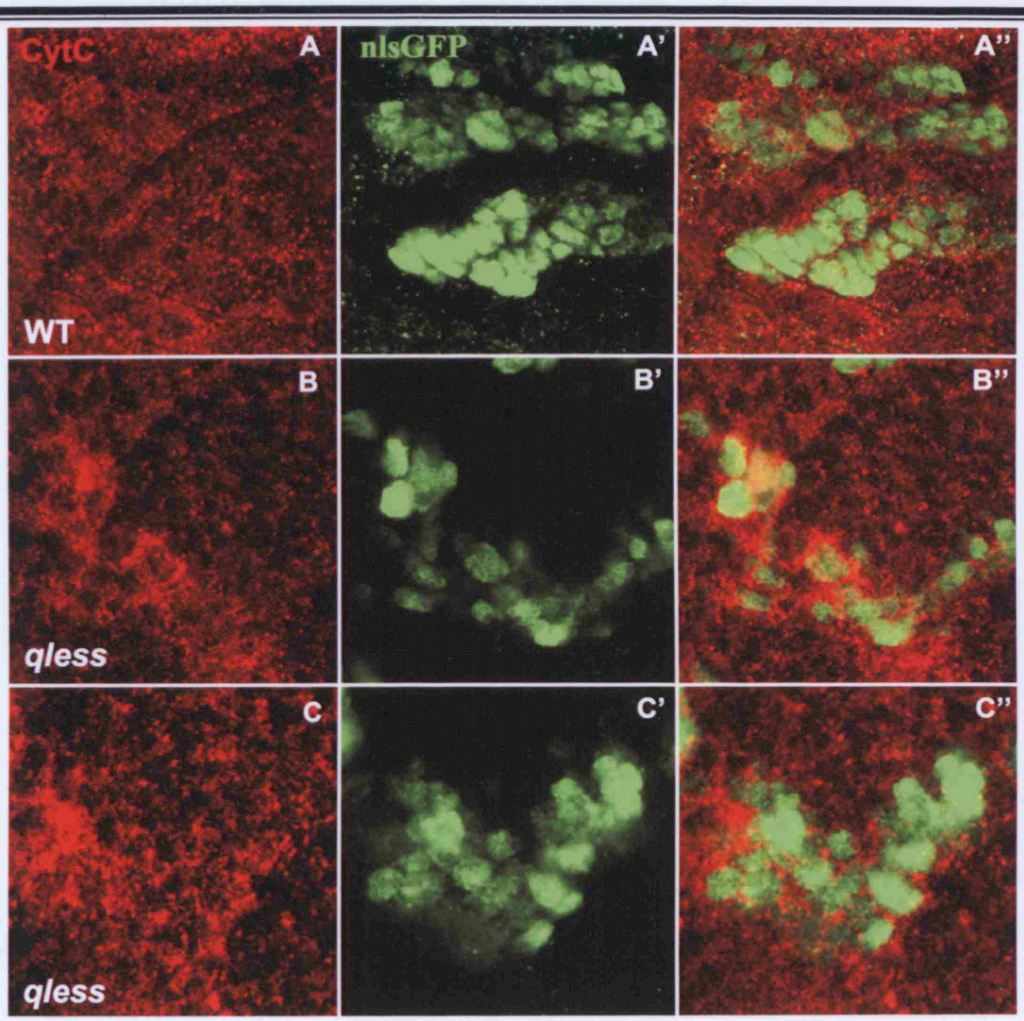

FIGURE 5.18. CYTOCHROME C CELL-DEATH EPITOPE IS UNMASKED IN *qless* CLONES. All images are brain-lobe clones at 96 hr ALH. Magnification is 1000x. Cytochrome *c* is labelled in red and clones are labelled with nlsGFP (green). **(A)** Wild-type clone shows that there is no difference in staining inside versus outside the clone. **(B** and **C)** ***qless*** clones. Staining reveals that the cell-death epitope of Cytochrome *c* is unmasked in *qless* clones.

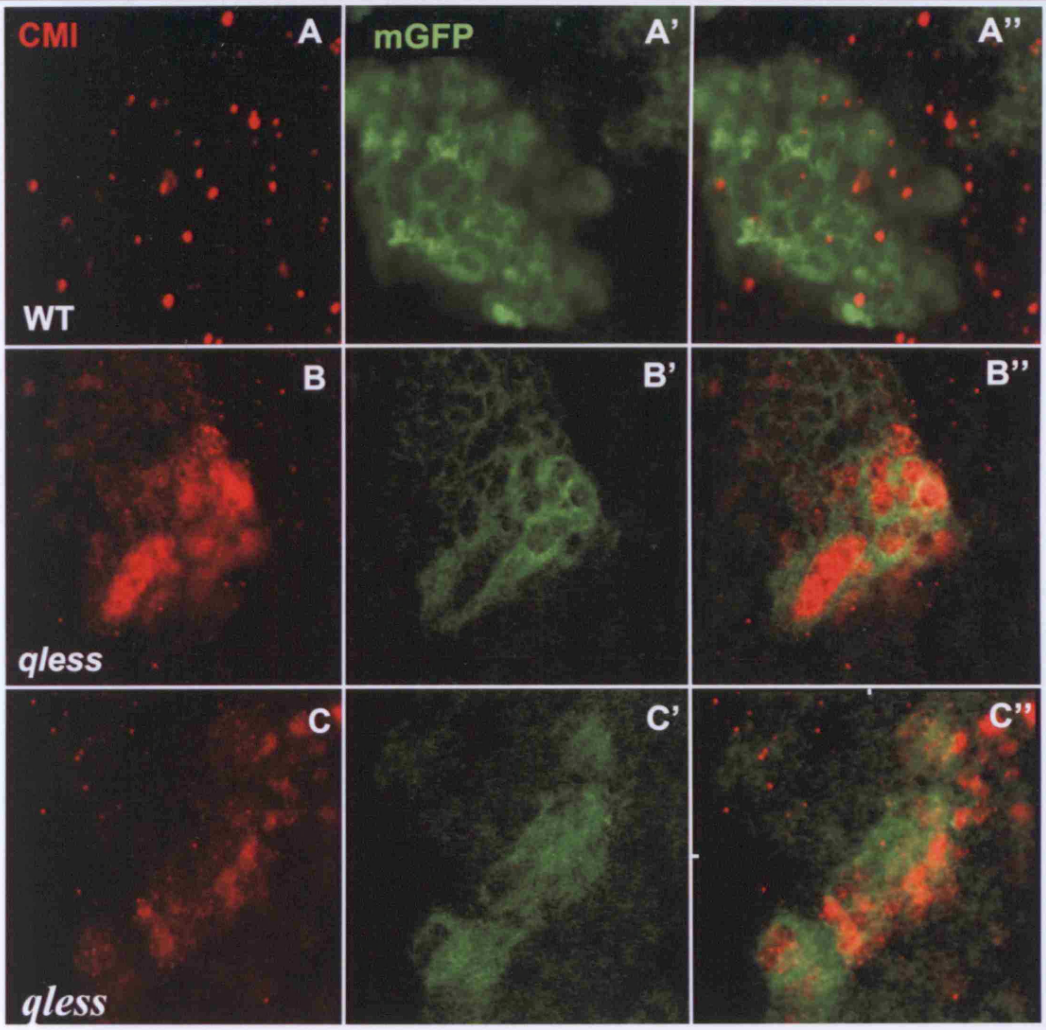

FIGURE 5.19. *qless* IS REQUIRED FOR THE SURVIVAL OF NEUROBLASTS AND NEURONS. All images are brain-lobe clones at 96 hr ALH. Magnification 1000x. Co-labelling is with CM1 (red), an antibody to activated caspases and membrane GFP (green) to label clones. **(A)** In wild-type clones neither the neuroblast (white dotted line) nor the neurons express activated caspase. **(B** and **C)** In *qless* clones, the neuroblast and neurons are activated-caspase positive indicating both cell types are undergoing apoptosis.

5.3. Discussion

I have shown that *qless* encodes the fly orthologue of human *PDSS1,* a *trans*-prenyl transferase which synthesises the isoprenoid side chain of Coenzyme Q. The S214N mutation in *qless*^{109} is close to a DDxxD catalytic site, and may therefore abolish or diminish catalytic activity. Direct evidence for this is provided by rescue of the clonal undergrowth phenotype by feeding CoQ to the larvae. However embryonic lethality cannot be rescued by feeding adult flies CoQ_{10} as no homozygous *qless* larvae were recovered. This suggests that exogenous CoQ may not be passed efficiently from mother to embryo. CoQs with different side-chain lengths between 4-10 can all rescue the MARCM undergrowth phenotype, showing they are functionally equivalent, at least in this context. These results correlate with various reports that CoQs of different isoprenoid side-chain lengths can rescue or partially rescue the effects of CoQ deficiencies. The worm homologue for the yeast gene *coq7* that encodes a mitochondrial protein involved in CoQ synthesis, is *clk-1*. When *clk-1 Caenorhabditis elegans* mutants were fed dietary CoQ_6, CoQ_7, CoQ_8 and CoQ_9, all could function normally with sustained growth in contrast to no CoQ at all, which causes growth arrest at the L2 stage. However, only CoQ_8 and CoQ_9 rescued fertility, indicating that the different side-chain lengths can rescue some but not all biological processes (Hihi et al., 2003). Studies in *S. cerevisae and E. coli* which normally use CoQ_6 and CoQ_8 respectively also indicated that side-chain length was not critical for biological function (Okada, 1998; Saiki et al., 2005). Furthermore, when genetically dystrophic mice deficient in CoQ_9 were treated therapeutically with CoQ_4 and CoQ_7 they showed a distinct improvement, with even severely dystrophic mice responding and able to walk (Farley et al., 1966; Scholler et al., 1970).

CoQ is an electron carrier located in the mitochondria and also protects the mitochondrial membrane due to its anti-oxidant properties. In addition, CoQ_{10} and its analogues are also thought to counteract mitochondrial depolarisation via the mitochondrial permeability transition pore. The inner mitochondrial membrane has a low permeability to ions and solutes in order to save energy in the form of an electron and pH gradient across the membrane. To facilitate trans-membrane transport, it possesses a number of macromolecules that act as transporters and ion channels. Disruption to the membrane due to increased permeability through the opening of the permeability transition pore e.g. due to the release of Ca^{2+} (this could

be tested using a UAS-GCaMP calcium sensor) (Wang et al., 2004), has been proposed as an early indicator of mammalian apoptosis resulting in cytochrome *c* release and caspase activation (Fontaine et al., 1998; Papucci et al., 2003; Turunen et al., 2003; Walter et al., 2002). Studies show that CoQ_{10} can counteract membrane depolarisation, cytochrome *c* release and caspase-9 activation and as such acts as an apoptotic inhibitor (Papucci et al., 2003; Turunen et al., 2003). Therefore, CoQ deficiency might be expected to cause disruption of the mitochondrial membrane, opening of the permeability pore, caspase activation and apoptosis. My Hsp60, cytochrome *c* and caspase results are consistent with this hypothesis. The mitochondrial Hsp60 antibody revealed mitochondrial stress. The unmasking of the cell-death epitope of cytochrome *c* points to disruption of the outer membrane, an indicator of apoptosis. As both neuroblasts and neurons are positive for activated caspase in *qless* clones, my results indicate that cell death operates at two levels to reduce clone size. First, size is reduced when post-mitotic neurons die and, second, there is a failure to proliferate due to neuroblast death.

Chapter 6

Discussion

6. Discussion

To identify genes regulating CNS growth, I conducted pupal-lethal and mosaic genetic screens. From a total of 1,600 mutagenised chromosomes, 90 mutations associated with undergrowth and overgrowth phenotypes were recovered. Seven mutations were successfully pinpointed using deficiency mapping and three of these were localised to a single gene. First, I will outline the successes and limitations of the genetic screens and second, I will discuss in depth the characterisation of a novel gene from the screens that I have named *qless*.

6.1. Screening for neural cell proliferation and death genes.

The MARCM and pupal-lethal screens together identified 90 mutations representing 6 distinct classes of growth phenotypes. These correspond to under-sized entire CNS, region-specific reduction of thorax and central brain/optic lobes, region-specific undergrowth of optic lobes and thorax with overgrowth of abdomen, region-specific undergrowth of the thorax, overgrowth of the entire CNS and region-specific overgrowth of the abdomen. Both screens have limitations. The mosaic screen misses non-cell autonomous mutations and the pupal-lethal screen is only able to analyse a small fraction of lethal genes as most lethals die earlier. In addition, although both screens have proved efficient in isolating genes affecting growth, they are not specific for death versus proliferation. Secondary screening of the 90 mutations using α-activated caspase and BrdU would need to be applied to distinguish between these two processes. From the pupal-lethal screen of 350 mutagenised chromosomes, 22 growth phenotypes falling into three distinct classes were selected. The Class A phenotype of reduced thoracic and brain lobe tissue with elongated abdomen was represented by 6 mutations, the Class B phenotype of a reduced CNS was represented by 15 mutations and finally the Class C phenotype of an oversized CNS was represented by 1 mutation. This suggests that overgrowth phenotypes are either much rarer than undergrowth phenotypes or that they are more frequently lethal at embryonic/early larval stages. For abdominal neuromeres at least, the latter possibility is consistent with the large number of overgrowth phenotypes recovered in the MARCM screen of embryonic-lethal mutations. Six pupal lethals, *2v71, 2v106, 2v206, 2v237, 2v290* and *2v316* were selected for mapping and four out

of the six were successfully mapped. *2v237* and *2v316* failed to map to 3R and most probably lie on 3L. *2v71* mapped to the heterochromatic region of the 3R telomere and had a MARCM phenotype of under-proliferation of thoracic neuromeres and brain lobes and over-proliferation of the abdomen confirmed by both BrdU and Mira/pH3 labelling. *2v106* was mapped to an interval containing 3 candidate genes, and *2v206* and *2v290* were mapped to the well known tumour-suppressor genes, *scribble* and *Enhancer of split m8* respectively. *scribble* is involved in asymmetric division and forms the Lgl/Scrib/Dlg complex, reported to be responsible for the basal targeting of Prospero/Miranda/Brat at metaphase, crucial for GMC fate (Albertson et al., 2004; Albertson and Doe, 2003; Betschinger et al., 2003; Doe and Bowerman, 2001; Humbert, 2003; Lee et al., 2006a; Wodarz, 2005). The *E(spl)complex* genes are transcriptional repressors of proneural genes, involved in the lateral inhibition process that determines which cells become neuroblastss and which become epidermal (Bray, 1997; Campos-Ortega and Hartenstein, 1997; Campuzano and Modolell, 1992; Kunisch M, 1994; Martin-Bermudo MD, 1995). Reported loss-of-function *scribble* mutations lead to overgrowth of neuronal tissue and giant L3 larvae and *E(spl)* loss-of-function mutations show neural hyperplasia with additional neuroblasts (Bilder and Perrimon, 2000; Buescher et al., 2002; Corbin et al., 1991; Ziemer et al., 1988). Intriguingly, both *2v206* and *2v290* are associated with an undersized CNS phenotype. This is in stark contrast to the over-proliferation phenotypes described for loss-of-function mutations in these genes. These two alleles may therefore be interesting to follow up in the future, perhaps determining whether their intriguing effect on the CNS is mediated by non-cell autonomous effects on other growth-promoting tissues.

A larger mosaic screen of 1,250 mutagenised chromosomes identified 68 embryonic-lethal mutations on 3R altering the number of neurons generated per neuroblast. The Class I phenotype of region-specific undergrowth of the thorax and central brain/brain lobes was represented by 5 complementation groups, the Class II phenotype of region-specific overgrowth in the abdomen was represented by 51 complementation groups, 30 of which had strong phenotypes and finally the Class III phenotype of region-specific undergrowth of the thorax was represented by 12 mutations. Class II was the most abundant phenotype recovered in the mosaic screen and is probably due to the MARCM technique being biased towards this phenotype

as the presence of even very small blue clones in the abdomen is easy to detect when compared to the wild-type pattern of none. Similarly, one caveat of the MARCM screen is that overgrowth of the already large thoracic and brain lobe clones is difficult to detect. Likewise, under-proliferation in the abdomen cannot be detected as the wild-type pattern is an absence of blue clones in the abdomen. Four complementation groups were selected for mapping from the MARCM screen: *63, 72* and *47/87* had Class II phenotypes whereas *109/264* have a Class I phenotype. Both *63* and *47/87* were successfully mapped to 8 and 9 candidate genes respectively. Finally *109/264* mapped to a single uncharacterised gene *CG31005*, encoding a *trans*-prenyl transferase required for Coenyme Q synthesis that I named *qless*.

Very similar frequencies of growth phenotypes were recovered from the pupal-lethal and mosaic screens, 6.4% for the former and 5.4% for the latter. The 3L screen carried out in the Gould lab (C. Maurange, L. Cheng, J. Pendred and A. Gould) recovered 90 mutants from 3000 EMS lines representing 3% of the total which is somewhat lower than the 5.6% recovered from the 3R screen. The higher percentage of recovered growth mutations in the 3R versus 3L screens may well reflect more lethal hits per chromosome arm (1.5 for 3L versus 2.5 in 3R, [A. Gould, personal communication]). Nevertheless, the 3R MARCM screen results also gave more hits than a more focused 3L MARCM screen by the William Chia lab using the same set of orthologue EMS lines. Although this screen scored Miranda localisation, it isolated alleles affecting neuroblast asymmetric division, cell fate and the orientation of the mitotic spindle, representing 2.8% of the total lines screened (Slack et al., 2006). Perhaps I recovered twice the frequency because more genes affect CNS growth and clone size than asymmetric cell division.

6.2. *qless* encodes the *Drosophila* orthologue of human *PDSS1*

Mapping and sequence analysis revealed that *109* and *264* are mutations in *qless (CG31005)*, annotated on Flybase as a *trans*-prenyl transferase. I used BLAST alignments to show that the closest human homologue is *PDSS1,* the catalytically active sub-unit of the PDSS1-PDSS2 holoenzyme that synthesises the isoprenoid

side chain of CoQ. The missense mutation found in *qless*^{109}, S214N, changes a conserved serine to an asparagine, ten residues downstream from the first DDxxD motif in the catalytic site, and reveals a new critical residue important for enzyme function. CoQ_{10} feeding experiments rescued the mutant phenotype demonstrating that the *qless* mutation causes a CoQ deficiency.

The *trans*-prenyl transferases act as complexes which can be homodimers, heterodimers or heterotetramers depending on the organism, and are only active after formation of the complex. The *trans*-prenyl transferases of *S.Cerevisiae* (CoQ_6) and *B.stearothermophilis* (CoQ_7) form heterodimers, whereas mice (CoQ_9) and *S. Pombe* (CoQ_{10}) form heterotetramers. This indicates that side-chain length is not specific to a certain type of multimeric enzyme complex (Koike-Takeshita et al., 1995; Saiki et al., 2005; Zhang et al., 2000b). The human enzyme is only functional as a heterotetramer composed of two PDSS1 and two PDSS2 subunits (Lopez et al., 2006; Mollet et al., 2007; Saiki et al., 2005). I used BLAST analysis of the *Drosophila* genome for human *PDSS2* orthologues and identified *CG10585* with an e-value of 2e-26, opening up the way to use *Drosophila* to dissect the functions of both *PDSS* subunits. As this analysis suggests that insects and humans may use the same heterotetrameric enzyme complex, *Drosophila* is likely to provide more insights relative to humans than yeast.

6.2.1. Functional equivalence between CoQ side-chain lengths

In yeast it is known that *COQ1*, a *PDSS1* orthologue, specifies the chain length of CoQ (Okada et al., 1996). To assess which CoQ chain length is functional in the *Drosophila* CNS, feeding experiments using CoQ_4, CoQ_9 and CoQ_{10} were carried out. As each CoQ variant rescued the phenotype, it can be concluded that they are functionally interchangeable. However which one is normally used in the fly is therefore still not clear. These results are consistent with studies on a *S. cerevisiae COQ1* mutant defective for hexaprenyl diphosphate synthesis. CoQs of side-chain lengths between 5-10 units were produced using different prenyl transferases from other species and were found to rescue the biological function of CoQ_6 (Okada, 1998). CoQ_6, CoQ_7, CoQ_8 and CoQ_9 all rescue growth in *C. elegans clk-1/coq7* null mutants (Hihi et al., 2003). Similarly, after treatment with CoQ_4 and CoQ_7,

genetically dystrophic CoQ_9 deficient mice improved greatly and even the most severely affected mice were able to walk (Farley et al., 1966; Scholler et al., 1970). As the *qless* mutant phenotype was rescued by CoQ_4, CoQ_9 and CoQ_{10}, this suggests that rather than a subtle change in side-chain length, it is more probable that the S214N mutation causes loss of enzyme activity, which could be due to the loss of serine phosphorylation or to a structural change in Qless that affects the tunnel-shaped substrate crevice or its ability to bind substrate or to form a complex with PDSS2/CG10585.

6.2.2. *qless* links mitochondrial function to apoptosis in *Drosophila*

In mammals, the mitochondrial role in cell death is well documented and understood (See Section 1.4. and Fig 1.5), but mitochondrial involvement in cell death in *Drosophila* remains unclear. Unlike the mammalian pathway which requires cytochrome *c* to trigger apoptosis, there is no conclusive evidence that it is required for cell death in *Drosophila* except in spermatid individualization and in the retina (Arama et al., 2003; Mendes et al., 2006; Rodriguez et al., 1999). Nevertheless, the presence of *Drosophila* homologues of the mammalian pro-apoptotic and anti-apoptotic Bcl-2 family, Drob-1/Debcl/dBorg-1/dBok (pro-apoptotic) and Buffy/dBorg2 (anti-apoptotic) suggests conservation of elements of this mitochondrial pathway (Igaki, 2004; Quinn et al., 2003; Quinn et al., 1999; Zhang et al., 2000a). In addition, there is a *Drosophila* homologue for Apaf-1 (Ark), for Omi/HtrA2 (DmHtrA2) (Challa, 2007) and, although there is no strong sequence similarity between the mammalian Smac/Diablo and *Drosophila* Hid/Reaper/Grim, both bind to IAPs and are localised to mitochondria (Brun et al., 2002; Claveria et al., 2002; Freel et al., 2008; Olson et al., 2003a; Wang et al., 1999; Yan et al., 2006). Further evidence for functional equivalence to Smac/Diablo is that Hid, Grim and Reaper can induce death in mammalian cells through the mitochondrial pathway (Claveria, 2004; Olson et al., 2003b). Recent studies report that the DmHtrA2 protein resides in the mitochondrial intermembrane space where it undergoes cleavage producing a mature protein that has two IBMs (IAP binding motifs). Upon apoptotic stimuli that induce mitochondrial permeabilization, the mature protein is

released and binds to dIAP to inactivate it, thus promoting apoptosis via the caspase pathway (Challa, 2007).

My observations that neurons lacking the Qless enzyme upregulate the mitochondrial stress marker Hsp60 and unmask the cytochrome *c* epitope, an indicator of mitochondrial membrane disruption, provide evidence that mitochondrial disruption can result in caspase activation and programmed cell death in *Drosophila.* The punctate unmasked cytochrome *c* epitope suggests that it remains localized to the mitochondria This contrasts with a recent study reporting that this cytochrome *c* epitope is released from mitochondria into a diffuse cytoplasmic pattern in cells expressing Hid and Reaper (Abdelwahid et al., 2007) but is consistent with previous studies reporting exposure but not delocalisation of the cytochrome c cell-death epitope in apoptotic cells (Dorstyn et al., 2004; Varkey et al., 1999).

In *qless* neurons, it is tempting to speculate that mitochondrial disruption/ permeabilization causes release of mature DmHtrA2. It would be interesting to see whether or not the pro-apoptotic proteins Reaper, Hid, Grim and Arc (Apaf-1) remain localised to mitochondria in *qless* neurons. Further analysis of *qless* thus offers the possibility of helping to define the mitochondrial death pathway in *Drosophila* that is independent of cytochrome *c* release.

6.2.3 *qless*, a fly model for human CoQ deficiencies

Primary CoQ_{10} deficiency in humans has been identified in 3 prenyl transferase enzymes involved in CoQ_{10} synthesis. Mutations in prenyl diphosphate synthase, subunit 1 (PDSS1), prenyl diphosphate synthase 2 (PDSS2) and OH-benzoate polyprenyltransferase (COQ2) result in CoQ deficiency and oxidative phosphorylation disorders, with tissues and organs with high energy demands such as brain, muscles, eyes, and kidneys being the most affected. Neurons, in particular, require large amounts of ATP with 95% of this generated in the mitochondria, with the result that the CNS is highly susceptible to low levels of CoQ_{10} (See Chapter 1, Section 1.4.2.). Primary deficiencies are autosomal recessive and fall into five major phenotypes: Infantile encephalomyopathies, severe infantile multisystemic disease, cerebellar ataxias, Leigh syndrome with growth retardation, ataxia and deafness and

isolated myopathy (Berbel-Garcia et al., 2004; DiMauro et al., 2006; DiMauro et al., 2007; Lopez et al., 2006; Quinzii et al., 2006; Rotig et al., 2000; Rotig et al., 2007; Zhang et al., 2007). Clinical conditions usually appear in childhood or adolescence and include general tiredness, muscle weakness, mental retardation, cerebellar symptoms, seizures, encephalopathy, renal failure (which requires a kidney transplant), optic atrophy, deafness, nephritic syndrome, psychomotor and developmental delay, progressive ataxia, cardiomyopathy, cerebral atrophy and infant death.

The recessive mutation found in the *PDSS1* gene (the *qless* orthologue) caused a multisystem disease in two related children due to CoQ_{10} deficiency (Mollet et al., 2007). This became more severe as the children grew older with progressive mental retardation, muscle weakness, deafness, obesity and optic atrophy. The recessive mutation in *PDSS2*, which encodes the small subunit of prenyl diphosphate synthase was extremely severe causing Leigh Syndrome and nephropathy in a male infant (Lopez et al., 2006). At 3 months he developed left-sided seizures which could not be cured with anti-epileptic drugs, his muscles became progressively weaker and he had feeding difficulties due to exhaustion. He died at the age of 7 months.

In addition to these diseases, low levels of CoQ_{10} are found in patients with neurodegenerative diseases such as Alzheimer's, Parkinson's and Huntington's, mitochondrial diseases caused by mitochondrial DNA mutations, cancer, Friederich's ataxia, asthma, hyperthyroidism, male infertility, AIDS and cardiovascular disease (Beal, 2007; Belardinelli et al., 2006; Celotto et al., 2006; Dias-Santagata et al., 2007; Folkers et al., 1991; Hausse et al., 2002; Lin and Beal, 2006; Mandemakers et al., 2007; Montero et al., 2007; Ross, 2007; Rustin et al., 2002; Young et al., 2007; Yuvaraj et al., 2007). Clinical trials using high doses of CoQ_{10} have shown distinct improvement in all of these illnesses. Of particular importance are clinical trials on breast cancer patients which have shown that CoQ_{10} inhibits metastases and has a tumour suppressor effect (Premkumar et al., 2007). In neurodegenerative diseases, administration delays progress of the disease, and patients show a distinct improvement. Similarly, for Freiderich's ataxia patients, either CoQ_{10} or the analogue CoQ_4 have benefited them clinically (Farley et al., 1966; Geromel et al., 2002; Hausse et al., 2002; Lerman-Sagie et al., 2001; Ross, 2007; Rotig et al., 2000; Rustin et al., 2002). It is therefore imperative that these

clinical diseases are diagnosed at the first signs of a possible CoQ_{10} deficiency so that rescue therapy can begin as soon as possible (Huntsman et al., 2005). Although there is abundant clinical evidence of the therapeutic effects of CoQ, more evidence for mechanism-of-action is needed. As the *qless* mutation causes defective neurogenesis in the fly CNS, it provides an important fly model to study CoQ deficiency diseases

6.3. Conclusion.

In conclusion, both genetic screens successfully isolated a total of 90 mutations affecting various aspects of CNS growth. The mapping technique identified a previously uncharacterised *Drosophila* gene *qless*, the homologue of the human *PDSS1* gene which encodes a trans-prenyl transferase required for CoQ synthesis. Sequence analysis revealed the serine residue downstream from the catalytic site as a new critical amino acid required for its function. Characterisation of *qless* clones revealed that Coenzyme Q deficiency causes neural defects in proliferation and apoptosis. CoQs of different side-chain length are functionally equivalent in the *Drosophila* CNS. Interestingly, CoQ supplementation also increases the frequency of clones generated in mosaic animals and is therefore a useful tool for boosting FLP-mediated recombination events. In *qless* clones, mitochondrial membrane disruption appears to lead to caspase activation and cell death, providing a new link between mitochondria and programmed cell death in *Drosophila* which to date is still unclear. Taken together, these results indicate that the *qless* mutant lines are a valuable genetic tool as a potential fly model for mitochondrial disruption and apoptosis in the fly. Importantly, as the primary CoQ_{10} deficiencies and mitochondrial diseases are rare and difficult to study in humans, the *qless* mutant will provide an important fly model to study these mutations.

Bibliography

Abdelwahid, E., Yokokura, T., Krieser, R.J., Balasundaram, S., Fowle, W.H., and White, K. (2007). Mitochondrial disruption in Drosophila apoptosis. Dev Cell *12*, 793-806.

Albertson, R., Chabu, C., Sheehan, A., and Doe, C.Q. (2004). Scribble protein domain mapping reveals a multistep localization mechanism and domains necessary for establishing cortical polarity. J Cell Sci *117*, 6061-6070.

Albertson, R., and Doe, C.Q. (2003). Dlg, Scrib and Lgl regulate neuroblast cell size and mitotic spindle asymmetry. Nat Cell Biol *5*, 166-170.

Almeida, M.S., and Bray, S.J. (2005). Regulation of post-embryonic neuroblasts by Drosophila Grainyhead. Mech Dev *122*, 1282-1293.

Alonso, J., Rodriguez, J.M., Baena-Lopez, L.A., and Santaren, J.F. (2005). Characterization of the *Drosophila melanogaster* Mitochondrial Proteome. Journal of Proteome Research *4*, 1636-1645.

Arama, E., Agapite, J., and Steller, H. (2003). caspase activity and a specific cytochrome c are required for for sperm differentiation in *Drosophila*. Dev Cell *4*, 687-697.

Arya, R., Mallik, M., and Lakhotia, S.C. (2007). Heat shock genes-integrating survival and death. J Biosci *32*.

Baehrecke, E.H. (2000). Steroid regulation of programmed cell death during *Drosophila* development. Cell Death Differ *7*, 1057-1062.

Baloh, R.H. (2008). Mitochondrial dynamics and peripheral neuropathy. Neuroscientist *14*, 12-18.

Beal, M.F. (2007). Mitochondria and Neurodegeneration. Novartis Found Symp *287*, 183-196.

Bebel-Garcia, A., Barbera-Farre, H., and al, e. (2004). Coenzyme Q10 improves lactic acidosis, strokelike episodes and epilepsy in a patient with MELAS. Clinical Neuropharmacology *27*, 187-191.

Belardinelli, R., Mucaj, A., Lacalaprice, F., Solenghi, M., Seddaiu, G., Principi, F., Tiano, L., and Littarru, G.P. (2006). Coenzyme Q10 and exercise training in chronic heart failure. Eur Heart J *27*, 2675-2681.

Belliveau, M.J., and Cepko, C.L. (1999). Extrinsic and extrinsic factors control the genesis of amacrine and cone cells in the rat retina. Development *126*, 555-566.

Bello, B., Holbro, N., and Reichert, H. (2007). Polycomb group genes are required for neural stem cell survival in postembryonic neurogenesis of Drosophila. Development *134*, 1091-1099.

Bello, B.C., Hirth, F., and Gould, A.P. (2003). A pulse of the Drosophila Hox protein Abdominal-A schedules the end of neural proliferation via neuroblast apoptosis. Neuron *37*, 209-219.

Berbel-Garcia, A., Barbera-Farre, H., and al, e. (2004). Coenzyme Q10 improves lactic acidosis, strokelike episodes and epilepsy in a patient with MELAS. Clinical Neuropharmacology *27*, 187-191.

Berry, M., Rogers, A.W., and Eayrs, J.J. (1964). Pattern of Cell MIgration Duting Cortical Histogenesis. Nature *203*, 591-593.

Betschinger, J., Mechtler, K., and Knoblich, J.A. (2003). The Par complex directs asymmetric cell division by phosphorylating the cytoskeletal protein Lgl. Nature *422*, 326-330.
Betschinger, J., Mechtler, K., and Knoblich, J.A. (2006). Asymmetric Segregation of the Tumour Suppressor Brat Regulates Self-Renewal in *Drosophila* Neural Stem Cells Cell *124*, 1241-1253.
Bhat, K.M. (1998). Cell-cell signaling during neurogenesis: some answers and many questions. Int J Dev Biol *42*, 127-139.
Bilder, D., and Perrimon, N. (2000). Localization of apical epithelial determinants by the basolateral PDZ protein Scibble. Nature *403*, 676-680.
Bossing, T., Udolph, G., Doe, C.Q., and Technau, G.M. (1996). The embryonic central nervous system lineages of Drosophila melanogaster. I. Neuroblast lineages derived from the ventral half of the neuroectoderm. Dev Biol *179*, 41-64.
Boyer, P.D. (1997). The ATP synthase -- a splendid molecular machine. Annual Rev Biochem *66*, 717-749.
Bray, S.J. (1997). Expression and function of Enhancer of split bHLH proteins during Drosophila neurogenesis. Perspect Dev Neurobiol *4*, 313-323.
Bray, S.J., Burke, B., Brown, N.H., and Hirsh, J. (1989). Embryonic expression pattern of a family of *Drosophila* proteins that interact with a central nervous system regulatory element Genes and Development *3*, 1130-1145.
Britton, J., and Edgar, B. (1998). Environmental control of cell cycle in *Drosophila:* nutrition activates mitotic and endoreplicative cells by distinct mechanisms. Development *125* (11), 2149-2158.
Broadus, J., Skeath, J.B., Spana, E.P., Bossing, T., Technau, G., and Doe, C.Q. (1995). New neuroblast markers and the origin of the aCC/pCC neurons in the Drosophila central nervous system. Mech Dev *53*, 393-402.
Brody, T., and Odenwald, W.F. (2000). Programmed transformations in neuroblast gene expression during Drosophila CNS lineage development. Dev Biol *226*, 34-44.
Brody, T., and Odenwald, W.F. (2005). Regulation of temporal identities during Drosophila neuroblast lineage development. Curr Opin Cell Biol *17*, 672-675.
Brown, M., Keynes, R., and Lumsden, A. (2001). The Developing Brain. Oxford University Press.
Brun, S., Rincheval, V., Gaumer, S., Mignotte, B., and Guenal, I. (2002). *reaper* and *bax* initiate two different apoptotic pathways affecting mitochondria and antagonized by *bcl-2* in *Drosophila* Oncogene *21*, 6458-6470.
Caldwell, M.C., and Datta, S. (1998). Expression of cyclin E or DP/E2F rescues the G1 arrest of trol mutant neuroblasts in the Drosophila larval central nervous system. Mech Dev *79*, 121-130.
Calhoun, M., Thomas, J., and Gennis, R. (1994). The cytochrome oxidase superfamily of redox-driven proton pumps. Trends Biochem Sci *19*, 325-330.
Campos-Ortega, J., and Hartenstein, V. (1997). The embryonic development of *Drosophila melanogaster*. Springer, Heidelburg.
Campos-Ortega, J.A. (1997). Asymmetic division: dynastic intricacies of neuroblast division. Curr Biol *7*, R726-728.
Campuzano, S., and Modolell, J. (1992). Patterning of the *Drosophila* nervous system:the *achaete-scute gene complex*. Trends Genet *8*, 202-208.
Cayre, M., Malaterre, J., Charpin, P., Strambi, C., and Strambi, A. (2000). Fate of neuroblast progeny during postembryonic development of mushroom bodies in the house cricket, Acheta domesticus. J Insect Physiol *46*, 313-319.

Cecchi, C. (2002). Emx2: a gene responsible for cortical development, regionalization and area specification. Gene *291*, 1-9.
Cecchini, G. (2003). Function and structure of complex II of the respiratory chain. Annual Rev Biochem *72*, 77-109.
Celotto, A.M., Frank, A.C., McGrath, S.W., Palladino, M.J., and al, e. (2006). Mitochondrial Encephalomyopathy in *Drosophila*. The Journal of Neuroscience *26*, 810-820.
Cenci, C., and Gould, A.P. (2005). Drosophila Grainyhead specifies late programmes of neural proliferation by regulating the mitotic activity and Hox-dependent apoptosis of neuroblasts. Development *132*, 3835-3845.
Cepko, C.L. (1999). The roles of intrinsic and extrinsic and bHLH genes in the determination of retinal cell fates.cues Curr Opin Neurobiology *9*, 37-46.
Chada, S.R., and Hollenbeck, P.J. (2004). Nerve growth factor signaling regulates motility and docking of axonal mitochondria. Current Biology *14*, 1272-1276.
Challa (2007). Drosophila Omi, a mitochondrial-localized IAP antagonist and proapoptotic serine protease. EMBO *26*, 3144-3156.
Chang, D.T.W., Honick, A.S., and Reynolds, I.J. (2006). Mitochondrial trafficking to synapses in cultured primary cortical cells. J Neuroscience *26*, 7035-7045.
Chang, D.T.W., and Reynolds, I.J. (2006). Mitochondrial trafficking and morphology in healthy and injured neurons. Progress in Neurobiology *80*, 241-268.
Chang, W.S., and Harris, W.A. (1998). Sequential genesis and determination of cone and rod receptors in *Xenopus*. J Neurobiology *35*.
Chen, F., Hersh, B.M., Conradt, B., Zhou, Z., Riemer, D., Gruenbaum, Y., and Horvitz, H.R. (2000). Translocation of *C. elegans* CED-4 to nuclear membranes during programmed cell death. Science *287*, 1485-1489.
Claveria (2004). A Bax/Bak-independent mitochondrial death Pathway triggered by Drosophila Grim GH3 domain in mammalian cells Biological Chemistry *279*, 1368-1375.
Claveria, C., Caminero, E., Martinez-A, C., Campuzano, S., and Torres, M. (2002). GH3 a novel proapoptotic domain in *Drosophila* Grim, promotes a mitochondrial death pathway. Embo J *21*, 3327-3336.
Corbin, V., Michelson, A.M., Young, M.W., and al, e. (1991). A role for the *Drosophila* neurogenic genes in mesoderm differentiation Cell *67*, 311-323.
Crane, F.L. (2001). Biochemical functions of coenzyme Q10. Journal of the American College of Nutrition *20*, 591-598.
Datta, S. (1995). Control of proliferation activation in quiescent neuroblasts of the Drosophila central nervous system. Development *121*, 1173-1182.
Datta, S. (1999). Activation of neuroblast proliferation in explant culture of the Drosophila larval CNS. Brain Res *818*, 77-83.
DeHahn, T., Barr, R., and Morre (1997). NADH oxidase activity present on both the external and internal surfaces of the soybean plasma membrane Biochim Biophys Acta *1328*, 99-108.
del Peso, L., Gonzalez, V.M., Inohara, N., Ellis, R.E., and Nunez, G. (2000). Disruption of the CED-9/CED-4 complex by EGL-1 is a critical step for programmed cell death in *C. elegans*. J Biol Chem *275*, 27205-27211.
Denault, J.B., Eckelman, B.P., Shin, H., Pop, C., and Salvesen, G.S. (2007). Caspase 3 attenuates XIAP (X-linked inhibitor of apoptosis protein) -mediated inhibition of caspase 9. Biochem J *405*, 11-19.
Denault, J.B., and Salvasen, G.S. (2008). Apoptotic Caspase activation and activity. Methods Mol Biol *414*, 191-220.

Desai, A.R., and McConnell, S.K. (2000). Progressive restriction in fate potential by neural progenitors during cerebral cortical development. Development *127*, 2863-2872.
Dias-Santagata, D., Fulga, T.A., Duttaroy, A., and Feany, M.B. (2007). Oxidative stress mediates tau-induced neurodegeneration in *Drosophila*. The Journal of Clinical Investigation *117*, 236-245.
DiMauro, S., Hirano, M., and Schon, E.A. (2006). Approaches to the treatment of mitochondrial diseases. Muscle Nerve *34*, 265-283.
DiMauro, S., Quinzii, C.M., and Hirano, M. (2007). Mutations in coenzyme Q10 biosynthetic genes. J Clin Invest *117*, 587-589.
Doe, C.Q. (2006). Chinmo and neuroblast temporal identity. Cell *127*, 254-256.
Doe, C.Q., and Bowerman, B. (2001). Asymmetric cell division: fly neuroblast meets worm zygote. Curr Opin Cell Biol *13*, 68-75.
Doe, C.Q., and Skeath, J.B. (1996). Neurogenesis in the insect central nervous system. Curr Opin Neurobiol *6*, 18-24.
Doetsch, F., Petreanu, L., Caille, I., Garcia-Verdugo, J.M., and Alvarez-Buyalla, A. (2002). EGF converts transit-amplifying neurogenic precursors in the adult brain into multipotent stem cells. Neuron *36*, 1021-1034.
Donovan, S.L., and Dyer, M.A. (2005). Regulation of proliferation during central nervous system development. Semin Cell Dev Biol *16*, 407-421.
Dorstyn, L., Mills, K., Lazebnik, Y., and Kumar, S. (2004). The two cytochrome *c* species, DC3 and DC4, are not required for caspase activation and apoptosis in *Drosophila* cells The Journal of Cell Biology *17*, 405-410.
Dorstyn, L., Read, S.H., Cakouros, D., Huh, J.R., Hay, B.A., and Kumar, S. (2002). The role of cytochrome *c* in caspase activation in *Drosophila melanogaster*. J Cell Biology *156*, 1089-1098.
Dumstrei, K., Wang, F., and Hartenstein, V. (2003). Role of DE-cadherin in neuroblast proliferation, neural morphogenesis, and axon tract formation in Drosophila larval brain development. J Neurosci *23*, 3325-3335.
Ebens, A.J., Garren, H., Cheyette, B.N., and Zipursky, S.L. (1993). The Drosophila anachronism locus: a glycoprotein secreted by glia inhibits neuroblast proliferation. Cell *74*, 15-27.
Egger, B., Boone, J.Q., Stevens, N.R., Brand, A.H., and Doe, C.Q. (2007a). Regulation of spindle orientation and neural stem cell fate in the Drosophila optic lobe. Neural Develop *2*, 1.
Egger, B., Chell, J.M., and Brand, A.H. (2008). Insights into neural stem cell biology from flies. Philos Trans R Soc Lond B Biol Sci. 363, 39-56
Ellis, H.M., and Horvitz, H.R. (1986). Genetic control of programmed cell death in the nematode *C elegans*. Cell *44*, 817-829.
Farley, T.M., Scholler, J., and Folkers, K. (1966). Response of genetically dystrophic mice to therapy with hexahydrocoenzyme Q_4. Biochemical and Biophysical Research Communications *24*, 299-303.
Fekete, D.M., Perez-Miguelsanz, J., Ryder, E.F., and Cepko, C.L. (1994). Clonal analysis in the chicken retina reveals tangential dispersion of clonally related cells. Developmental Biology *166*, 666-682.
Fernandez, S.M.S., Kellogg, B.A., and Poulter. C, D. (2000). Farnesyl diphosphate synthase. Altering the catalytic site to slect for geranyl diphosphate synthase activity. Biochemistry *39*, 15316-15321.

Folkers, K., Ellis, J., and al, e. (1991). Coenzyme Q_{10} deficiency in cancer patients: potential for immunotherapy with Coenzyme Q_{10}. Vitamins and cancer prevention, New York, 103-110.
Fontaine, E., Ichas, P., and Bernardi, P. (1998). A ubiquinone-binding site regulates the mitochondrial permeability transition pore. J Biol Chem *273*, 25734-25740.
Frantz, G.D., and McConnell, S.K. (1996). Restriction of late cerebral cortical progenitors to an upper-layer fate. Neuron *17*, 55-61.
Freel, C.D., Richardson, D.A., Thomenius, M.J., Gan, E.C., Horn, S.R., Olson, M.R., and Kornbluth, S. (2008). Mitochondrial Localization of Reaper to Promote Inhibitors of Apoptosis Protein Degradation Conferred by GH3 Domain-Lipid Interactions J Biol Chem *283*, 367-379.
Geromel, V., Darin, N., Chretian, D., and al, e. (2002). Coenzyme Q10 and idebenone in the therapy of respiratory chain diseases: rationale and comparative benefits. Molecular Genetics and Metabolism *77*, 21-30.
Gille, L., and Nohl, H. (2000). The existence of a lysosomal redox chain and the role of ubiquinone. Arch Biochem Biophys *375*, 347-354.
Gotz, M., and Hunter, W.B. (2005). The Cell Biology of Neurogenesis. Nature Reviews/Molecular Cell Biology *6*, 777-778.
Greenspan, R.J. (1997). Fly Pushing. The Theory and Practice of *Drsosophila* Genetics. Cold Spring HarbourLab Press.
Grosskortenhaus, R., Pearson, B.J., Marusich, A., and Doe, C.Q. (2005). Regulation of temporal identity transitions in Drosophila neuroblasts. Dev Cell *8*, 193-202.
Grosskortenhaus, R., Robinson, K.J., and Doe, C.Q. (2006). Pdm and Castor specify late-born motor neuron identity in the NB7-1 lineage. Genes and Development *20*, 2618-2627.
Guo, R., Kuo, C., and al, e. (2004). A molecular ruler for chain elongation catalyzed by octaprenyl pyroposphate synthase and its structure-based engineering to produce unprecedented long chain *trans*-prenyl products Biochemistry *43*, 7678-7686.
Hanashima, C., Li, S.C., Shen, L., Lai, E., and Fishell, G. (2004). Foxg1 suppresses early cortical fate. Science *303*, 56-59.
Hartenstein, V., Rudloff, E., and Campos-Ortega, J. (1987). The pattern of proliferation of the neuroblasts in wild-type embryo of *Drosophila melanogaster* Development Biology *196*, 473-485. division in the Drosophila neurectoderm: spatiotemporal pattern, cytoskeletal
Hartenstein, V., Younossi-Hartenstein, A., and Lekven, A. (1994). Delamination and dynamics, and common control by neurogenic and segment polarity genes. Dev Biol *165*, 480-499.
Hausse, A.O., Aggoun, Y., Bonnet, D., Rustin, P., and al, e. (2002). Idebenone and reduced cardiac hypertrophy in Freidreich's ataxia Heart *87*, 346-349.
Hay, B.A., and Guo, M. (2006). Caspase-dependent cell death in Drosophila. Annu Rev Cell Dev Biol *22*, 623-650.
Hay, B.A., Huh, J.R., and Guo, M. (2004). The genetics of cell death:approahes, insights and opportunities in *Drosophila*. Nat Rev Genetics *5*, 911-922.
Hihi, A.K., Kebir, H., and Hekimi, S. (2003). Sensitivity of *Caenorhabditis elegans clk-1* Mutants to Ubiquinone Side-Chain lenghts reveals Multiple Ubiquinone-dependent Processes. Journal of Biological Chemistry *278*, 41013-41018.
Holt, C.E., Bertsch, T.W., Ellis, H.M., and Harris, W.A. (1988). Cellular determination in the *Xenopus* retina is independent of lineage and birth date. Neuron *1*.

Horvitz, H.R. (1999). Genetic control of programmed cell death in the nematode *Caenorhabditis elegans*. Cancer Res *59*, 1701-1706.
Hu, M., and Easter, S.S. (1999). Retinal neurogenesis: the formation of the initial central patch of postmitotic cells. Developmental Biology *207*, 309-321.
Humbert, P., Russell, S., Richardson H (2003). Dlg, Scribble and Ll in cell proliferation and cancer. BioEssays *25*, 542-553.
Hunte, C., Palsdottir, H., and Trumpower, B. (1990). Protonmotive pathways and mechanisms in the cytochrome bc1 complex. FEBS Lett *545*, 39-46.
Huntsman, R.J., Sinclair, D.B., Bhargava, R., and Chan, A. (2005). Atypical Presentations of Leigh Syndrome: A Case Series and Review. Pediatric Neurology *32*, 334-340.
Igaki (2000). Drob-1, a Drosophila member of the Bcl-2/CED-9 family that promotes cell death. Proc Natl Acad Sci USA *97*, 662-667.
Igaki (2004). Role of Bcl-2 family members in veterbrates. BBA *1644*, 73-81.
Igaki (2007). Evolution of mitochondrial cell death pathway: Proapoptotic role of HtrA2/Omi in Drosophila. Biochemical and Biophysical Research communications *356*, 993-997.
Igaki, T., Yamamoto-Goto, Y., Tokushige, N., Kanda, H., and Miura, M. (2002). Down-regulation of DIAP 1 triggers a novel *Drosophila* cell death pathway mediated by Dark and DRONC. J Biol Chem *277*, 23103-23106.
Isshiki, T., Pearson, B., Holbrook, S., and Doe, C.Q. (2001). Drosophila neuroblasts sequentially express transcription factors which specify the temporal identity of their neuronal progeny. Cell *106*, 511-521.
Jacobson, M.D., Weil, M., and Raff, M.C. (1997). Programmed cell death in animal development. Cell *1997*, 347-354.
Kambadur, R., Koizumi, K., Stivers, C., Nagle, J., Poole, S.J., and Odenwald, W.F. (1998). Regulation of POU genes by castor and hunchback establishes layered compartments in the Drosophila CNS. Genes Dev *12*, 246-260.
Kann, O., and Kovacs, R. (2007). Mitochondria and neural activity. American J Physiol Cell Physiol *292*, 641-657.
Karcavich, R., and Doe, C.Q. (2005). *Drosophila* neuroblast NB7-3 cell lineage: a model system for studying programmed cell death, Notch/Numb signalling, and sequential specification of ganglion mother cell identity. J Comp Neurol *481*, 240-251.
Kessaris, N., Pringle, N., and Richardson, W.D. (2001). Ventral neurogenesis and the neuron-glial switch. Neuron *31*, 677-680.
Kinai MI, O.M., Hiromi Y (2005). seven-up controls switching of transcription factors that specify temporal identities of Drosophila neuroblasts. Dev Cell *8*, 203-213.
Knust, E., Schrons, H., Grawe, F., and Campos-Ortega, J. (1992). Seven genes of the Enhancer of split complex of *Drosophila melanogaster* encode helix-loop-helix proteins. Genetics *132*, 505-518.
Koike-Takeshita, A., Koyama, T., Obata, S., and Ogura, K. (1995). Molecular cloning and nucleotide sequences of the genes for two essential proteins constituting a novel enzyme system for heptaprenyl diphosphate synthase. The Journal of Biological Chemistry *270*, 18396-18400.
Koyama, T., Obata, S., Nishino, T., and Ogura, K. (1995). Significance of Phe220 and Gln-221 inthe catalytic mechanism of farnesyl diphosphate synthase of *Bacillus stearothermophilus* farnesyl pyrophosphate synthase. Biochem Biophys Res Commun *212*, 681-686.

Koyama, T., Obata, S., Saito, K., Takeshita-Koike, A., and Ogura, K. (1994). Structural and functional roles of the cysteine residues of *Bacillus stearthermophilus* farnesyl pyrophosphate synthase Biochemistry *33*, 12644-12648.
Kunisch M, H.M., Campos-Ortega JA (1994). Lateral inhibition mediated by the Drosophila neurogenic gene delta is enhanced by proneural proteins. Proc Natl Acad Sci USA *91*, 10139-10143.
Lee, C.Y., Robinson, K.J., and Doe, C.Q. (2006a). Lgl, Pins and aPKC regulate neuroblast self-renewal versus differentiation. Nature *439*, 594-598.
Lee, C.Y., Wilkinson, B.D., Siegrist, S.E., Wharton, R.P., and Doe, C.Q. (2006b). Brat is a Miranda cargo protein that promotes neuronal differentiation and inhibits neuroblast self-renewal. Dev Cell *10*, 441-449.
Lee, T., and Luo, L. (1999). Mosaic analysis with a repressible cell marker for studies of gene function in neuronal morphogenesis. Neuron *22*, 451-461.
Lerman-Sagie, Lev.D, Rustin, P., and Munnich, A. (2001). Dramatic improvement in mitochondrial cardiomyopathy following idebenone treatment. J Inher Metab Dis *24*, 28-34.
Liang, P., Ko, T., and Wang, A. (2002). Structure, mechanism and function of prenyltransferases. Eur J Biochem *269*, 3339-3354.
Lin, M.T., and Beal, M.F. (2006). Mitochondrial dysfunction and oxidative stress in neurodegeneative diseases. Nature *443*, 785-795.
Lindner, J.R., Hillman, P.R., Barrett, A.L., Jackson, M.C., Perry, T.L.P., Y., and Datta, S. (2007). The *Drosophila* Perlecan gene *trol* regulates multiple signaling pathways in different developmental contexts. BMC Developmental Biology *7*.
Liu, Q.A., and Hengartner, M.O. (1999). The molecular mechanisms of programmed cell death in *C. elegans*. Ann N Y Acad Sci *887*, 92-104.
Livesey, F.J., and Cepko, C.L. (2001). Vertebrate neural cell-fate determination: lessons from the retina. . Nat Rev Neuroscience *2*, 109-118.
Lopez, L.C., Schuelke, M., Quinzii, C.M., Kanki, T., Rodenburg, R.J., Naini, A., Dimauro, S., and Hirano, M. (2006). Leigh syndrome with nephropathy and CoQ10 deficiency due to decaprenyl diphosphate synthase subunit 2 (PDSS2) mutations. Am J Hum Genet *79*, 1125-1129.
Lundell, M.J., Lee, H.K., Perez, E., and Chadwell, L. (2003). the regulation of apoptosis by Numb/Notch signaling in the serotonin lineage of *Drosophila*. Development *130*, 4109-4121.
Lyons, D.A., Guy, A.T., and Clarke, J.D.W. (2003). Monitoring neural progenitor fate through multiple rounds of division in the intact vertebrate brain. Development *130*, 3427-3436.
Madden, K., Sheu, Y., Baetz, K., Andrews, B., and Snyder, M. (1997). SBF cell cycle regulator as a target of the yeast PKC-MAP kinase pathway. Science *275*, 1781-1784.
Mandemakers, W., Morais, V.A., and De Strooper, B. (2007). A cell biological perspective on mitochondrial dysfunction in Parkinson disease and other neurodegenerative diseases. JCell Science *120*, 1707-1716.
Martin-Bermudo MD, C.A., Jimenez F (1995). Neurogenic genes control gene expression at the transcriptional level in early neurogenesis and in mesectoderm specification. Development *121*, 219-224.
Matthews, F.S. (1985). The structure, function and evolution of the cytochromes. Prog Biophys Mol Biol *45*, 1-56.

Maurange, C., Cheng, L., and Gould, A.P. (2008). Temporal Transcription Factors and Their Targets Schedule the End of Neural proliferation in *Drosophila* Cell *133*, 891-902.
Maurange, C., and Gould, A.P. (2005). Brainy but not too brainy: starting and stopping neuroblast divisions in Drosophila. Trends Neurosci *28*, 30-36.
McConnell, S.K. (1988). Development and decision-making in the mammalian cortex. Brain Res *472*, 1-23.
McQuibban, G.A., Lee, J.R., Zheng, L., Juusola, M., and Freeman, M. (2006). Normal mitochondran dynamics requires Rhomboid-7 and affects *Drosophila* lifespan and neuronal function. Current Biology *16*, 982-989.
Melzig, J., Rein, K.H., Schafer, U., Pfister, H., Jackle, H., Heisenberg, M., and Raabe, T. (1998). A protein related to p21-activated kinase (PAK) that is involved in neurogenesis in the Drosophila adult central nervous system. Curr Biol *8*, 1223-1226.
Mendes, C.S., Arama, E., S, B., Scherr, H., and Mollereau, B. (2006). Cytochrome c-d regulates developmental apoptosis in the *Drosophila* retina. Embo reports *7*, 933-939.
Mettler, U., Vogler, G., and Urban, J. (2006). Timing of identity: spatiotemporal regulation of hunchback in neuroblast lineages of Drosophila by Seven-up and Prospero. Development *133*, 429-437.
Miguel-Aliaga, I., and Thor, S. (2004). Segment-specific prevention of pioneer neuron apoptosis by cell-autonomous, postmitotic Hox gene activity. Development *131*, 6093-6105.
Miguel-Aliaga, I., Thor, S., and Gould, A.P. (2008). Postmitotic specification of *Drosophila* insulinergic neurons from pioneer neurons. PLOS Biology *6*.
Mizuguchi, R., Sugimori, M., Takebayashi, H., Kosako, H., Nagao, M., and al, e. (2001). Combinatorial roles of olig2 and neurogenin 2 in the coordinated induction of pan-neuronal and subtype-specific properties of motoneurons Neuron *31*, 757-771.
Mollet, J., Giurgea, I., Schlemmer, D., Dallner, G., Chretien, D., Delahodde, A., Bacq, D., de Lonlay, P., Munnich, A., and Rotig, A. (2007). Prenyldiphosphate synthase, subunit 1 (PDSS1) and OH-benzoate polyprenyltransferase (COQ2) mutations in ubiquinone deficiency and oxidative phosphorylation disorders. J Clin Invest *117*, 765-772.
Molyneaux, B.J., Arlotta, P., Menezes, J.R.L., and Macklis, J.D. (2007). Neuronal subtype specification in th cerebral cortex. Nature Reviews/Neuroscience *8*, 427-437.
Montero, R., Pineda, M., Aracil, A., Vilaseca, M.A., Briones, P., Sanchez-Alcazar, J.A., Navas, P., and Artuch, R. (2007). Clinical, biochemical and molecular aspects of cerebellar ataxia and Coenzyme Q10 deficiency. Cerebellum *6*, 118-122.
Moody, S.A., Chow, I., and Huang, S.A. (2000). Intrinsic bias and lineage restriction in the phenotype determnation of dopamine and neuropeptide Y amacrine cells. J Neuroscience *20*, 3244-3253.
Morre, D.J. (1994). The hormone and growth factor-stimulated NADH oxidase. J Bioenerg Biomemb *26*, 421-433.
Novitch, B.G., Chen, A.I., and Jessell, T.M. (2001). Coordinate regulation of motor neuron sub-type identity and pan-neuronal properties by the bHLH repressor Olig2. . Neuron *31*, 773-789.

Novotny, T., Eiselt, R., and Urban, J. (2002). Hunchback is required for the specification of the early sublineage of neuroblast 7-3 in the Drosophila central nervous system. Development *129*, 1027-1036.
Ohnuma, S., Hirroka, K., and al, e. (1998). A pathway where polyprenyl diphosphate elongates in prenyltransferase. The Journal of Biological Chemistry *273*, 26705-26713.
Okada (1998). Biological significance of the side chain length of ubiquinone in Saccharomyces cerevisae. FEBS *431*, 241-244.
Okada, K., Suzuki, K., Kamiya, Y., Zhu , X., Fujisaki, S., Nishino, T., Nishimura, T., Nakagawa, T., Kawamukai, M., and Matsuda, Y. (1996). Polyprenyl diphosphate synthase essentially defines the length of the side chain of ubiquinone. Biochim Biophys Acta *1302*, 217-223.
Olson, M.R., Holley, C.L., Gan, E.C., Colon-Ramos, D.A., Kaplan, B., and Kornbluth, S. (2003a). A GH3-like domain in reaper is required for mitochondrial localization and induction of IAP degradation J Biol Chem *278*, 44758-44768.
Olson, M.R., Holley, C.L., Gan, E.C., Colon-Ramos, D.A., Kaplan, B., and Kornbluth, S. (2003b). A GH3-like domain in reaper is required for mitochondrial localization and induction of IAP degradation. J Biol Chem *278*, 44758-44768.
Oppenheim, R.W. (1991). Cell death during development of the central nervous system. Annual Rev Neuroscience *14*, 453-501.
Papucci, L., Schavione, N., Witort, E., Donnini, M., and al, e. (2003). Coenzyme Q10 prevents apoptosis by inhibiting mitochondrial depolorazation independently of its free radical scavenging property. J Biol Chem *278*, 28220-28228.
Pearson, B.J., and Doe, C.Q. (2003). Regulation of neuroblast competence in Drosophila. Nature *425*, 624-628.
Pearson, B.J., and Doe, C.Q. (2004). Specification of Temporal Identity in the Developing nervous System. Ann Rev Cell Developmental Biology *20*, 619-647.
Peterson, C., Carney, G.E., Taylor, B.J., and White, K. (2002). reaper is required for neuroblast apoptosis during Drosophila development. Development *129*, 1467-1476.
Pettmann, B., and Henderson, C.E. (1998). Neuronal cell death. Neuron *20*, 633-647.
Premkumar, V.G., Yuvara, S., Vuayasarathy, K., and al, e. (2007). Effect of Coenzyme Q_{10}, Riboflavin and Niacin on Serum CEA and CA 15-3 Levels in Breast Cancer Patients undergoing Tamoxifen Therapy. Biol Pharm Bull *30*, 367-370.
Prokop, A., Bray, S., Harrison, E., and Technau, G.M. (1998). Homeotic regulation of segment-specific differences in neuroblast numbers and proliferation in the Drosophila central nervous system. Mech Dev *74*, 99-110.
Prokop, A., and Technau, G.M. (1991). The origin of postembryonic neuroblasts in the ventral nerve cord of Drosophila melanogaster. Development *111*, 79-88.
Putcha, G.V., and Johnson Jr., E.M. (2004). Men are but worms:neuronal cell death in *C elegans* and verterbrates. Cell Death Differ *11*, 28-48.
Quinn, L., Coombe, M., Mills, K., Daish, T., Colussi, P., Kumar, S., and Richardson, H. (2003). Buffy, a *Drosophila* Bcl-2 protein, has anti-apoptotic and cell cycle inhibitory functions. Embo J *22*, 3568-3579.
Quinn, P., Fabisiak, J., and Kagan, V. (1999). Expansion of the antioxidant vitamin E by Coenzyme Q. Biofactors *9*, 149-154.
Quinzii, C.M., DiMauro, S., and Hirano, M. (2006). Human Coenzyme Q_{10} Deficiency. Neurochem Res.
Rakic, P. (1974). Neurons in rhesus monkeys visual cortex: systematic relation between time of origin and eventual disposition. Science *183*, 425-427.

Rattan, S.I. (2006). Theories of biological ageing: genes, proteins and free radicals. Free Radic Res *40*, 1230-1238.
Richardson, H., and Kumar, S. (2002). Death to flies: *Drosophila* as a model system to study programmed cell death. J Immunol Methods *265*, 21-38.
Riedl, S.J., and Shi, Y. (2004). Molecular mechanisms of caspase regulation during apoptosis. Nat Rev Mol Cell Biology *5*, 897-907.
Rodriguez, A., Oliver, H., Zou, H., P, C., Wang, X., and Abrams, J.M. (1999). Dark is a *Drosophila* homologue of Apaf-1/CED-4 and functions in an evolutionary conserved death pathway. Nat Cell Biology *1*, 272-279.
Rogulja-Ortmann, A., Luer, K., Seibert, J., Rickert, C., and Technau, G.M. (2007). Programmed cell death in the embryonic central nervous system of Drosophila melanogaster. Development *134*, 105-116.
Ross, S.M. (2007). Coenzyme q10: ubiquinone: a potent antioxidant and key energy facilitator for the heart. Holist Nurs Pract *21*, 213-214.
Rotig, A., Appelkvist, E.L., Geromel, V., Rustin, P., and al, e. (2000). Quinone-responsive mitochondrial encephalomyopathy due to a CoQ_{10} biosynthesis defect. Lancet *356*, 391-395.
Rotig, A., Mollet, J., Rio, M., and Munnich, A. (2007). Infantile and pediatric quinone deficiency diseases. Mitochondrion *7*, 12-121.
Rustin, P., Rotig, A., Munnich, A., and Sidi, D. (2002). Heart hypertrophy and function are improved by idebenone in Freidreich's ataxia. Free Radic Res *36*, 467-470.
Saiki, R., Nagata, A., Kainou, T., Matsuda, H., and Kawamukai, M. (2005). Characterization of solanesyl and decaprenyl diphosphate synthases in mice and humans. Febs J *272*, 5606-5622.
Salvesen, G.S., and Riedl, S.J. (2008). Caspase mechanisms. Adv Exp Med Biol *615*, 13-23.
Schmid, A., Chiba, A., and Doe, C.Q. (1999). Clonal analysis of Drosophila embryonic neuroblasts: neural cell types, axon projections and muscle targets. Development *126*, 4653-4689.
Schmidt, H., Rickert, C., Bossing, T., Vef, O., Urban, J., and Technau, G.M. (1997). The embryonic central nervous system lineages of Drosophila melanogaster. II. Neuroblast lineages derived from the dorsal part of the neuroectoderm. Dev Biol *189*, 186-204.
Scholler, J., Jones, D., Littarru, G.P., and Folkers, K. (1970). Therapy of hereditary mouse muscular dystrophy with Coenzyme Q_7 Biochemical and Biophysical Research Communications *41*, 1298-1305.
Schrons, H., Knust, E., and Campos-Ortega, J. (1992). The Enhancer of split complex and adjacent genes in the 96F region of *Drosophila melanogaster* are required for segregation of neural and epidermal progenitor cells. Genetics *132*, 481-503.
Schultz, B., and Chan, S. (2001). Structures and proton-pumping strategies of mitochondrial respiratory enzymes Annual Rev Biophys Biomol Struct *30*, 23-65.
Shen, Q., Wang, Y., Dimos, J.T., Fasano, C.A., Phoenix, T.N., Lemischka, I.R., Ivanova, N.B., Stifani, S., Morrisey, E.E., and Temple, S. (2006). The timing of cortical neurogenesis is encoded within lineages of individual progenitor cells. Nature Neuroscience *9*, 743-751.
Shi, Y. (2002). Mechanisms of caspase activation and inhibition during apoptosis. Mol Cell *9*, 459-470.

Silhankova, M., Jindra, M., and Asahina, M. (2005). Nuclear receptor NHR-25 is required for cell-shape dynamics during epidermal differentiation in Caenorhabditis elegans. J Cell Sci *118*, 223-232.
Skeath, J.B., and Doe, C.Q. (1996). The achaete-scute complex proneural genes contribute to neural precursor specification in the Drosophila CNS. Curr Biol *6*, 1146-1152.
Skeath, J.B., and Thor, S. (2003). Genetic control of Drosophila nerve cord development. Curr Opin Neurobiol *13*, 8-15.
Skeath, J.B., Zhang, Y., Holmgren, R., Carroll, S.B., and Doe, C.Q. (1995). Specification of neuroblast identity in the Drosophila embryonic central nervous system by gooseberry-distal. Nature *376*, 427-430.
Slack, C., Somers, W.G., Sousa-Nunes, R., Chia, W., and Overton, P.M. (2006). A mosaic genetic screen for novel mutations affecting Drosophila neuroblast divisions. BMC Genet *7*, 33.
Song, L., and Poulter. C, D. (1994). YeastfFarnesyl diphosphate synthase: site-directed mutagenesis of residues in highly conserved prenyltransferase domain I and II. . Proc Natl Acad Sci USA *91*, 3044-3048.
Sun, I.L., Sun, E.L., Crane, F.L., D.J, M., Lindgren, A., and Low, H. (1992). Requirement for CoQ in plasma membrane electron transpor. Proc Natl Acad Sci USA *89*, 11126-11130.
Technau GM, Berger C., Urbach R (2006). Generation of cell diversity and segmental pattern in the embryo. Dev Dyn. *235* (4), 861-869.
Truman, J.W., and Bate, M. (1988). Spatial and temporal patterns of neurogenesis in the central nervous system of Drosophila melanogaster. Dev Biol *125*, 145-157.
Truman, J.W., Taylor, B.J., and Awad, T.A. (1993). Formation of the Adult Nervous System. The Development of *Drosophila melanogaster Chapter 21*, 1245-1275.
Trumpower, B. (1990). The protonmotive Q cycle. Energy transduction by coupling of proton translocation to electron transfer by the cytochrome bc1 complex. J Biol Chem *265*, 11409-11412.
Turner, D.L., and Cepko, C.L. (1987). A common progenitor for neurons and glia persists in rat retina late in development. Nature *328*, 131-136.
Turner, D.L., Snyder, E.y., and Cepko, C.L. (1990). Lineage-independent determination of cell type in the embryonic retina. Neuron *14*.
Turunen, M., Olsson, J., and Dallner, G. (2003). Metabolism and function of coenzyme Q. Biochimica et Biophysica Acta *1660*, 171-199.
Twomey, C., and McCarthy, J.V. (2005). Pathways of apoptosis and importance in development. J Cell Mol Med *9*, 345-359.
Urbach, R., Schnabel, R., and Technau, G.M. (2003). The pattern of neuroblast formation, mitotic domains and proneural gene expression during early brain development in Drosophila. Development *130*, 3589-3606.
Urbach, R., and Technau, G.M. (2003a). Molecular markers for identified neuroblasts in the developing brain of Drosophila. Development *130*, 3621-3637.
Urbach, R., and Technau, G.M. (2003b). Segment polarity and DV patterning gene expression reveals segmental organization of the Drosophila brain. Development *130*, 3607-3620.
Urbach, R., and Technau, G.M. (2004). Neuroblast formation and patterning during early brain development in Drosophila. Bioessays *26*, 739-751.
Urbach R, T.G. (2004). Neuroblast formation and patterning during early brain development in Drosophila. Bioessays *26*, 739-751.

Urbach, R., Volland, D., Seibert, J., and Technau, G.M. (2006). Segment-specific requirements for dorsoventral patterning genes during early brain development in Drosophila. Development *133*, 4315-4330.
Valko, M., Leibfritz, D., Moncol, J., Cronin, M.T., Mazur, M., and Telser, J. (2007). Free radicals and antioxidants in normal physiological functions and human disease. Int J Biochem Cell Biol *39*, 44-84.
Van de Bor, V., and Giangrande, A. (2001). Notch signalling represses the glia fate in Fly PNS. Development *128*, 1381-1390.
Varkey, J., Chen, P., Jemmerson, R., and Abrams, J.M. (1999). Altered cytochrome *c* display precedes apoptotic cell death in *Drosophila*. J Cell Biology *144*, 701-710.
Waid, D.K., and McLoon, S.C. (1998). Ganglion cells influence the fate of dividing retinal cells in culture. Development *125*, 1059-1066.
Walter, L., Miyoshi, H., Leverve, X., Bernardi, P., and Fontaine, E. (2002). Regulation of the mitochondrial permeability transition pore by ubiquinone analogs, A progress report. Free Radic Res *36*, 401-412.
Wang, S.L., Hawkins, C.J., Yoo, S.J., Muller, H.A., and Hay, B.A. (1999). The *Drosophila* caspase inhibitor DIAP1 is essential for cell survival and is negatively regulated by HID. Cell *98*, 453-463.
Wang, Y., Guo, H.F., Pologruto, T.A., Hannan, F., Hakker, I., Svobodo, K., and Zhong, Y. (2004). Stereotyped odor-evoked activity in the mushroom body of *Drosophila* revealed by green fluorescent protein-based Ca2+ imaging. Journal of Neuroscience *24*, 6507-6514.
Wetts, R., and Fraser, S.E. (1988). Multipotent precursors can give rise to all major cell types of the frog retina. Science *239*, 1142-1145.
White, K., Abrams, J.M., M.E., G., Abrams, J.M., Young, L., Farrell, K., and Steller, H. (1991). Genetic Control of Programmed Cell Death in *Drosophila*. Science *29*, 677-683.
White, K., Grether, M.E., Abrams, J.M., Young, L., and Steller, H. (1994). Genetic control of programmed cell death in *Drosophila* Science *264*, 677-683.
Wodarz, A. (2005). Molecular control of cell polarity and asymmetric cell division in Drosophila neuroblasts. Curr Opin Cell Biol *17*, 475-481.
Wu, L., Choe, K., Lu, Y., and Anderson, K. (2001). *Drosophila* immunity: genes on the third chromosome required for the response to bacterial infection Genetics *159*, 189-199.
Yan, N., Huh, J.R., Schirf, V., Demeler, B., Hay, B.A., and Shi, Y. (2006). Structure and activation mechanism of the *Drosophila* initiator caspase Dronc. J Biol Chem *281*, 8667-8674.
Yoshida, M., Muneyuki, E., and Hisabori, T. (2001). ATP synthase -- a marvellous rotary engine of the cell. Nat Rev Mol Cell Biol *2*, 669-677.
Yoshikawa, S., Muramoto, K., and Shinzawa-Itoh, K. (2006). Proton pumping mechanism of bovine heart cytochrome c oxidase. Biochim Biophys Acta *1757*, 1110-1116.
Youle, R.J., and Karbowski, M. (2005). Mitochondrial fision in apoptosis. Nature Reviews/Molecular Cell Biology *6*, 657-663.
Young, A.J., Johnson, S., Steffens, D.C., and Doraiswamy, P.M. (2007). Coenzyme Q10: a review of its promise as a neuroprotectant. CNS Spectr *12*, 62-68.
Young, R.W. (1985). Cell differentiation in the retina of the mouse. Anat Rec *212*, 199-205.
Yuvaraj, S., Premkumar, V.G., Vijayasarathy, K., Gangadaran, S.G., and Sachdanandam, P. (2007). Ameliorating effect of coenzyme Q10, riboflavin and

niacin in tamoxifen-treated postmenopausal breast cancer patients with special reference to lipids and lipoproteins. Clin Biochem *40*, 623-628.
Zhang, H., Huang, Q., Ke, N., Matsuyama, S., Hammock, B., Godzik, A., and Reed (2000a). *Drososphila* pro-apoptotic Bcl-2/Bax homologue reveals evolutionary conservation of cell death mechanisms. J Biol Chem *275*, 27303-27306.
Zhang, X.M., and Yang, X.J. (2001). Regulation of retinal ganglion cell production by Sonic hedgehog. Development *128*, 943-957.
Zhang, Y., Sun, F., Yang, Y.L., Chang, X.Z., Qi, Y., Qi, Z.Y., Xiao, J.X., Qin, J., and Wu, X.R. (2007). [Leigh syndrome due to pyruvate dehydrogenase E1 alpha subunit gene mutation: a complicated and difficult case study]. Zhongguo Dang Dai Er Ke Za Zhi *9*, 216-219.
Zhang, Y.W., Li, X.Y., and Koyama, T. (2000b). Chain length determination of prenyltransferases: both heteromeric subunits of medium-chain (E)-prenyl diphosphate synthase are involved in the product chain length determination. Biochemistry *39*, 12717-12722.
Zhao, G., Wheeler, S.R., and Skeath, J.B. (2007). Genetic control of dorsoventral patterning and neuroblast specification in the Drosophila Central Nervous System. Int J Dev Biol *51*, 107-115.
Zhou, Q., Choi, G., and Anderson, D.J. (2001). The bHLH transcription factor Olig2 promotes oligodendrocyte differentiation in collaboration with Nkx2.2. Neuron, 791-807.
Zhu, S., Lin, S., Kao, C., Awasaki, T., Chiang, A., and Lee, T. (2006). Gradients of the *Drosophila* Chinmo BTB-Zinc Finger Protein Govern Neuronal Temporal Identity. Cell *127*, 409-422.
Ziemer, A., Tietze, K., Knust, E., and Campos-Ortega, J. (1988). Genetic analysis of Enhancer of Split locus involved in neurogenesis in *Drosophila melanogaster*. Genetics *119*, 63-74.
Zou, H., Henzel, w.j., Liu, X., Lutschug, A., and Wang, X. (1997). Apaf-1, a human protein homolgous to *C. elegans* CED-4, participates in cytochrome c-dependent activation of caspase-3. Cell *90*, 405-413.